

NASA Contractor Report 178083

**The Evaluation of the
OSGLR Algorithm
for Restructurable Control**

W. Bonnice, E. Wagner, S. Hall, P. Motyka

**THE CHARLES STARK DRAPER LABORATORY, INC.
555 Technology Square
Cambridge, Massachusetts 02139**

**CONTRACT NAS1-17556
May 1986**



National Aeronautics and
Space Administration

Langley Research Center
Hampton, Virginia 23665

NASA Contractor Report 178083

**The Evaluation of the
OSGLR Algorithm
for Restructurable Control**

W. Bonnice, E. Wagner, S. Hall, P. Motyka

**THE CHARLES STARK DRAPER LABORATORY, INC.
555 Technology Square
Cambridge, Massachusetts 02139**

CONTRACT NAS1-17556

May 1986



National Aeronautics and
Space Administration

Langley Research Center
Hampton, Virginia 23665

TABLE OF CONTENTS

<u>Section</u>	Page
1	INTRODUCTION 1
2	BACKGROUND 5
2.1	Introduction 5
2.2	C-130 Simulation Description 5
2.3	Description of FDI Algorithms Evaluated 9
2.3.1	The Detection Filter 9
2.3.2	The Modified Detection Filter 12
2.3.3	The Generalized Likelihood Ratio (GLR) Test for Dynamic Systems 15
2.3.4	Orthogonal Series Generalized Likelihood Ratio (OSGLR) Test 21
2.4	Evaluation and Comparison of the FDI Algorithms 26
2.4.1	Failure Modes 28
2.4.2	Type of Failure 28
2.4.3	Magnitude of Failure 29
2.4.4	False Alarm Performance 29
2.4.5	Detection Time 30
2.4.6	Computational Burden 31
2.4.7	Robustness 33
2.4.8	Maturity 33
2.4.9	Summary and Overall Comparison 34
2.5	System Monitoring Strategy 34
2.5.1	Local Actuator FDI 37
2.5.2	Analytic FDI 37
2.5.3	Control Surface Position Sensors 38
2.5.4	System Monitoring Strategy Selected 39
2.6	Conclusions 40
3	A SURVEY OF FDI TECHNIQUES APPLICABLE TO AIRCRAFT CONTROL SURFACE FAILURE DETECTION AND ISOLATION 42
3.1	Introduction 42
3.2	Failure Sensitive Filters 42
3.3	Innovations-based Systems 43

TABLE OF CONTENTS (Cont.)

<u>Section</u>	<u>Page</u>
3.4 Multiple Hypothesis Filtering	44
3.5 Generalized Bayesian Tests	45
3.6 Conclusions	45
4 ACCOMMODATION OF MODELING ERRORS FOR THE OSGLR ALGORITHM	47
4.1 Dynamic Thresholds	48
4.2 Dynamic Decision Regions	52
4.3 Model Error Estimation	53
4.4 Robust Residual Generation	53
4.5 Summary and Conclusions	67
5 DETAILED EVALUATION OF THE OSGLR ALGORITHM USING A SINGLE CRUISE LINEAR MODEL	72
5.1 Introduction	72
5.2 Sensor Errors and Dynamics	73
5.3 Off-Nominal, No-Failure Flight Conditions	75
5.3.1 Maneuvering Test Case	75
5.3.2 Turning Test Case	78
5.3.3 Maximum Rate-of-Climb Test Case	81
5.3.4 Accelerating Test Cases	81
5.3.5 Decelerating and Descending Test Cases	84
5.3.6 Non-Zero Flap Deflections	84
5.3.7 Off-Nominal Turbulence and Steady Winds	89
5.4 Failures	92
5.4.1 Elevator Failure Test Case	92
5.4.2 Off-Nominal Elevator Failure Test Cases	95
5.4.3 Right Aileron Failure Test Case	99
5.4.4 Rudder Failure Test Case	99
5.4.5 Right Flap Failure Test Case	103
5.4.6 Largest Failure Decision Functions as a Function of Time and Failure Magnitude	106
5.5 Summary and Conclusion	113
6 SCHEDULING	120
6.1 Introduction	120
6.2 Scheduling of Zero Flap Deflection Linear Models	120
6.3 Nonzero Flap Deflections	127

TABLE OF CONTENTS (Cont.)

<u>Section</u>	<u>Page</u>
6.4 Failure Detection and Scheduling	129
6.5 Scheduling of Age-Weighted Filter and OSGLR Steady-State Matrices	135
6.6 Summary and Conclusions	139
7 SUMMARY AND CONCLUSIONS	141
REFERENCES	145
 <u>Appendix</u>	
A SUMMARY OF TEST CASES	148
B SCHEDULING IMPLEMENTATION DETAILS	156
B.1 Introduction	156
B.2 Linear Model Formulation	156
B.3 Steady-State OSGLR Equations	157
B.4 Scheduling	158

LIST OF ILLUSTRATIONS

<u>Figure</u>		<u>Page</u>
2.1	Detection filter block diagram	10
2.2	Block diagram of the modified detection filter	16
4.1	Sensitivity measure for the OSGLR algorithm	49
4.2	State estimation errors and standard deviations for a nonlinear, no-failure, nominal cruise flight condition test case	54
4.3	Decision functions for the nonlinear, no-failure, nominal cruise flight condition test case	56
4.4	OSGLR decision functions for a -0.01745 rad (-1°) elevator bias failure which occurred at 10 seconds at the nominal cruise flight condition of 77.2 m/s (150 knots) and 304.8 m (1000 ft)	58
4.5	OSGLR decision functions for a no-failure case at an off-nominal cruise flight condition of 102.9 m/s (200 knots) and 1524 m (5000 ft)	59
4.6	OSGLR decision functions for a -0.01745 rad (-1°) elevator bias failure at 10 seconds at the nominal cruise condition of 77.2 m/s and 304.8 m using a Kalman filter with process noise added	60
4.7	OSGLR decision functions for a no-failure case at an off-nominal cruise flight condition of 102.9 m/s and 1524.0 m using a Kalman filter with process noise added	61
4.8	Decision functions produced by an age-weighted OSGLR algorithm: no failures, off-nominal cruise flight condition of 102.9 m/s and 1524.0 m, age-weighting time constant of 15 s	65

LIST OF ILLUSTRATIONS (Cont.)

<u>Figure</u>		<u>Page</u>
4.9	Decision functions produced by an age-weighted OSGLR algorithm: -0.01745 rad (-1°) elevator bias failure at 10 s, nominal flight condition of 77.2 m/s and 304.8 m, age-weighting time constant of 15 s	66
4.10	Estimated rudder basis function coefficients for a 0.001745 rad/s (0.1° deg/s) rudder ramp failure starting at $t=0$ produced by an age-weighted OSGLR algorithm with age-weighted time constant of 3 seconds	68
4.11	Decision functions produced by an age-weighted OSGLR algorithm: no failures, off-nominal cruise flight condition of 102.9 m/s and 1524 m, age-weighting time constant of 3 s	69
4.12	Decision functions produced by an age-weighted OSGLR algorithm: -0.01745 rad (-1°) elevator bias failure at 10 s, nominal cruise flight condition of 77.2 m/s and 304.8 m, age-weighting time constant of 3 s	70
5.1	Decision functions for the maneuvering test case	77
5.2	Decision functions for the maneuvering test case with thrust as an input	79
5.3	Decision functions with the aircraft turning right for 3.32 rad (190 deg) and then left for 3.14 rad (180 deg)	80
5.4	Decision functions for the maximum rate-of-climb test case	82
5.5	Decision functions for the acceleration from 51.44 m/s (100 knots) to 102.9 m/s (200 knots) test case	83
5.6	Decision functions for the decelerating at constant altitude from 102.9 m/s to 51 m/s test case	85
5.7	Decision functions for the descending from 1524 m (5000 ft) test case	86

LIST OF ILLUSTRATIONS (Cont.)

<u>Figure</u>		<u>Page</u>
5.8	Decision functions for the 50% flap deflection test case	87
5.9	Decision functions for the 75% flap deflection test case	88
5.10	Decision functions for the maneuvering test case with light turbulence	90
5.11	Decision functions for the aircraft flying at the nominal cruise flight condition in thunderstorm turbulence	91
5.12	Decision Functions for a 10.3 m/s (20 knots) crosswind test case	93
5.13	Decision functions for a -0.0873 rad (-5 deg) elevator bias failure	94
5.14	Isolation decision functions for a -0.0873 rad (-5 deg) elevator bias failure	96
5.15	Decision functions for a -0.0873 rad (-5 deg) elevator bias failure with the aircraft flying at an off-nominal cruise airspeed of 64.3 m/s (125 knots) at the time of failure	97
5.16	Decision functions for a -0.0873 rad (-5 deg) elevator bias failure with the aircraft flying at an off-nominal cruise airspeed of 90 m/s (175 knots) at the time of failure	98
5.17	Decision functions for a 0.0873 rad (5 deg) right aileron bias failure	100
5.18	Isolation decision functions for a 0.0873 rad (5 deg) right aileron bias failure	101
5.19	Decision functions for a -0.0873 rad (-5 deg) rudder bias failure	102

LIST OF ILLUSTRATIONS (Cont.)

<u>Figure</u>		<u>Page</u>
5.20	Decision functions for a 5% right flap bias failure	104
5.21	Isolation decision functions for a 5% right flap bias failure	105
5.22	The largest decision function values produced by elevator bias failures	107
5.23	The largest decision function values produced by right aileron bias failures	108
5.24	The largest decision function values produced by right flap bias failures	109
5.25	The largest decision function values produced by rudder bias failures	110
5.26	The smallest of the isolation decision functions DF_{1i} ($i \neq 1$) produced by elevator bias failures	114
5.27	The smallest of the isolation decision functions DF_{2i} ($i \neq 2$) produced by right aileron bias failures	115
5.28	The smallest of the isolation decision functions DF_{5i} ($i \neq 5$) produced by right flap bias failures	116
6.1	Decision functions produced by an age-weighted, scheduled OSGLR algorithm for the acceleration from 51.44 m/s test case: 51.44, 77.2, 102.9 m/s linear models, 77.2 m/s age-weighted filter and OSGLR steady-state matrices	122
6.2	Decision functions produced by an age-weighted, scheduled OSGLR algorithm for an acceleration from 51.44 m/s test case: 46.3, 51.44, 77.2, 102.9 m/s linear models, 77.2 m/s age-weighted filter and OSGLR steady-state matrices	124

LIST OF ILLUSTRATIONS (Cont.)

<u>Figure</u>		<u>Page</u>
6.3	Decision functions for a 51.44 m/s, no-failure, cruise test case using the 51.44 m/s linear model and associated steady-state Kalman filter and OSGLR matrices	125
6.4	Decision functions for a 77.2 m/s cruise no-failure test case using the 77.2 m/s linear model and associated steady-state Kalman filter and OSGLR matrices	126
6.5	Decision functions produced by an age-weighted, scheduled OSGLR algorithm for a 50% flap deflection test case: 46.3, 51.44, 77.2, 102.9 m/s linear models, 77.2 m/s age-weighted filter and OSGLR steady-state matrices	128
6.6	Decision functions produced by an age-weighted, scheduled OSGLR algorithm for a 50% flap deflection test case: 38.6, 51.44, 77.2 m/s with 50% flap linear models, 77.2 m/s With 50% flap age-weighted filter and OSGLR steady-state matrices	130
6.7	Decision functions produced by an age-weighted, scheduled OSGLR algorithm for a 75% flap deflection test case: 38.6, 51.44, 77.2 m/s with 50% flap linear models, 77.2 m/s With 50% flap age-weighted filter and OSGLR steady-state matrices	131
6.8	Decision functions produced by an age-weighted, scheduled OSGLR algorithm for a 100% flap deflection test case: 100% flap deflection from the start of the test case, 38.6, 51.44, 77.2 m/s with 100% flap linear models, 77.2 m/s With 100% flap age-weighted filter and OSGLR steady-state matrices	132
6.9	Decision functions produced by an age-weighted, scheduled OSGLR algorithm for a -0.0873 rad (-5 deg) elevator bias failure at 90.0 m/s (175 knots) test case: 46.4, 51.44, 77.2, 102.9 m/s linear models, 77.2 m/s age-weighted filter and OSGLR steady-state matrices	133

LIST OF ILLUSTRATIONS (Cont.)

<u>Figure</u>	<u>Page</u>
6.10	Decision functions produced by an age-weighted, scheduled OSGLR algorithm for a -0.0873 rad (-5 deg) elevator bias failure at 64.3 m/s (125 knots) test case: 46.4 , 51.44 , 77.2 , 102.9 m/s linear models, 77.2 m/s age-weighted filter and OSGLR steady-state matrices 134
6.11	Decision functions produced by an age-weighted, scheduled OSGLR algorithm for a -0.0873 rad (-5 deg) elevator bias failure at 64.3 m/s (125 knots) test case: 46.3 , 51.44 , 77.2 , 102.9 m/s linear models, steady-state age-weighted filter and OSGLR matrices also scheduled 136
6.12	Decision functions for a -0.0873 rad (-5 deg) elevator bias failure at 175 knots test case produced by an age-weighted, linearly scheduled OSGLR algorithm: linear interpolation scheduling approach, 46.3 , 51.44 , 77.2 , 102.9 m/s linear models, steady-state age-weighted filter and OSGLR matrices also scheduled 138

LIST OF TABLES

<u>Table</u>	<u>Page</u>
2.1 Inputs, Outputs, and States of the C-130 Aircraft	7
2.2 Standard Deviation of Sensor Noise	8
2.3 Comparison of FDI Algorithms	35
5.1 C-130 control surface definition	73
5.2 Sensor errors	74
5.3 Maneuvering test case	76
5.4 Symbols for time after onset of bias failure	111
A.1 Summary of Test Cases	149

LIST OF ACRONYMS

CSDL	The Charles Stark Draper Laboratory
FDI	Failure Detection and Isolation
GLR	Generalized Likelihood Ratio
LLR	Log Likelihood Ratio
LR	Likelihood Ratio
NASA	National Aeronautics and Space Administration
OSGLR	Orthogonal Series Generalized Likelihood Ratio
STOL	Short Take Off or Landing

LIST OF SYMBOLS

a_i	unknown coefficients of series expansion of failure mode shape for OSGLR algorithm
\underline{a}	column vector which augments $A - \lambda I$ matrix; vector of a_i 's
A	linear system state matrix, dimension $n \times n$
A_a	state transition matrix of the unknown coefficient vector \underline{a} in the discrete time OSGLR algorithm
A_ϕ	state matrix that defines the OSGLR basis functions ϕ_i in discrete time
\underline{b}_i	i th column of B matrix
$\underline{b}(k)$	known vector denoting type of failure and its effect on the system
B	linear system state input matrix of dimension $n \times m$
\underline{c}	P_r^\dagger ; projection of residuals onto the normalized $C(\underline{b}_i - K\underline{d}_i)$ vectors and \tilde{d}_{1N} and \tilde{d}_{2N} ; also column vector which augments C
\underline{c}_f	components of \underline{c} which correspond to \underline{d}_i and have been filtered with the same eigenvalue as the detection filter
c_i	i th component of the C vector
C	linear system output matrix, dimension $r \times n$
\underline{d}_i	i th column of the D matrix
$\underline{d}(k)$	known vector denoting type of failure and its effect on the measurement
$\tilde{d}_{1N}, \tilde{d}_{2N}$	linearly independent normalized columns of D
D	linear system control input matrix for the output equation, dimension $r \times m$

LIST OF SYMBOLS (Cont.)

DF_i	detection decision function for control surface i , $i = 1, 2, \dots, 6$
DF_{ij}	isolation decision function between control surfaces i and j , $i, j = 1, 2, \dots, 6$
$DF(k)$	OSGLR decision function at time k ; GLR decision function at k
$\underline{e}(k)$	estimation error
$E(\)$	mean or expected value
\underline{f}	vector of nonlinear functions of the states and controls
$f(k)$	mode shape of failure
$\underline{f}(k, \theta)$	influence of failure mode on the state estimation error at increment k , failure occurring at time θ
$F(k)$	influence of vector of coefficients \underline{a} on the estimation error
\underline{g}	vector of nonlinear functions of the states and controls
$\underline{g}(k)$	known bias vector of dimension n
$\underline{g}(k, \theta)$	signature of failure at increment k , failure occurring at time θ
$G(k)$	influence of vector of coefficients \underline{a} on the residuals
$\underline{h}(k)$	known bias vector of dimensional r
H_0	no failure hypothesis
H_1	failure hypothesis
I	identity matrix
k	k th discrete time step
\underline{k}_i	i th column of the K matrix
K	detection filter, Kalman filter, or age-weighted filter gain matrix
$\ell(k_f, \theta, \nu)$	log likelihood ratio at final iteration k_f for failure of magnitude ν occurring at time θ
$\ell(k_f)$	log likelihood ratio at time k_f

LIST OF SYMBOLS (Cont.)

$M(k)$	covariance of Kalman or age-weighted filter residual at time step k
$n(t)$	unexpected control input
$n(k, \theta)$	failure mode shape
$N(a, b)$	normal distribution with mean a and variance b
p	number of basis functions of OSGLR algorithm
$p(x/y)$	conditional probability of x given that y has occurred
\underline{P}	the columns of \underline{P} are the normalized $C(\underline{b}_i - K\underline{d}_i)$, $\tilde{\underline{d}}_{1N}$ and $\tilde{\underline{d}}_{1N}$ vectors
$P(k)$	covariance of Kalman or age-weighted filter estimation error
\underline{q}	$\underline{x} - \underline{x}'$, difference between the system state vector and the detection filter state vector
\underline{q}'	state vector of the secondary filter used in the modified detection filter
$Q(k)$	state driving noise covariance
r	number of measurements
\underline{r}	$\underline{y} - \underline{y}'$, residual vector
r_f	components of \underline{r} which correspond to \underline{d}_i and have been filtered with the same eigenvalue as the detection filter
R	matrix operator which, when applied to \underline{c} , nulls out the components corresponding to the projections of the residual onto the $\tilde{\underline{d}}_{1N}$ and $\tilde{\underline{d}}_{2N}$ vectors
$R(k)$	measurement noise covariance
s	Laplace transform variable
S	variance or matrix operator which, when applied to \underline{c} , forms a two-dimensional vector containing the components corresponding to the projections of the residual onto the $\tilde{\underline{d}}_{1N}$ and $\tilde{\underline{d}}_{2N}$ vectors.

LIST OF SYMBOLS (Cont.)

$S(k_f, \theta)$	discrete-time information matrix at increment k_f , failure occurring at time θ
t	time
T, T^2	threshold
\underline{u}	nonlinear or linear system control input vector, dimension m
\underline{u}'	detection filter control input vector
\underline{u}_c	control system commands to the actuators
$\underline{u}_{\text{nominal}}$	nominal control surface deflections
$\underline{v}(k)$	zero mean Gaussian white noise vector with covariance matrix $R(k)$
$\underline{w}(k)$	zero mean Gaussian white noise vector with covariance matrix $Q(k)$
\underline{x}	nonlinear or linear system state vector, dimension n
\underline{x}'	detection filter state vector, dimension n
\underline{y}	nonlinear or linear system output vector, dimension r
\underline{y}'	detection filter output vector, dimension r
$\underline{y}_{\text{nominal}}$	nominal output vector, dimension r
\underline{z}	z -transform variable or exponential decay term
$\underline{\gamma}(k)$	Kalman or age-weighted residual at time step k
$\underline{\Delta u}$	linear input vector, dimension m
$\underline{\Delta u}'$	linear input vector to the detection filter, dimension m
$\underline{\Delta x}$	linear state vector, dimension n
$\underline{\Delta x}'$	linear detection filter state vector, dimension n
$\underline{\Delta y}$	linear output vector, dimension r
$\underline{\Delta y}'$	linear detection filter output vector, dimension r
θ	time of failure
λ	detection filter eigenvalue

LIST OF SYMBOLS (Cont.)

$\Lambda(k_f, \theta, v)$	likelihood ratio at final iteration k_f for failure of magnitude v occurring at time θ
v	magnitude of failure
$\phi_i(k)$	i th basis function of OSGLR algorithm at increment k
$\underline{\phi}(k)$	vector of basis functions
$\Phi(k)$	linear system discrete time state transition matrix, dimension $n \times n$
$\underline{\chi}(k)$	information vector at time k

Superscript

-1	inverse
\dagger	pseudo inverse
$-$	quantity prior to filter update
$+$	quantity after filter update

Subscript

a	refers to OSGLR basis function coefficients
d	discrete
f	final
N	vector has been normalized
0	initial or nominal
ϕ	refers to OSGLR basis functions

SECTION 1

INTRODUCTION

Recently, there has been much interest in the problem of restructuring the control law of aircraft following the failure of control surfaces or actuators (References 1,2,3). This interest is motivated in part by two incidents involving commercial aircraft. In the case of Delta flight 1080 on April 12, 1977, the left elevator became stuck in the 19° up position at takeoff (Reference 4). The pilot was able to compensate for the failure, in part by manipulating thrust to control the pitch axis. However, the pilot of the DC10 that crashed in Chicago (Reference 5) was unable to recover from the left engine breaking loose and the resulting retraction of the left wing's outboard leading edge slats. Simulations indicate that the aircraft could have been flown if impending stall conditions had been recognized and the proper corrective action taken. Restructuring the control system on-line to counteract the effect of these failures may be one solution to such problem situations. Although the need for restructurable control has been demonstrated for state-of-the-art aircraft systems, it can be expected to be most applicable to future aircraft where redundant control surfaces will very likely be extensively employed.

A feasible and practical restructurable control system requires the correct and timely detection and isolation of the control surface failure so that the proper corrective action can be taken. The Charles Stark Draper Laboratory, Inc. (CSDL) has investigated and evaluated practical FDI techniques for the NASA Langley Research Center under contract NAS1-17556 entitled, "Evaluation of Failure Detection and Identification

Techniques for Application in Aircraft Restructurable Control Systems." Reference 6 and this report document the results of this contractual effort.

The initial phase of the CSDL study, Reference 6, compared three failure detection and isolation techniques for detecting and isolating control surface or actuator failures: the detection filter, the generalized likelihood ratio (GLR) test, and the orthogonal series generalized likelihood ratio (OSGLR) test. A modification to the basic detection filter was also considered. The algorithms were evaluated by testing their ability to detect and isolate control surface failures in a non-linear simulation of a C-130 aircraft. The testing was in general limited to a single cruise operating condition. All the algorithms were capable of detecting failures. However isolating aileron and flap failures was difficult since these surfaces produce similar effects on the aircraft. Since the algorithms had difficulty isolating wing surface failures, the system monitoring strategy for implementing the FDI algorithms would augment the FDI algorithm with position measurements of these surfaces.

The detection filter (References 7,8,9) has the form of an observer with the feedback gain matrix chosen so that each type of failure produces a uniquely defined residual. With direct input-output coupling resulting from the use of acceleration measurements, the residuals produced by control surface failures may only be constrained to a known plane. The modification to the basic detection filter uses secondary filtering of the residuals to produce unidirectional control surface failure signatures with acceleration measurements.

The GLR and OSGLR algorithms (References 10 and 11 respectively) are sequential hypothesis tests. The failure hypothesis for the GLR algorithm assumes an additive failure of a known behavior or, equivalently, failure mode with unknown onset time and unknown magnitude. The failure mode assumed for this study was a step. Based on the residuals from the Kalman filter designed for the no-failure system, the maximum likelihood

estimate of the failure magnitude is determined for each possible failure onset time. Using this estimate of the failure magnitude, the likelihood ratio is maximized over the possible onset times to produce the generalized likelihood ratio test statistic.

Instead of assuming a fixed failure mode, the OSGLR algorithm expresses the failure mode as a truncated series of orthonormal basis functions. Based on the residuals of a no-failure Kalman filter, the coefficients of the series expansion are estimated using maximum likelihood estimation and a generalized likelihood ratio is formed using these estimates. The rationale for adopting this approach is that most failures should be represented fairly well using a truncated orthogonal series expansion and this algorithm should be more robust to failure mode uncertainty than the conventional GLR test. Unlike the GLR algorithm, the onset time of the failure does not need to be estimated and therefore the algorithm is computationally more efficient.

The OSGLR algorithm provided the best detection and isolation performance. The disadvantage of the OSGLR algorithm is its robustness to modeling errors was worse than the other algorithms. The GLR algorithm performed almost as well as the OSGLR algorithm. However, the computational burden of the GLR algorithm is very heavy and it is not robust to failure mode uncertainty. The OSGLR and GLR algorithms were less sensitive to severe turbulence than the basic and modified detection filter algorithms because the turbulence model was incorporated into the no-failure Kalman filter. The sensitivity of the detection filter algorithms to turbulence degraded their detection performance relative to the OSGLR and GLR algorithms. The advantage of the detection filter algorithms is their relatively low computational processing. Based on this comparison, the OSGLR algorithm was selected for further study as the most promising of the algorithms.

This report focuses on an in-depth evaluation of the OSGLR algorithm. This evaluation considers a variety of steady winds and wind turbulence levels and a number of flight conditions or flight regimes repre-

sentative of the range of environments in which a transport aircraft must operate. Detection and false alarm performance issues are also addressed. Sensor dynamics and errors are included in the simulation.

In addition, to ensure all promising practical FDI techniques have been evaluated, the literature is searched for FDI techniques that might be applicable to control surface and actuator failure detection and isolation in addition to those already studied. Any promising techniques are to be included in the detailed evaluation described above.

This report is organized as follows. Section 2 reviews the initial phase of this study and summarizes the results. Section 3 surveys the literature for other applicable FDI algorithms. Since the major drawback to the OSGLR algorithm is robustness to modeling errors, Section 4 examines possible methods of reducing the effects of modeling errors on the algorithm. The testing at a number of off-nominal flight and wind conditions of the algorithm designed using a single cruise linear model is described in Section 5. Also a number of failure cases are described in order to determine the detection performance of the algorithm. Section 6 examines scheduling as a means of extending the algorithm to a larger flight envelope. The report is summarized and the major conclusions presented in Section 7. Appendix A contains a table summarizing the test cases presented in this report for easy reference and comparison. Appendix B contains additional implementation details of the scheduling approach.

SECTION 2

BACKGROUND

2.1 Introduction

The previous work done on this contract (Reference 6) analyzed and compared the feasibility of using three FDI algorithms to detect and isolate aircraft control surface and actuator failures. The three algorithms were the detection filter, the generalized likelihood ratio (GLR) test, and the orthogonal series generalized likelihood ratio (OSGLR) test. A modification to the detection filter was also developed and tested. In addition, a system monitoring strategy was developed. The present effort further investigates the most promising of the FDI algorithms evaluated - the OSGLR algorithm. In order to provide the necessary background for this effort and to motivate our selection of the OSGLR algorithm as the most promising, this section reviews the preliminary evaluation of the FDI algorithms and system monitoring strategy described in Reference 6. The nonlinear C-130 aircraft simulation used in the evaluation is described in the next section. A description of the algorithms evaluated, a comparison of the algorithms, and the selection of the system monitoring strategy follows.

2.2 C-130 Simulation Description

The FDI algorithms were evaluated by testing their ability to detect and isolate control surface failures that have occurred in a simulation of a Lockheed C-130 aircraft. The C-130 aircraft is a military, medium- to long-range transport propelled by four turboprop engines

located on a high wing. The particular version of the C-130 aircraft used for this program has short takeoff and landing (STOL) capability provided by trailing edge double-slotted flaps.

The simulation of the C-130 aircraft uses the standard six degree-of-freedom aircraft nonlinear equations of motion. The aerodynamic forces and moments are described by one-, two-, or three-dimensional look-up tables. These look-up tables are functions of angle of attack, sideslip angle, thrust, and the control surface deflections. Each of the four engines are assumed to provide the same thrust. Actuator dynamics have been included; however, sensor dynamics were not included.

The surfaces available for control of the aircraft are the ailerons, flaps, rudder and elevator. The simulation allows for independent motion of the left and right ailerons and the left and right flaps. Since aileron and flap failures are similar in their effect on the dynamics of the vehicle, detecting and isolating aileron and flap failures provided an adequate test for the algorithms that were evaluated.

The eleven measurements available for detecting and isolating failures are those typically available onboard aircraft. These measurements are listed in Table 2.1, along with the six control inputs described above and the ten states that describe the aircraft dynamics. The measurements are generated in the simulation by superimposing zero-mean Gaussian distributed noise on the output variables. The noise statistics used for this study are shown in Table 2.2.

Wind turbulence is also incorporated in the simulation. The turbulence velocity along each body axis is modeled by passing white noise through shaping filters to produce signals with desired one-dimensional power spectral densities. The Dryden form of the spectra, defined in Reference 12, is modeled. The turbulence intensities used in the preliminary evaluation are presented later in this section. The turbulence scale lengths were the clear air values defined in Section 3.7.3.2 of Reference 12.

Table 2.1. Inputs, Outputs, and States of the C-130 Aircraft

Inputs

Elevator
Right aileron
Left aileron
Right flap
Left flap
Rudder

Outputs

Airspeed
Acceleration at the cg along the y body axis
Acceleration at the cg along the z body axis
Angular velocity about the x body axis
Angular velocity about the y body axis
Angular velocity about the z body axis
Roll
Pitch
Yaw
Altitude rate
Altitude

States

Airspeed
Sideslip angle
Angle of attack
Angular velocity about the x body axis
Angular velocity about the y body axis
Angular velocity about the z body axis
Roll
Pitch
Yaw
Altitude

Table 2.2. Standard Deviation of Sensor Noise

SENSOR	STANDARD DEVIATION	
Airspeed	3.35 m/s	11 ft/s
Accelerometers	.3 m/s ²	.98 ft/s ²
Roll Rate Gyro	.0024 rad/s	.1375 deg/s
Pitch and Yaw Rate Gyros	.0007 rad/s	.04 deg/s
Attitude Gyros	.01 radians	.573 degrees
Altitude Rate	.08 m/s	.25 ft/s
Altitude	3.05 m	10 ft

2.3 Description of FDI Algorithms Evaluated

The three FDI algorithms considered, the detection filter, the generalized likelihood ratio test, and the orthogonal series generalized likelihood ratio test, are described in this section. A modification to the detection filter was also developed and tested. The modification will be referred to as the modified detection filter and will be discussed as a separate algorithm.

2.3.1 The Detection Filter¹

The detection filter (References 7,8,9) is a linear, time-invariant observer of the system (see Figure 2.1). Therefore, the nonlinear system excluding the actuator dynamics must be linearized about a nominal operating condition for use in the observer. The model can be expressed as

$$\dot{\underline{x}}(t) = A\underline{x}(t) + B\underline{u}(t) \quad (2.1)$$

$$\underline{y}(t) = C\underline{x}(t) + D\underline{u}(t) \quad (2.2)$$

where $\underline{x}(t)$, $\underline{u}(t)$, and $\underline{y}(t)$ are the deviations in the states, controls, and outputs respectively from their nominal values. The superscript tilde in Figure 2.1 denotes the actual nonlinear quantities. Detection filter theory cannot account for the effects of disturbances, measurement noise, or mismodeling. Their effects on the performance of the detection filter will be determined via simulation.

The detection filter state and residual satisfy

$$\dot{\underline{x}}'(t) = A\underline{x}'(t) + B\underline{u}'(t) + K\underline{r}(t) \quad (2.3)$$

$$\underline{r}(t) = \underline{y}(t) - \underline{y}'(t) \quad (2.4)$$

¹ This description was taken from Reference 13.

where

$$\underline{y}'(t) = C\underline{x}'(t) + D\underline{u}'(t) \quad (2.5)$$

Here, the prime denotes the detection filter state, output, and expected (no-failure) control input. In the absence of failures, the detection filter state estimation error satisfies the differential equation

$$\dot{\underline{q}}(t) = (A - KC)\underline{q}(t) \quad (2.6)$$

and the residual in terms of the state estimation error is given by

$$\underline{r}(t) = C\underline{q}(t) \quad (2.7)$$

In the presence of a failure of the i th actuator or control surface, the filter error and residual dynamics are given by

$$\dot{\underline{q}}(t) = (A - KC)\underline{q}(t) + (\underline{b}_i - K\underline{d}_i)n(t) \quad (2.8)$$

$$\underline{r}(t) = C\underline{q}(t) + \underline{d}_i n(t) \quad (2.9)$$

where \underline{b}_i and \underline{d}_i are the i th columns of the B and D matrices, and $n(t)$ is a function of time which represents the failure mode (i.e., the behavior of the failed surface relative to the expected behavior). Detection filter theory allows $n(t)$ to be any arbitrary function of time.

Since the gain matrix K must be chosen such that the filter is stable, the detection filter will track the system when there are no failures. However, when a failure occurs, the actuator models or the linear model incorporated into the filter no longer accurately model the system, and a nonzero residual results. The objective of detection filter design is to constrain the residual produced by a particular failure to a single direction or plane. A failure is detected, then, when one or

more of the residual projections along a known failure direction or in a known failure plane are sufficiently large. Isolating a failure may be possible if one of the residual projections is significantly greater than the rest.

Prior to this work, the development of the detection filter assumed no direct coupling between the inputs and the outputs (i.e., no D matrix). Without input-output coupling, present design procedures may be able to determine K such that the residual is unidirectional in response to a control surface or actuator failure. If such a gain matrix exists, the residual will be constrained to the direction $CA^k \underline{b}_i$ where k is the smallest positive integer for which $CA^k \underline{b}_i$ is nonzero. Since $n(t)$ does not affect the failure direction, the failure direction is independent of the failure mode. This is an important advantage of the detection filter.

Using acceleration measurements to detect actuator and control surface failures, however, results in direct input-to-output coupling. In this case, the residual produced by such failures may be constrained to a plane spanned by the vectors \underline{d}_i and $C(\underline{b}_i - K\underline{d}_i)$ if the part of the residual produced by the $(\underline{b}_i - K\underline{d}_i)n(t)$ term can be restricted to a single direction. The difficulty in determining a gain matrix K to do this is that present design procedures assume the direction of the additive term to the filter state error equation is known. However, the direction of the $(\underline{b}_i - K\underline{d}_i)n(t)$ term is not known until the gain matrix is determined. Fortunately, knowledge of this direction is not necessary when the system is fully measured (i.e., the rank of C is equal to the number of states). The system used in the preliminary evaluation was fully measured.

2.3.2 The Modified Detection Filter²

Secondary filtering of the detection filter residual was found to restore the unidirectional failure signature property even when there is direct coupling between the inputs and the measurements. Assuming that

² This description was taken from Reference 13.

the detection filter gain matrix, K , is calculated to satisfy the relationship $K = A - \lambda I$, the transfer function between the residual and the unexpected input from the i th actuator is

$$r(s) = \left[\frac{C(\underline{b}_{-i} - K\underline{d}_{-i})}{s - \lambda} + \underline{d}_{-i} \right] n(s) \quad (2.10)$$

If the contribution $\underline{d}_{-i}n(s)$ could be filtered with the same time constant as in the detection filter, the failure signature would be unidirectional, lying along $C(\underline{b}_{-i} - K\underline{d}_{-i}) + \underline{d}_{-i}$.

The secondary filtering scheme, then, has several elements. First, the components of the residual along the event vectors \underline{d}_{-i} are separated from the residual. Next they are filtered using the detection filter time constant. Finally, these filtered components are then added to the other components, forming a new residual which is used for failure detection and isolation.

In order for the initial separation of the components along \underline{d}_{-i} to be possible, all event vectors \underline{d}_{-i} must be mutually independent, and each must be independent of the hyperplane formed by the $C(\underline{b}_{-i} - K\underline{d}_{-i})$ vectors. To obtain the components of the residual in the directions \underline{d}_{-i} , first write the residual

$$\underline{r}(t) = \left[C(\underline{b}_{-1} - K\underline{d}_{-1})_N \mid \cdots \mid C(\underline{b}_{-6} - K\underline{d}_{-6})_N \mid \tilde{\underline{d}}_{-1N} \mid \tilde{\underline{d}}_{-2N} \mid \right] \begin{bmatrix} c_1(t) \\ c_2(t) \\ \cdot \\ \cdot \\ c_8(t) \end{bmatrix} \quad (2.11)$$

$$= \underline{Pc}(t) \quad (2.12)$$

Here, $C(\underline{b}_{-i} - K\underline{d}_{-i})$ has been normalized for each of the six actuators considered in the preliminary evaluation, giving $C(\underline{b}_{-i} - K\underline{d}_{-i})_N$, and $\tilde{\underline{d}}_{-1N}$

and $\tilde{\underline{d}}_{-2N}$ are the two distinct directions among the columns of the D matrix resulting from the two acceleration measurements. The vector $\underline{c}(t)$ is obtained using

$$\underline{c}(t) = P^\dagger \underline{r}(t) \quad (2.13)$$

where P^\dagger is the Moore-Penrose pseudo inverse of P.

The magnitudes c_7 and c_8 are passed through a secondary two-state filter:

$$\dot{\underline{q}}'(t) = \lambda I \underline{q}'(t) + \begin{bmatrix} c_7(t) \\ c_8(t) \end{bmatrix} \quad (2.14)$$

Substituting these filtered components for the unfiltered ones in $\underline{c}(t)$ leads to

$$\underline{c}_f(t) = \begin{bmatrix} c_1(t) \\ \vdots \\ c_6(t) \\ q_1'(t) \\ q_2'(t) \end{bmatrix} \quad (2.15)$$

Transforming this vector of components back into the original residual space results in

$$\underline{r}_f(t) = P \underline{c}_f(t) \quad (2.16)$$

Actuator failures may be detected and (simultaneously) isolated through projection of $\underline{r}_f(t)$ onto each of the six signature vectors

$$C(\underline{b}_i - K\underline{d}_i) + \underline{d}_i.$$

In using the transformation P , $\underline{r}(t)$ has been assumed to lie, in this case, in the eight-dimensional space spanned by columns of P . Applying transformations P^\dagger and P leads to suppression of noise in the residual that is in directions orthogonal to the range of P . Because noise in these directions only interferes with failure detection and isolation, this suppression could be very beneficial. However, the transformation is model-dependent and therefore will be sensitive to modeling errors.

The modified detection filter is shown in Figure 2.2

2.3.3 The Generalized Likelihood Ratio (GLR) Test for Dynamic Systems³

The GLR test (Reference 10) assumes a linear, time-varying system. The discrete-time case will be considered here. In the normal or unfailed mode of operation, the state equation and measurement equation are given by

$$H_0: \underline{x}(k+1) = \Phi(k)\underline{x}(k) + B(k)\underline{u}(k) + \underline{w}(k) \quad (2.17)$$

$$\underline{y}(k) = C(k)\underline{x}(k) + D(k)\underline{u}(k) + \underline{v}(k) \quad (2.18)$$

where $\underline{x}(k)$ is an n -dimensional state vector, $\underline{y}(k)$ is an m -dimensional measurement vector, $\Phi(k)$ is the state dynamics matrix, and $C(k)$ is the measurement matrix. $B(k)$ and $D(k)$ are the input matrices for state and output equations with $\underline{u}(k)$ being the control input. $\underline{w}(k)$ and $\underline{v}(k)$ are zero-mean, independent, Gaussian white processes with intensities $Q(k)$ and $R(k)$, respectively. For the analysis that follows, the effects of the control input may be omitted, due to the linearity of the equations.

³ This description of the GLR test was partially taken from Reference 6.

The GLR failure hypothesis is that

$$H_1: \underline{x}(k+1) = \Phi(k)\underline{x}(k) + \underline{w}(k) + \underline{b}(k)n(k, \theta)v \quad (2.19)$$

$$\underline{y}(k) = C(k)\underline{x}(k) + \underline{v}(k) + \underline{d}(k)n(k, \theta)v \quad (2.20)$$

where $\underline{b}(k)$ and $\underline{d}(k)$ are known vectors that depend on the type of the failure. For example, if an actuator failure is modeled, $\underline{b}(k)$ will be the column of the matrix $B(k)$ corresponding to that actuator, and $\underline{d}(k)$ will be the corresponding column of $D(k)$. $n(k, \theta)$ is the mode shape, or simply mode, of the failure, which occurs at time θ . Generally, we have that

$$n(k, \theta) = 0, \quad k < \theta \quad (2.21)$$

For example, if a bias failure is assumed, then

$$n(k, \theta) = \begin{cases} 0 & k < \theta \\ 1 & k \geq \theta \end{cases} \quad (2.22)$$

Finally, v is the magnitude of the failure.

One of the difficulties with the GLR test is that the failure mode is assumed to be known in advance. While specifying the mode of the failure will most likely improve the detection performance of a failure for that specific mode shape, the detection performance of other failure modes probably will be degraded. Adequately enumerating all the possible failure modes is a practical consideration which must be dealt with.

Suppose the data $\underline{y}(k)$ are observed over the observation interval

$$k_0 \leq k \leq k_f \quad (2.23)$$

For a given time of failure, θ , and magnitude of failure, v , the Likelihood Ratio (LR) is given by

$$\Lambda(k_f, \theta, v) = \frac{p(\underline{y}(k_0), \underline{y}(k_0+1), \dots, \underline{y}(k_f) | H_1, \theta, v)}{p(\underline{y}(k_0), \underline{y}(k_0+1), \dots, \underline{y}(k_f) | H_0)} \quad (2.24)$$

Because the $\underline{y}(k)$ are not independent from time step to time step, the evaluation of the conditional probabilities is difficult. To evaluate the LR, a Kalman filter is implemented, based on the normal mode (H_0) system. The filter equations are

$$\hat{\underline{x}}^-(k+1) = \Phi(k)\hat{\underline{x}}^+(k) \quad (2.25)$$

$$\hat{\underline{x}}^+(k) = \hat{\underline{x}}^-(k) + K(k)\underline{\gamma}(k) \quad (2.26)$$

where $K(k)$ is the Kalman gain matrix, and $\underline{\gamma}(k)$ is the residual, given by

$$\underline{\gamma}(k) = \underline{y}(k) - C(k)\hat{\underline{x}}^-(k) \quad (2.27)$$

The Kalman gain matrix is given by

$$K(k) = P^-(k)C^T(k)M^{-1}(k) \quad (2.28)$$

where $P^-(k)$ is the covariance of the estimation error

$$\underline{e}^-(k) = \underline{x}(k) - \hat{\underline{x}}^-(k) \quad (2.29)$$

and $M(k)$ is the covariance of $\underline{\gamma}(k)$, given by

$$M(k) = C(k)P^-(k)C^T(k) + R(k) \quad (2.30)$$

The covariance is propagated by

$$P^-(k+1) = \Phi(k)P^+(k)\Phi^T(k) + Q(k) \quad (2.31)$$

$$P^+(k) = [I - K(k)C(k)]P^-(k) \quad (2.32)$$

The LR may then be written in terms of the residual sequence $\underline{\gamma}(k)$ rather than the measurement sequence. Because the residual sequence is (conditionally) a white Gaussian sequence, the LR is easier to determine in terms of $\underline{\gamma}(k)$ than in terms of $\underline{y}(k)$.

Due to the linearity of the state equation and the filter equations, the residual may be expressed under each hypothesis as

$$H_0: \underline{\gamma}(k) = \underline{\gamma}_0(k) \quad (2.33)$$

$$H_1: \underline{\gamma}(k) = \underline{\gamma}_0(k) + \underline{g}(k, \theta)v \quad (2.34)$$

where $\underline{\gamma}_0(k)$ is a zero-mean, white Gaussian sequence with covariance $M(k)$. $\underline{g}(k, \theta)$ is the failure signature of a failure occurring at time θ . $\underline{g}(k, \theta)$ is given by

$$\underline{g}(k, \theta) = C(k)\underline{f}(k, \theta) + \underline{d}(k)n(k, \theta) \quad (2.35)$$

where $\underline{f}(k, \theta)$ is the influence of the failure mode $n(k, \theta)$ on the state estimation error. $\underline{f}(k, \theta)$ may be generated recursively by

$$\underline{f}(k+1, \theta) = \Phi(k)[I - K(k)C(k)]\underline{f}(k, \theta) + [\underline{b}(k) - \Phi(k)K(k)\underline{d}(k)]n(k, \theta) \quad (2.36)$$

with the initial condition

$$\underline{f}(k_0, \theta) = \underline{0} \quad (2.37)$$

It can be seen therefore that

$$\underline{f}(k, \theta) = \underline{0}, \quad k \leq \theta \quad (2.38)$$

Because the residual sequence is (conditionally) Gaussian and white, the Log Likelihood Ratio (LLR) ratio has a particularly simple form:

$$l(k_f, \theta, v) = v \chi(k_f, \theta) - \frac{1}{2} v^2 S(k_f, \theta) \quad (2.39)$$

where

$$\chi(k_f, \theta) = \sum_{k=\theta}^{k_f} \underline{g}^T(k, \theta) M^{-1}(k) \underline{y}(k) \quad (2.40)$$

$$S(k_f, \theta) = \sum_{k=\theta}^{k_f} \underline{g}^T(k, \theta) M^{-1}(k) \underline{g}(k) \quad (2.41)$$

Now, the generalized likelihood ratio is given by

$$l(k_f) = \max_{\hat{\theta}, \hat{v}} l(k_f, \hat{\theta}, \hat{v}) \quad (2.42)$$

Performing the maximization over \hat{v} first, we have that

$$\hat{v}(k_f, \theta) = \frac{\chi(k_f, \theta)}{S(k_f, \theta)} \quad (2.43)$$

Hence, the GLR test statistic is given by

$$l(k_f) = \max_{\hat{\theta}} \frac{1}{2} \frac{\chi^2(k_f, \hat{\theta})}{S(k_f, \hat{\theta})} \quad (2.44)$$

As a matter of convenience, the GLR decision function is defined by

$$DF(k_f) = 2 \ell(k_f) = \max_{\hat{\theta}} \frac{\chi^2(k_f, \hat{\theta})}{S(k_f, \hat{\theta})} \quad (2.45)$$

A failure is detected when the decision function exceeds the detection threshold.

A closed-form solution to the above maximization does not exist in general. Therefore, in order to implement the GLR, the statistic $\ell(k_f, \theta)$ must be computed for all possible times of failure, θ . As a result, a bank of matched filters that grows linearly with time is required. To avoid this unlimited growth in the amount of computation, the assumed time of failure may be restricted, say, to be in the range $k_f - N < \theta \leq k_f$. Even so, the amount of computation required to implement the GLR can be quite large, especially if N is large. This problem arises because the unknown parameter θ enters the equations in a nonlinear fashion. Hence, a nonlinear estimation structure is required to estimate θ . This problem is typical of FDI tests in which the onset time of the failure appears as an unknown parameter of the failure hypothesis.

2.3.4 Orthogonal Series Generalized Likelihood Ratio (OSGLR) Test⁴

The OSGLR test (Reference 11) is similar in many ways, to the GLR test discussed previously. The discrete-time version will be presented here. A linear, time-varying system is assumed. The unfailed system is the same as the unfailed system assumed for the GLR test (Eqs. 2.17 and 2.18). However, the OSGLR failure hypothesis is assumed to have the form

$$H_1: \underline{x}(k+1) = \Phi(k)\underline{x}(k) + \underline{w}(k) + \underline{b}(k)f(k) \quad (2.46)$$

$$\underline{y}(k) = C(k)\underline{x}(k) + \underline{v}(k) + \underline{d}(k)f(k) \quad (2.47)$$

⁴ This description of the OSGLR test was partially taken from Reference 14.

where $\underline{b}(k)$ and $\underline{d}(k)$ are known vectors that depend on the type of the failure, and $f(k)$ is the mode shape, or simply mode, of the failure. Because the failure mode is generally not known a priori, it would be desirable to allow the failure mode $f(k)$ to be completely arbitrary. The approach that will be taken here is to represent the mode shape $f(k)$ by a truncated series expansion. The motivation is that if the basis functions of the expansion are chosen properly, it should be possible to approximate any well-behaved failure mode. In this sense, the OSGLR test is similar to the detection filter which assumes the failure mode to be unknown.

The data is assumed to be observed over the interval $[k_o, k_f]$. A constraint is imposed on the form of the series expansion, namely, that it has the form

$$f(k) = \sum_{i=1}^p a_i(k_f) \phi_i(k_f - k) \quad (2.48)$$

where p is the number of basis functions used in the series expansion. That is, the series expansion is expressed in terms of basis functions which are defined relative to the end of the observation interval, k_f . Eq. 2.48 may be expressed more conveniently in vector form as

$$f(k) = \underline{\phi}^T(k_f - k) \underline{a}(k_f) \quad (2.49)$$

Eqs. 2.46, 2.47, and 2.49 specify the failure hypothesis H_1 .

Note that the left side of Eq. 2.49 is a function only of k , whereas the right side is a function of both k and k_f . This apparent contradiction is resolved by choosing the basis functions and coefficients such that the right side of Eq. 2.49 is invariant with respect to k_f . This requires that $\underline{a}(k_f)$ satisfy the difference equation

$$\underline{a}(k_f + 1) = \underline{A} \underline{a}(k_f) \quad (2.50)$$

where A_a is a constant matrix. Furthermore, the vector of basis functions $\underline{\phi}(i)$ must satisfy the difference equation

$$\underline{\phi}(i+1) = A_a \underline{\phi}(i) \quad (2.51)$$

where A_ϕ is a constant matrix and i is a dummy time index defined by

$$i = k_f - k \quad (2.52)$$

That is, i defines a time scale that runs backwards from the end of the observation interval, k_f . The matrices A_a and A_ϕ are related by

$$A_a = A_\phi^{-T} \quad (2.53)$$

The measurement process $y(k)$ over the interval $[k_0, k_f]$ is used to form the likelihood ratio for the hypotheses H_0 and H_1 . Because the measurement process is correlated in time, it is difficult to determine the likelihood ratio in terms of $y(k)$. Instead, the data are filtered using a Kalman filter based on H_0 to produce the residual process, $\underline{\gamma}(k)$. Because the residual process is white (when no failure has occurred), it is more easily used to obtain the likelihood ratio. The Kalman filter discrete-time equations are given in the GLR test description (Eqs. 2.25 - 2.32).

Due to the linearity of the state and measurement equations and of the Kalman filter, the OSGLR hypotheses may be written as

$$H_0: \underline{\gamma}(k) = \underline{\gamma}_0(k) \quad (2.54)$$

$$H_1: \underline{\gamma}(k) = \underline{\gamma}_0(k) + G(k)\underline{a}(k) \quad (2.55)$$

where $\underline{y}_0(k)$ is a zero-mean, Gaussian white processes with intensity $M(k)$. $G(k)$ represents the influence of the coefficient vector $\underline{a}(k)$ on the residual. The residual influence matrix $G(k)$ is given by

$$G(k) = C(k)F(k) + \underline{d}(k)\underline{\phi}^T(0) \quad (2.56)$$

where $F(k)$ is the matrix that represents the influence of $\underline{a}(k)$ on the estimation error. $F(k)$ satisfies the difference equation

$$F(k) = \{A(k)[I - K(k)C(k)]F(k) + [\underline{b}(k) - A(k)K(k)\underline{d}(k)]\underline{\phi}^T(0)\}A_{\phi}^T \quad (2.57)$$

with initial condition

$$F(k_0) = 0 \quad (2.58)$$

The information in the residual process may be reduced to a sufficient statistic $\underline{\chi}(k)$ that contains all the information in the residuals about the two hypotheses (Reference 15). $\underline{\chi}(k)$ satisfies the difference equation

$$\underline{\chi}(k+1) = A_{\phi}\underline{\chi}(k) + G^T(k+1)M^{-1}(k+1)\underline{y}(k+1) \quad (2.59)$$

with initial condition

$$\underline{\chi}(k_0) = G^T(k_0)M^{-1}(k_0)\underline{y}(k_0) \quad (2.60)$$

Now, $\underline{\chi}(k)$ is a Gaussian random vector, because $\underline{y}(k)$ is a Gaussian random process. Under H_0 , the mean of $\underline{\chi}(k)$ is the zero vector. The covariance of $\underline{\chi}(k)$, $S(k)$, satisfies the difference equation

$$S(k+1) = A_{\phi}S(k)A_{\phi}^T + G^T(k+1)M^{-1}(k+1)G(k+1) \quad (2.61)$$

with initial condition

$$S(k_0) = G^T(k_0)M^{-1}(k_0)G(k_0) \quad (2.62)$$

Under H_1 , $\chi(k)$ has the same covariance, but its mean is given by

$$E[\chi(k) | H_1] = S(k)\underline{a}(k) \quad (2.63)$$

Therefore, the OSGLR hypotheses may be rewritten as

$$H_0: \chi(k_f) \sim N(\underline{0}, S(k_f)) \quad (2.64)$$

$$H_1: \chi(k_f) \sim N(S(k_f)\underline{a}(k_f), S(k_f)) \quad (2.65)$$

Finally, the log likelihood ratio for these hypotheses is given by

$$\ell(k_f, \underline{a}(k_f)) = \underline{a}^T(k_f)\chi(k_f) - \frac{1}{2} \underline{a}^T(k_f)S(k_f)\underline{a}(k_f) \quad (2.66)$$

Because the vector of coefficients $\underline{a}(k_f)$ is unknown, an appropriate test statistic to use is the generalized likelihood ratio. In this case, the decision function $DF(k)$ is defined by

$$\begin{aligned} DF(k_f) &= \max_{\hat{\underline{a}}(k_f)} 2\ell(k_f, \hat{\underline{a}}(k_f)) \\ &= \chi^T(k_f)S^{-1}(k_f)\chi(k_f) \end{aligned} \quad (2.67)$$

A failure is detected whenever the decision function exceeds a threshold. That is, the detection test is given by

$$\begin{array}{ccc} & \text{declare a failure} & \\ DF(k) & > & T^2 \\ & < & \\ & \text{continue testing} & \end{array} \quad (2.68)$$

where T^2 is the detection threshold. The decision function is written with k as the time argument, rather than k_f , to emphasize the fact that the test is to be implemented as a sequential test, although it is derived as a fixed-data test.

Note that the OSGLR test has a relatively simple structure. The differential equations for $\underline{\chi}(k)$ and $S(k)$ are simply the Kalman filter equations for estimating $\underline{a}(k)$ in information form. The state equation for $\underline{a}(k)$ is given by Eq. 2.50, and the measurement equation is given by Eq. 2.55. The only other equation required to implement the OSGLR test is the decision function calculation of Eq. 2.68. Hence, the OSGLR test is no more difficult to implement than a single Kalman filter of order p .

In many respects, the OSGLR test is similar to the GLR test. The GLR test also employs a Kalman filter to estimate the unknown failure magnitude, v . Because v is a constant, and the Kalman filter is implemented in information form, the resulting estimator is simply a matched filter. However, a bank of filters is required, because v must be estimated for each possible time of failure, θ . Thus, the GLR test may be computationally burdensome, especially if the number of possible failure times (i.e., the width of the "data window") is large.

2.4 Evaluation and Comparison of the FDI Algorithms

The evaluation and qualitative comparison of the four FDI algorithms described in Section 2.3 in detecting and isolating control surface failures is presented here (Reference 6). The evaluation was conducted as follows. Each algorithm was designed and tested at a single flight condition of 1000 ft. altitude and 150 knot airspeed. An additional flight condition was tested to determine the effects of modeling errors. Only the time-invariant, steady state implementation of the GLR and OSGLR algorithms was tested. The assumed failure mode of each GLR failure hypothesis was a step function of unknown magnitude occurring at time θ . For each OSGLR failure hypothesis, six basis functions were used

in the truncated series expansion. The basis functions used were the discrete-time equivalent of the Laguerre function with a 3 s time constant. The GLR and OSGLR algorithms were tested in turbulence of intensity 1.98 m/s (6.5 ft/s) while the detection filter and the modified detection filter were tested mostly in turbulence of intensity 0.3 m/s (1 ft/s) although turbulence intensity of 1.98 m/s (6.5 ft/s) was also briefly considered. The Kalman filter, used by both the GLR and OSGLR algorithms, incorporated the turbulence model. Bias failures were introduced into the nonlinear C-130 simulation to test the two detection filter algorithms. To test the GLR and OSGLR algorithms, bias failures were introduced into a linear simulation of the C-130 aircraft. In addition, the nonlinear C-130 simulation was used to determine the effects of nonlinearities on the GLR and OSGLR algorithms and to test their ability to detect ramp and stuck failures. Thresholds were not selected for the two detection filter algorithms and a general detection and isolation logic was not developed. In spite of these limitations, we believe that a sufficiently accurate picture of the capabilities of each algorithm was obtained to allow the algorithms to be qualitatively compared.

In comparing the four algorithms, the following issues were considered:

- Failure modes (bias, stuck, ramp, etc.) that can be detected
- Type of failure (rudder, elevator, etc.) that can be detected and isolated
- Magnitude (or degree) of failures that can be detected
- False alarm performance
- Detection time (time delay between failure and detection)
- Computational burden
- Robustness
- Maturity

Each issue will now be individually addressed.

2.4.1 Failure Modes

Failure modes describe the behavior of the failed surface. Some of the important failure modes for restructurable control applications are stuck, hardover, and bias failures and the loss of part or all of a surface. The ability of the algorithms to detect these and other failure modes will be considered here.

The GLR test uses models of failure modes to detect failures. It is therefore, most capable of detecting the modes that are modeled. However, each mode modeled requires a separate bank of filters which makes modeling even a small number of possible modes computationally costly. With only the bias failure mode modeled, the GLR algorithm was able to detect bias and ramp failures. The GLR algorithm had difficulty deciding if a stuck failure existed with only a 2 second data window; but had no difficulty in doing so with a 5 second data window.

In the OSGLR algorithm, the failure modes are represented by a truncated series expansion rather than a fixed function. The series expansion chosen and the number of terms used determine how well a particular failure mode can be represented. Using the first six terms in the expansion, the OSGLR test was able to detect bias, ramp, and stuck failures (the only failure modes tested). These same six terms should be adequate to detect most other failure modes.

One advantage of both the unmodified and the modified detection filter is that all failure modes should be detectable as the residual direction is independent of the failure mode, depending only on the surface which failed.

2.4.2 Type of Failure

All four algorithms were able to detect elevator, rudder, right and left aileron, and right and left flap failures. The left and right elevators were assumed to move together as a unit. Elevator and rudder failures could be isolated by all four algorithms. However, isolating

wing surface (aileron and flap) failures was difficult for all of the algorithms. Based on the few test cases simulated, the modified detection filter could isolate a moderate wing surface failure (0.0349 rad (2°) aileron bias, 10% flap bias) to one of two possible surfaces in minor turbulence. The detection filter algorithm could eliminate one wing surface from consideration at most. It was demonstrated that false isolation could result with the GLR algorithm. Isolation to a specific wing surface is possible with the OSGLR algorithm with a significant delay of perhaps 10 seconds or more.

2.4.3 Magnitude of Failure

The magnitude of the failures that can be detected depends on the sensor noise, disturbances, and modeling errors. The GLR and OSGLR algorithms were able to detect moderate (0.01745 rad or 1° elevator, rudder and aileron) bias failures in the presence of noise and severe turbulence ($\sigma_\omega = 1.98$ m/s or 6.5 ft/s).

The detection filter and the modified detection filter were able to detect moderate (-0.0349 rad or -2° elevator, aileron, and 10% flap) failures in minor turbulence ($\sigma_\omega = 0.3$ m/s or 1 ft/s). However, detecting moderate failures in severe turbulence was more difficult. While hardover failures were not tested, they should be easily detected even in severe turbulence.

Modeling errors also degraded the ability of all the algorithms to detect small failures. Detection of hard failures, though, should still be possible.

2.4.4 False Alarm Performance

False alarm rates can only be determined via simulation because analytic estimates are not available. (The analytic estimates of false alarm rates for the OSGLR algorithm cannot account for the effect of modeling errors.) However, determining even large false alarm rates using simulation is difficult because of the limited number of conditions

that can be tested and the large computational burden. Therefore, the false alarm performance of each of the algorithms will be qualitatively assessed by its sensitivity to noise, turbulence, and modeling errors. Algorithms that are sensitive to these effects can be expected to have larger false alarm rates than algorithms that are less sensitive.

The OSGLR and GLR algorithms were least sensitive to noise and turbulence. This is true for two reasons: the system model incorporated into these algorithms included a turbulence model, and a Kalman filter is used to provide an estimate of the state. The unmodified detection filter was sensitive to turbulence while the modified detection filter was very sensitive to turbulence.

Since each algorithm incorporated a linear model of the aircraft, all four of the algorithms were very sensitive to modeling errors. The OSGLR algorithm appeared to be the most sensitive to modeling errors.

2.4.5 Detection Time

The failure detection times depend on the magnitude of the failure, the sensor noise, the disturbances present, and the thresholds selected. Selecting thresholds for the GLR and OSGLR algorithms higher than the largest no-failure decision function levels at the nominal cruise flight condition (nonlinear simulation) would result in detection time for 0.01745 rad (1°) elevator and right aileron bias failures in severe turbulence on the order of a second. Using the same thresholds for detecting rudder failures as for other control surface failures, would result in longer detection times. The rudder decision functions are smaller than those of the other control surface decision functions for the same magnitude failure. However, the effects of mismodeling affect the rudder decision functions less than the other decision functions. Therefore, smaller thresholds for the rudder decision function could be used, allowing the rudder detection times to be comparable to the other control surface detection times.

Detection times for both the modified and unmodified detection filters also depend on the filter eigenvalue chosen and the time constant of the low-pass filter, if any, required to suppress noise in the residual. The detection times were estimated based on the time delay between failure onset and a clear indication that a failure has occurred. For the unmodified detection filter, approximately two seconds would be required to detect 0.0349 rad (2 deg) elevator or right aileron failure in minor turbulence with the residual being low-pass filtered with a time constant of one second. A 0.0349 rad (2 deg) rudder failure would take a second longer. Detection times for the modified detection filter would be on the same order as for the unmodified detection filter.

While the detection times were comparable for all the algorithms, the GLR and OSGLR algorithms were tested in turbulence of intensity 1.98 m/s (6.5 ft/s) as opposed to 0.3 m/s (1 ft/s) turbulence intensity for the detection filter algorithms.

2.4.6 Computational Burden

The computational burden of all of the algorithms has not been quantitatively determined. Yet, some approximate comparisons will be made here. Each of the algorithms consists of a filter of the system to generate a residual, some type of residual processing, and a test for failures. The filter portion of each algorithm is computationally equivalent. Therefore, the relative computational burden can be determined by examining the computations required to process the residual and to test for the failure.

The least additional computations are required by the unmodified detection filter. The residual processing would likely consist of several banks of low-pass filters to give the algorithm the ability to quickly detect hard failures and still detect soft failures. To test for a failure, the residual must be projected onto the failure signature plane segments for each control surface.

The modified detection filter requires slightly more computational processing than the detectiton filter. The additional computations result from the secondary filtering of the residual which restores the property of a unidirectional residual in response to a control surface failure.

The relative computational burden of the OSGLR algorithm is primarily determined by the number of actuators or control surfaces and by the number of terms in the series used to represent the possible failure modes. The residual is used to drive an additional filter for each control surface to produce an information vector whose dimension is the number of terms used in the series expansion to represent the failure mode. The test for a failure in each actuator or control surface is the information vector weighted by an information matrix. For the time-invariant case considered in the preliminary evaluation, the information matrix is a constant matrix. For a large number of both actuators and terms used in the series, the computational burden would be very heavy. However, keeping only the first six terms of the series expansion was found to be adequate in the preliminary evaluation. With the six control surfaces considered in the preliminary evaluation, the computational burden of the OSGLR algorithm is at least 50% greater than the unmodified detection filter.

The relative computational burden for the GLR algorithm is mainly a function of the number of actuators, the number of failure modes modeled, and the data window chosen. Each actuator requires N correlation receivers for each failure mode modeled where N is the length of the data window divided by the time step. For a realistic data window of 2 seconds, a 0.02 second time step, six actuators, and only modeling the bias failure mode, the GLR algorithm would be computationally very burdensome. A comparison of CPU times for this window suggests that the GLR algorithm would require approximately 18 times more computation than the OSGLR test.

2.4.7 Robustness

As each of the algorithms considered here relies upon a linear model of the system to detect and isolate failures, these algorithms will be sensitive to modeling errors. Modeling errors caused large GLR and OSGLR decision functions. However, The OSGLR test was shown to be more sensitive to modeling errors than the GLR test. An off-nominal cruise flight condition produced biases in the unmodified and modified detection filter residual projections. With these biases, detecting small wing failures at the nominal flight condition would be difficult, if not impossible, unless dynamic thresholds or some other compensating approach is used.

Another source of modeling errors for the GLR and OSGLR algorithms are the failure mode models incorporated into each of the algorithms. The OSGLR algorithm is likely to be robust to actuator failure mode modeling errors as the model is sufficiently general to represent most modes adequately. However, the GLR algorithm required specific models of failure modes such as bias failures. As only bias failures were modeled in the preliminary evaluation, the GLR algorithm is likely to be less robust to other failure modes than the other three algorithms.

2.4.8 Maturity

The GLR algorithm is mature in both theory and in application. The OSGLR algorithm is almost as mature in theory as the GLR algorithm. However, as the OSGLR test is a recently developed FDI algorithm, there is very little experience in applying it.

Detection filter theory is mature for restructurable controls application to linear, time-invariant systems with no input-to-output coupling (i.e. no acceleration measurements). However, no theory exists for applying the detection filter to time-varying systems. In addition, for systems with input-to-output coupling, systematic methods of using the extra degrees of freedom in the gain matrix calculation (which result

from having more measurements than states) and scaling to improve detection filter performance are needed. Finally, there is limited experience in applying the detection filter with only a couple of applications having been reported.

The modified detection filter, developed for this application, needs additional investigation to be considered mature in both theory and application. The problems of time-varying systems, improving performance through scaling, and the extra degrees of freedom in the gain matrix calculation mentioned above for the detection filter also apply to the modified detection filter.

2.4.9 Summary and Overall Comparison

The eight issues addressed in this memorandum are summarized in Table 2.3. The GLR and OSGLR algorithms performed the best, especially in severe turbulence. However, the computational burden of the GLR algorithm is heavy and its ability to isolate wing surface failure modes is uncertain. The most significant advantage of the detection filter algorithms is their relatively low computational processing requirements. If the sensitivity of the detection filter algorithms to turbulence could be reduced, their performance might be comparable to the GLR and OSGLR algorithms. The most significant disadvantage of the OSGLR algorithm is its sensitivity to modeling errors. Still, the OSGLR algorithm is the most promising of these four algorithms evaluated.

2.5 System Monitoring Strategy

A second program task was to develop a system monitoring strategy for the detection and isolation of aircraft actuator and control surface failures. Before discussing the issues, the advantages and limitations of three applicable FDI techniques will be considered: local actuator FDI, analytic FDI algorithms such as those considered in this program, and the use of surface position measurements.

Table 2.3. Comparison of FDI Algorithms*

ALGORITHM	GLR	OSGLR	DETECTION FILTER	MODIFIED DETECTION FILTER
Failure Modes Detectable	Bias, Ramp**	Most failure modes	All (Only bias tested)	All (Only bias tested)
	Detect	All	All	All
Type of Failure	Elevator, Rudder, False isolation of wing surface failures possible	Elevator, Rudder, Wing surface with a moderate time delay	Elevator, Rudder	Elevator, Rudder
Magnitude	0.01745 rad(1°) bias in severe turbulence and no modeling errors	0.01745 rad(1°) bias in severe turbulence and no modeling errors	0.0349 rad(2°) bias in minor turbulence and no modeling errors	0.0349 rad(2°) bias in minor turbulence and no modeling errors; larger failures in heavier turbulence and modeling errors
False Alarm Performance	Insensitive to turbulence; sensitive to modeling errors	Analytic results available; insensitive to turbulence; very sensitive to modeling errors	Sensitive to turbulence and modeling errors	Very sensitive to turbulence; sensitive to modeling errors

*The comparison is based on the test cases used to evaluate each algorithm the preliminary evaluation. Only a limited number of flight conditions and environments were simulated. Also, the comparison is qualitative as thresholds were not chosen in all cases and a general detection and isolation logic was not selected.

**A bias failure mode was assumed in the GLR hypotheses.

Table 2.3. Comparison of FDI Algorithms (Cont.)

ALGORITHM	GLR	OSGLR	DETECTION FILTER	MODIFIED DETECTION FILTER
Detection Time	Less than 0.5 seconds for 0.01745 rad(1°) bias failure in severe turbulence	Less than a half second for 0.01745 rad (1°) bias failure in severe turbulence	Approximately two seconds for 0.0349 rad (2°) bias failure in minor turbulence; longer in severe turbulence	Approximately two seconds for 0.0345 rad(2°) bias failure in minor turbulence; probably longer in severe turbulence
Computation Burden	Heavy	Moderate	Light	Light
Robustness to failure mode uncertainty	Poor to good	Good	Good	Good
Robustness to model uncertainty	Poor	Poor, worse than the other three algorithms	Poor	Poor
Maturity in Theory	Mature	Mature	Mature for linear time-invariant systems with no input-to-output coupling	Needs more investigation
Experience in Application	Much	No previous experience	Some	No previous experience

2.5.1 Local Actuator FDI

Direct duplication of actuation has been the practice for most military and large commercial aircraft for quite some time. Whole actuation channels may be duplicated several times. There have been several methods devised for dealing with failures of elements in these channels. The subsystems and channels must be substantially identical in order to give the same control inputs and to enhance the performance of the system. Some differences are inevitable because of tolerances, and these must be taken into account so that disengagement of a channel will occur only under genuine failure conditions. The performance of the subsystems and channels is continuously adjusted, in a process called equalization (Reference 16). As a part of equalization, inter-channel differences are minimized through feedback. If a difference is too great, then the failed channel is disengaged or bypassed. Frangible elements (shear pins, for example) have also been used, allowing a jammed actuator to be broken by the others. Thus, a large degree of actuator FDI (and reconfiguration) already takes place on a local level. However, there are failures such as jams, actuator bias, inappropriate overall actuation gain, or control surface damage which the local FDI scheme will be unable to detect.

2.5.2 Analytic FDI

Analytic FDI schemes, such as those considered in this program, look for control surface failure signatures in the whole-system dynamics. That they detect failures at the system level (ultimately the most important one) is what makes these schemes potentially of great value. They can be considered most useful in the context of aircraft actuator FDI in identifying failures that the low-level FDI schemes have missed. Such failures might include inaccuracy or breakdown of the local schemes and actual physical damage to the control surface itself. However, analytic FDI schemes have been shown to have difficulty in fully isolating failures among control surfaces that are functionally redun-

dant. Thus, isolating a wing surface failure to a specific flap or aileron was difficult. The quantitative measures developed to determine the maximum discrimination of such failures showed the inherent difficulty.

The value of actually isolating a failure of a surface that is functionally redundant might be questioned to some degree. After a surface fails, it is required that sufficient capability remain to end the flight in an acceptable way. If there is sufficient capability and if this can be appropriately determined then complete failure isolation might be considered optional. However, the ability to quickly and accurately determine the functional capability of the aircraft while in flight does not exist at the present time. Furthermore, there are reasons why isolation to a specific surface would be preferred. It is likely that a failure could be more quickly and appropriately compensated if it were fully isolated. Moreover, full isolation might allow for more flexibility and confidence in continuing a flight after a failure has occurred. Therefore, full isolation capability is taken as the simpler and more desirable option.

2.5.3 Control Surface Position Sensors

Position sensors mounted on or near the control surface itself could be considered to provide information on a level just below that of the whole system. Information from these transducers can be expected to be reasonably easy to obtain and use. Position transducers of the synchro, potentiometer, and linear variable differential (LVDT) types have been extensively used and are simple (Reference 17). For these position transducers to be an independent source of information on any type of failure, however, they should not be part of the actual flight control loop. (Position sensors are not presently used by aircraft control systems.)

Flight control systems in which control loops are closed using aircraft dynamic information will automatically compensate for some actuator failures, such as small surface bias errors. To identify larger

biases, comparing actuator position expected (using a reference model) with that actually measured by position transducers might suffice to isolate a failed surface. Alternately, in a separate actuator positioning flight control mode in benign flight conditions, commanding the surface to move to some absolute position or to move a certain fixed amount could suffice to detect and isolate biases or incorrect gains. If the surface is jammed, FDI using outputs from position transducers is also possible, using tests similar to those described for biases.

Employing an FDI scheme based on surface position measurements involves additional hardware and perhaps the design of separate flight or test modes. In addition, FDI of the surface position sensors may also be required. It should be stressed, too, that position transducers would still be of only limited use in identifying certain types of failures, such as actual control surface damage.

2.5.4 System Monitoring Strategy Selected

An analytic whole-system FDI scheme is preferable as it can detect failures that may not be detectable by either the local FDI scheme or by position sensors. However, since analytic algorithms have some difficulty isolating failures, they could be augmented with direct surface position sensors to provide information for complete failure isolation, eliminating the uncertainties inherent in fully identifying the failure of a functionally redundant surface. Only a limited number of transducers might then be required, and limited use made of their information. Use of position sensors to augment analytic FDI schemes also implies that each scheme could serve as a limited check on the other, providing a more reliable FDI system. While information from the local actuator FDI scheme may be of limited use also in this regard, this information will not be considered.

The system monitoring strategy for the C-130 aircraft considered in this evaluation (assuming that the elevators move together) would be a

combination of the best analytic FDI algorithm (the OSGLR test) with position sensors on each of the wing surfaces.

2.6 Conclusions

The major conclusion which may be drawn from the results of this study is that algorithmic failure detection and isolation may be feasible for restructurable control applications. This conclusion must be qualified by the results obtained during this preliminary evaluation which have been basically limited to a single operating condition and to the investigation of a small subset of the potential failures. In particular, failure detection at the nominal flight condition does not appear to be a problem. Each of the algorithms was able to detect small elevator, rudder, aileron and flap failures for the C-130 aircraft in turbulence. The isolation of control surface failures was not a problem for elevator and rudder failures. However, difficulties arose in the isolation of wing surface, i.e., aileron and flap, failures. These failures have a similar effect on the responses of the aircraft system. This difficulty highlights the potential need to augment the analytic FDI algorithms with the direct measurement of failures using, for example, position sensors on some of the control surfaces.

The OSGLR algorithm performed best of those evaluated. The general representation of the failure mode implies that most failure modes should be detectable. All failure types investigated during this study were detected and isolated, although there was a long time delay associated with isolating the wing surface failures. Bias failures on the order of a degree of surface deflection were detected in approximately a second for a system without modeling errors. The computation and burden associated with this algorithm is moderate relative to the others, and the theory associated with it is mature. However, robustness properties of the OSGLR test are worse than those of the other algorithms. In addition, the OSGLR algorithm has not been previously applied to any system.

The GLR algorithm also performed well in the C-130 application. The major drawbacks associated with it are its heavy computational burden, its lack of robustness to failure mode uncertainty, and its poor wing surface isolation performance. The most significant advantage of the detection filter algorithms is their relatively low computational processing requirements. If the sensitivity of these algorithms to turbulence could be reduced, their performance might be comparable to the GLR and OSGLR algorithms. None of the algorithm was robust to model uncertainty.

In our judgement, the OSGLR algorithm is the most promising of the algorithms evaluated and, therefore, will be investigated further. The poor robustness to modeling errors of the OSGLR algorithm can, we believe, be improved; reducing the sensitivity to these errors of the OSGLR algorithm is the subject of Section 4. Many of the ideas presented there are applicable to other FDI algorithms as well.

SECTION 3

A SURVEY OF FDI TECHNIQUES APPLICABLE TO AIRCRAFT CONTROL SURFACE FAILURE DETECTION AND ISOLATION

3.1 Introduction

In order to determine if there are practical FDI alternatives to the three algorithms already evaluated, a survey of FDI techniques that might be applicable to detecting and isolating aircraft control surface and actuator failures is presented. This survey is based largely on Reference 18. A discussion of several general categories of FDI algorithms will follow, with attention to those algorithms that might be usable in the aircraft application. The conclusions section summarizes the results of this search.

3.2 Failure Sensitive Filters

The detection filter can be considered one of the class of failure sensitive filters used for FDI. This class also includes limited memory filters and filters augmented with the parameters of hypothesized failures included as state variables. Limited memory filters are effectively used only for failure detection, because they are not failure specific. By keeping the residual gain high, it is hoped that a failure can be expected to result in a sudden and pronounced change in the filter behavior. Filter state augmentation does help in this regard, but at the expense of potentially quite large dimensionality. The augmented filter will not be able to match the detection filter's ability to respond to any failure manifested in a known direction, and the augmentation serves to decrease performance of the filter when there are no failures.

3.3 Innovations-based Systems

The GLR and OSGLR algorithms belongs to the group of FDI schemes known as innovations-based systems. These monitor the innovations of the (typically) Kalman filter designed for the unfailed system. This group also includes simple residual magnitude monitoring for failure detection. The GLR algorithm attempts to detect and isolate additive failures using knowledge of the different effects such failures have on the (linear) system innovations. Because the exact form of the failure is generally unknown, some estimate is needed in order to have an accurate indication of failure. This failure estimation is inherent in any GLR scheme. Matched correlation detectors, in general each assuming a particular direction, mode, and time of failure, use as inputs the residuals of the normal mode filter and estimate the unknown associated with the failure. These estimates are then used in composite tests for the presence of particular failures.

The OSGLR algorithm is similar to the GLR algorithm in many ways. However, the OSGLR algorithm represents the failure mode by a truncated series expansion. A matched filter for each control surface is used to estimate the coefficients of the truncated series expansion. The order of the matched filter is the number of terms in the truncated series expansion. Also, no explicit estimation of the time of failure is required by the OSGLR approach.

In aircraft application, in which the direction of the failure is known, effective use of the traditional GLR algorithm would probably involve hypothesizing one or more different failure modes, e.g., bias or ramp. Assuming only certain limited modes can give the GLR algorithm some robustness with respect to other, different modes of failures. The OSGLR algorithm, however, avoids the complexity of specifying different modes, since inherently it allows for any.

The traditional GLR algorithm explicitly estimates time of failure onset, resulting in a time-linear growth in the number of detectors. Limiting the possible times of failure onsets to the recent past limits this growth. However, this "windowing" may degrade detection and isolation performance, especially if the window is chosen such that the GLR algorithm is computationally efficient. The windowing approximation need not be made in the OSGLR algorithm, however. Although the OSGLR algorithm cannot explicitly estimate time of failure, no new matched filters need be created.

The FDI algorithms evaluated so far have been used with a linearized model of the C-130. FDI performance suffers when the operating condition is far from nominal. Caglayan and Lancraft have applied the GLR ideas to systems for which the no-failure filter is an EKF (Reference 19). The nonlinear filter formulation gives a more complex but flight path-independent scheme, eliminating the need for gain scheduling. In the C-130 application, much of the model information is available only through tables. This makes the prospect of EKF filtering unlikely without extensive changes in the modeling representation. This may merit some consideration, however.

3.4 Multiple Hypothesis Filtering

Multiple hypothesis filtering schemes have also been proposed for FDI. In the exact application of this concept, a "bank" of full-order linear filters is constructed, with each filter based on a different hypothesis concerning system behavior. The innovations from the filters are then used to compute the probability that each system model is the correct one. This type of scheme has all of the drawbacks of the traditional GLR algorithm, in that the number of filters grows with time. Windowing of data is also possible here. Unlike the GLR algorithm, state estimation for the failed system is immediately available with the multiple hypothesis filter schemes since there is a filter valid for each failure hypothesis. However, state estimation for the failed system with

the innovation-based systems is possible by approximately compensating for the effects of an additive failure on the no-failure filter. If a complete set of failure types and modes can be delineated, multiple hypothesis filtering schemes can be expected to give the best possible FDI performance. Their complexity, however, renders them impractical.

3.5 Generalized Bayesian Tests

Generalized Bayesian tests (Reference 20), as another class of sequential algorithms, seek to provide optimal failure detection and isolation through the assignment of costs for making certain decisions at certain times. The optimal FDI strategy minimizes the expected overall cost. This class of algorithms can be considered the most general at the present time. Potential application is to any system for which a priori information concerning possible failures is available. (This is implied in the term Bayesian.) Moreover, unlike most schemes, probabilistic information about the overall FDI scheme is a byproduct of the optimization.

The optimal FDI rule is generally not computable, but the structure of the approach can be expected to be useful in deriving a practical suboptimal FDI algorithm. Reference 20 considers several possible approximations.

3.6 Conclusions

The detection filter can readily be considered the best of the failure-sensitive filters and the OSGLR algorithm the best of the innovations-based schemes for the linear time-invariant system with additive failures. They have been implemented, and it is doubtful that more complex schemes would significantly enhance practical FDI performance. It is likely that simpler schemes would not be able to provide timely and accurate full failure identification. It should be noted that generalized Bayesian schemes are relatively new and undeveloped; a good characterization of their potential suitability will come only as a result of future

research. The attractive decision-cost optimality comes, however, with solution of a difficult problem.

Based on this survey and the results of the initial evaluation (described in Section 2), the OSGLR algorithm, in our opinion, has the most potential of the algorithms that are mature for the Restructurable Controls Application. Therefore, only the OSGLR algorithm will be investigated further.

SECTION 4

ACCOMMODATION OF MODELING ERRORS FOR THE OSGLR ALGORITHM

Effective analytic fault detection and isolation schemes require accurate system models. All the FDI algorithms investigated in the preliminary evaluation, especially the OSGLR algorithm, were found to be sensitive to modeling errors. Certain modeling errors are introduced in linearizing aircraft nonlinear dynamics and in using a model during periods of off-nominal flight conditions. These errors will, at least to some extent, be attributed to control surface failures, and, consequently, lead to larger decision functions than if there were no such errors. In fact, with significant mismodeling, the decision functions are unbounded in their growth. Therefore, it is not always possible to avoid false alarms associated with modeling errors by judicious selection of the detection thresholds.

There are several ways of better accommodating modeling errors in analytic FDI algorithms. These might be considered as the following:

- Dynamic thresholding - choosing decision thresholds based on estimates of the system state or, perhaps, the disturbances present (e.g., turbulence).
- Dynamic decision regions - determining the statistics of the FDI residual, and choosing the threshold given those statistics.
- Actual model error estimation, and use of those estimates in offsetting residual errors.
- Robust design of the actual residual generator, leading to a sub-optimal scheme over the expected range of model errors.

While some of the above approaches have been used to reduce modeling errors in a number of FDI applications, no applications of FDI techniques in which the errors are propagated through a filter have been discovered. The F-8 study (References 21 and 22), for example, uses some fairly sophisticated modeling error accommodation, but the FDI is for sensors whose output can be more or less directly compared.

This section will consider each of the four approaches in attempting to reduce the sensitivity of the OSGLR algorithm to midmodeling.

4.1 Dynamic Thresholds

Detection thresholds can be tied to estimates of the state or of system disturbances or expressed as increasing functions of time during a maneuver, perhaps, e.g., $T = (a + bt)^2$. While it is difficult to see how dynamic thresholds can be systematically designed for filter residual-based FDI schemes (like the detection filter and OSGLR), one approach was investigated.

One measure of the sensitivity of the OSGLR algorithm to mismodeling is

$$\min \frac{\underline{\chi}^T \underline{S}^{-1} \underline{\chi}}{\underline{\chi}^T \bar{\underline{S}}^{-1} \underline{\chi}} \quad (4.1)$$

where $\underline{\chi}$ is the information vector, $\bar{\underline{S}}$ is the nominal information matrix used to calculate the decision function, and \underline{S} is the actual information matrix. A graphical interpretation of this measure is shown in Figure 4.1. This minimization both determines the direction (in $\underline{\chi}$ space) in which the nominal implementation is sensitive to a particular mismodeling and the largest σ ellipse of the actual decision function $\underline{\chi}^T \underline{S}^{-1} \underline{\chi}$ that is contained in the 1σ ellipse of the nominal decision function $\underline{\chi}^T \bar{\underline{S}}^{-1} \underline{\chi}$.

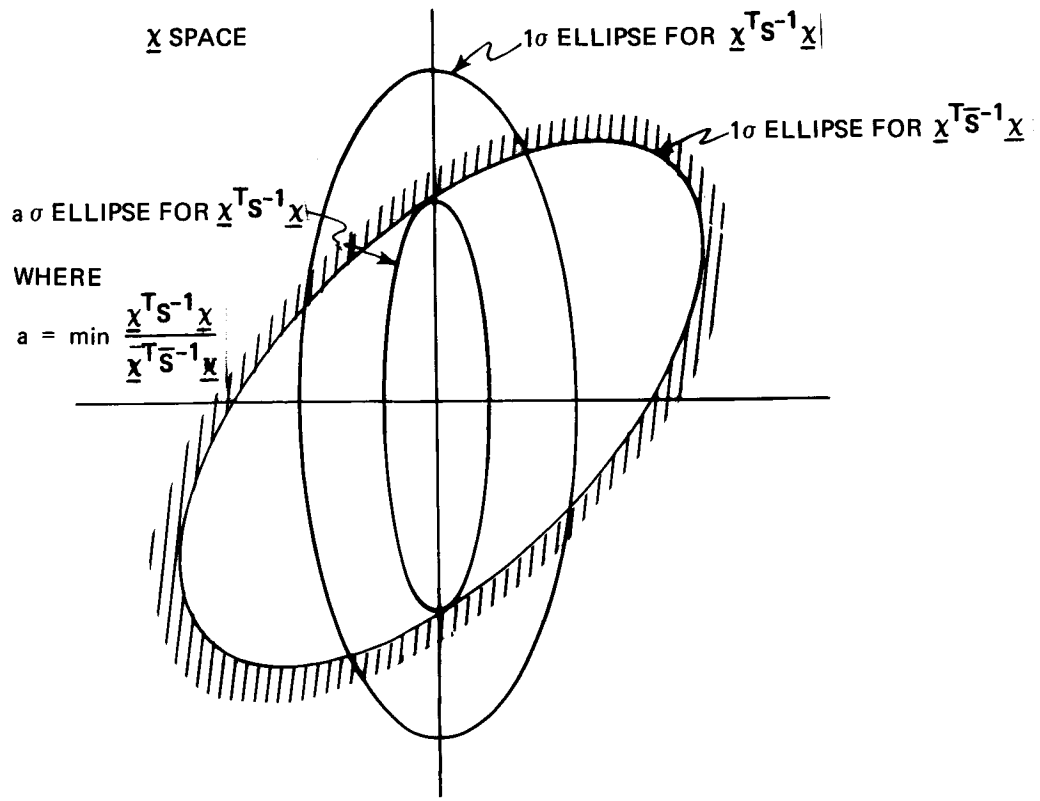


Figure 4.1 Sensitivity measure for the OSGLR algorithm

If determining the actual information matrix S is possible, one approach for compensating for the mismodeling effects might be to increase the threshold, T^2 , of the nominal decision function such that the $T\sigma$ ellipse would contain or mostly contain a $T_1\sigma$ ellipse for $\chi^T S^{-1} \chi$. T_1^2 is the threshold that yielded adequate performance with no mismodeling.

For mismodeling that results in changes in the linear model, the actual information vector S can be determined by combining the Kalman filter and OSGLR equations as implemented with the actual linear model (including the effects of mismodeling) into a single linear system.

$$\begin{bmatrix} \underline{x}(k+1) \\ \hat{\underline{x}}^-(k+1) \\ \chi_1(k+1) \end{bmatrix} = \begin{bmatrix} \phi & 0 & 0 \\ \phi^*K^*C & \phi^*(I-K^*C^*) & 0 \\ G^{*T}M^{*-1}C & -G^{*T}M^{*-1}C^* & \phi_\phi \end{bmatrix} \begin{bmatrix} \underline{x}(k) \\ \hat{\underline{x}}^-(k) \\ \chi_1(k) \end{bmatrix} \\
 + \begin{bmatrix} B \\ B^* + \phi^*K^*\Delta D \\ G^{*T}M^{*-1}\Delta D \end{bmatrix} \underline{u}(k) + \begin{bmatrix} \underline{w}(k) \\ \phi^*k^*v(k) \\ G^{*T}M^{*-1}v(k) \end{bmatrix} \quad (4.2)$$

where $\underline{x}(k)$ and $\hat{\underline{x}}^-(k)$ are the linear system state and the Kalman filter state estimate respectively. $\chi_1(k)$ is the information vector time shifted one time step:

$$\chi_1(k) = \chi(k-1)$$

The superscript (*) indicates that the matrix is either a nominal linear model matrix or steady-state Kalman filter and OSGLR matrices based on the nominal linear model. The actual linear model matrices are not superscripted and

$$\Delta D \stackrel{\Delta}{=} D - D^* \quad (4.4)$$

The process and measurement noise are represented by $w(k)$ and $v(k)$. Since the information matrix is simply the covariance of \underline{x} , the actual information matrix S is the lower right-hand block of the augmented state covariance matrix:

$$\begin{bmatrix} E[x(k)x^T(k)] & E[x(k)\hat{x}^T(k)] & \dots \\ \dots & E[\hat{x}(k)\hat{x}^T(k)] & \dots \\ \dots & \dots & S \end{bmatrix} \quad (4.5)$$

One difficulty with this approach is that the actual information matrix is a function of the covariance of the inputs unless modeling errors do not affect the B and D matrices. Instead of trying to appropriately describe the covariance of the inputs, the control system could be included in the augmented linear system (Eq. 4.2). However, the actual information matrix then becomes a function of the covariance of the commands to the control system. One approximation might be to assume the covariance of the commands to be zero. A much better approximation would be to assume the pilot is a feedback system.

Assuming the covariance of the inputs is somehow described, the actual information vector can be determined by propagating forward in time the augmented state covariance matrix or by solving a Lyapunov

equation for the steady-state covariance matrix. In the latter case, the actual linear model must be stable unless the control system is included. Then the sensitivity of the OSGLR algorithm to this change in the linear model could be determined and the threshold compensated. This analysis alone is not adequate in selecting thresholds as nonlinearities not represented in the linear models are not taken into account. Also, mismodeling may cause the information vector to become biased, or worse, to grow without bound.

This sensitivity analysis was not performed in this effort as describing the control system of the C-130 aircraft was prohibitive. Without a systematic method to design dynamic thresholds, a trial-and-error procedure would have to be used.

4.2 Dynamic Decision Regions

Filter sensitivity results can also be used to implement dynamic decision regions for the detection test used in the OSGLR algorithm. The form of the detection test is the information vector weighted by the information matrix and compared to a threshold.

$$\chi^T S^{-1} \chi \gtrsim T_x \quad (4.6)$$

The information matrix reflects the expected uncertainty associated with the basis function coefficient estimates. The certainty predicted in the filter generally does not take into account modeling errors, however. In order to reduce false alarms, one might like S to reflect the uncertainties associated with modeling errors even in the absence of failures.

The basic idea then is to use the actual information matrix as opposed to the nominal information matrix in calculating the decision function $\chi^T S^{-1} \chi$. The actual information matrix could be calculated as outlined in the previous section. Instead of continuously updating the information matrix, it would be more efficient to bound S in an

approximate manner, Even better would be to approximate S as a function of operating parameters, states, or inputs. As discussed in the previous section, certain nonlinearities and biases or unbounded growth in the information vector caused by mismodeling cannot be dealt with using this approach.

4.3 Model Error Estimation

A third option in accommodating modeling errors in FDI involves estimating these errors directly. This could be, of course, a highly effective option, but it would probably be difficult to account for much of the error and would thus be computationally prohibitive. Moreover, this extensive estimation could probably be foregone without bad consequences if one of the other accommodation options were employed.

4.4 Robust Residual Generation

The OSGLR algorithm nominally depends on residuals produced by a Kalman filter to detect and isolate failures. Either improving the robustness of the Kalman filter or using a more robust filter than the Kalman filter will reduce the effects of modeling errors on the OSGLR algorithm. The need for reducing the sensitivity of the Kalman filter to modeling errors is apparent even at the nominal cruise flight condition.

Figure 4.2 shows the predicted state covariance and the actual aircraft state estimation errors for a segment of nominal, no-failure flight, using a single linear model in the Kalman filter. Even here, a case for which the modeling errors are expected to be small, the estimation errors are not well bounded by the covariance. Figure 4.3 shows the corresponding OSGLR decision functions, which are large.¹ Practical improvements might involve adding process noise to the Kalman filter (in

¹ Appendix A contains a summary of test cases presented in this report for easy reference and comparison.

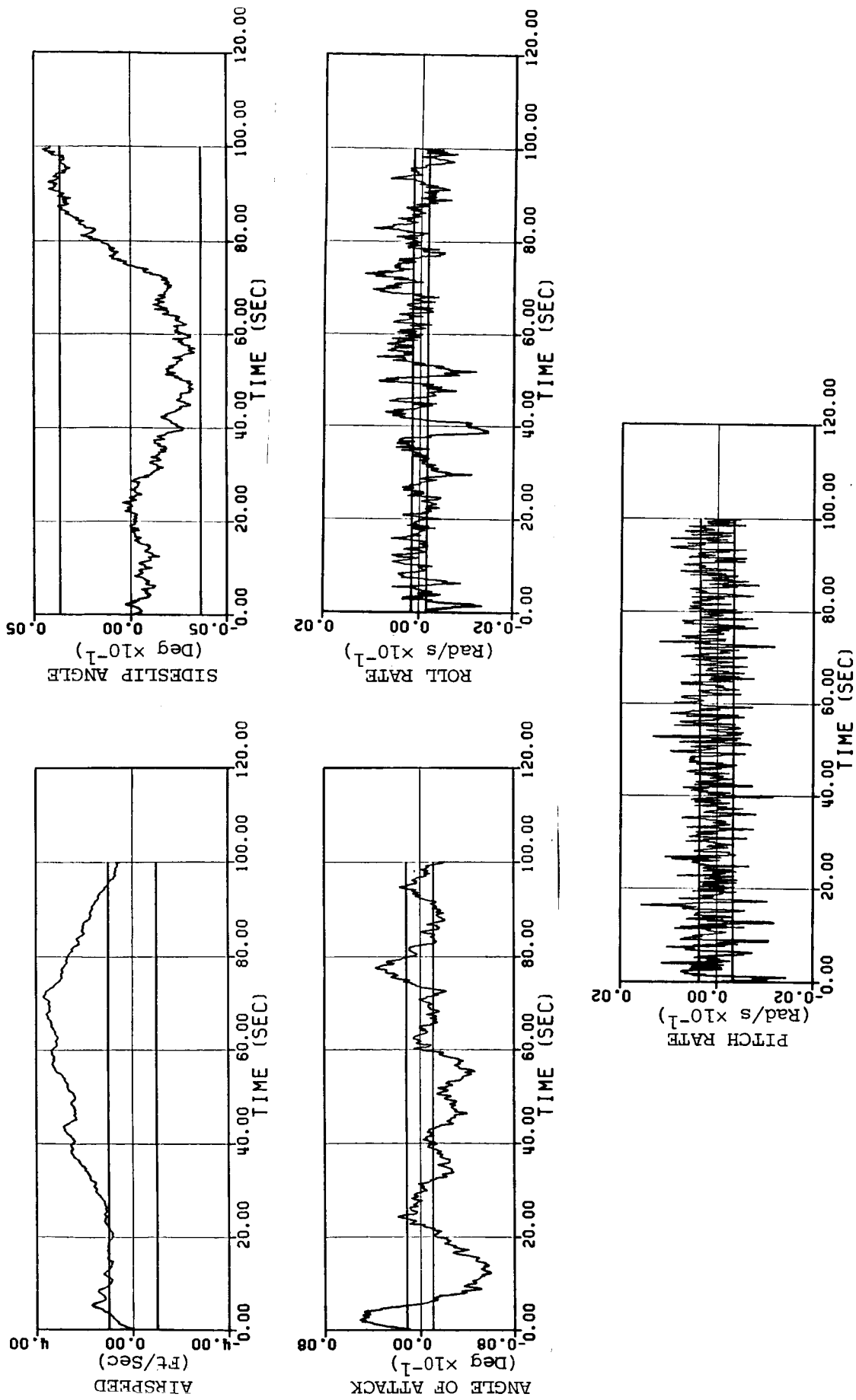


Figure 4.2 State estimation errors and standard deviations for a nonlinear, no-failure, nominal cruise flight condition test case

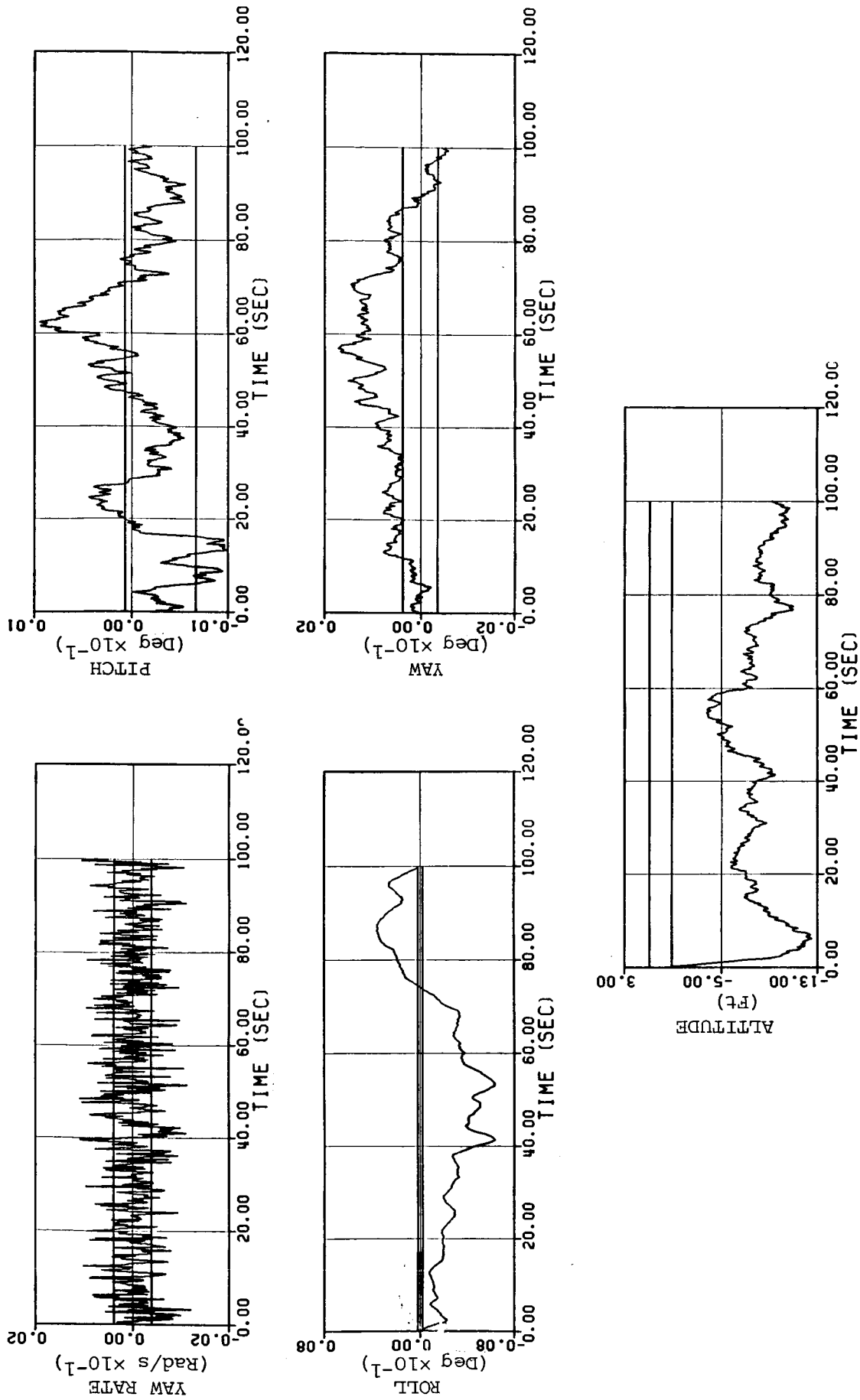


Figure 4.2 State estimation errors and standard deviations for a nonlinear, no-failure, nominal cruise flight condition test case (Cont.)

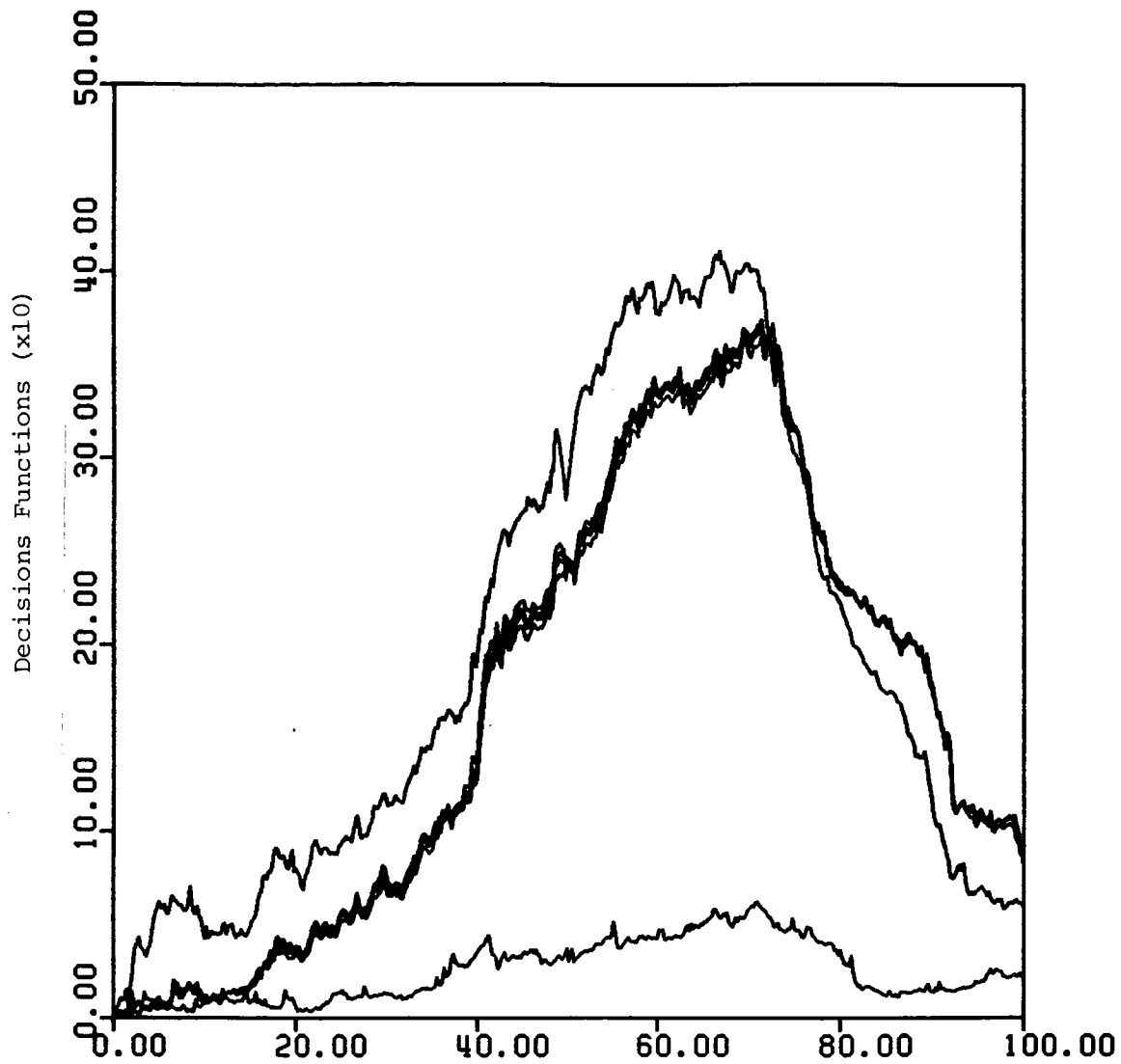


Figure 4.3 Decision functions for the nonlinear, no-failure, nominal cruise flight condition test case.

addition to the turbulence process noise already present), or perhaps using so-called limited memory filtering in the OSGLR. Either technique curtails growth of the actual estimation error covariance and increases predicted covariance. Use of either technique could also be expected to desensitize the decision functions to errors due to both linearization of the nonlinear dynamics and off-nominal maneuvering of the aircraft.

There is no method of systematically selecting process noise to reduce the effects of mismodeling on the Kalman filter. The designer must resort to a trial-and-error procedure of selecting the process noise and testing the resulting Kalman filter. The other difficulty with this approach is that the choice of process noise may reduce the effect of a failure on the Kalman filter residuals, degrading the ability of the OSGLR algorithm to detect and isolate that failure. In spite of these difficulties, this approach was briefly investigated. A set of state covariance weightings were determined such that 0.01745 rad (1°) elevator and right aileron bias failures, 0.0349 rad (2°) rudder bias failures, and 5% right flap bias failures still could be detected and isolated at the nominal cruise condition 77.2 m/s (150 knots) at 304.8 m (1000 ft) while greatly reducing the no-failure decision function at the off-nominal cruise condition 102.9 m/s (200 knots) at 1524.0 m (5000 ft). (The process noise added was in addition to the turbulence process noise already driving the system.) The decision functions for the 0.01745 rad (1°) elevator bias failure and the off-nominal no-failure test cases using the nominal (no process noise) Kalman filter and OSGLR algorithm are shown in Figures 4.4 and 4.5, respectively. The decision functions for the same two test cases using the Kalman filter and OSGLR algorithm designed using process noise are shown in Figures 4.6 and 4.7. Scheduling the threshold in terms of distance from the nominal point might allow for quick detection of failures close to the nominal cruise condition while reducing the effects of mismodeling.

Limited memory filtering is to be preferred as it can be implemented in such a way that it is general, simple, and quite effective. The

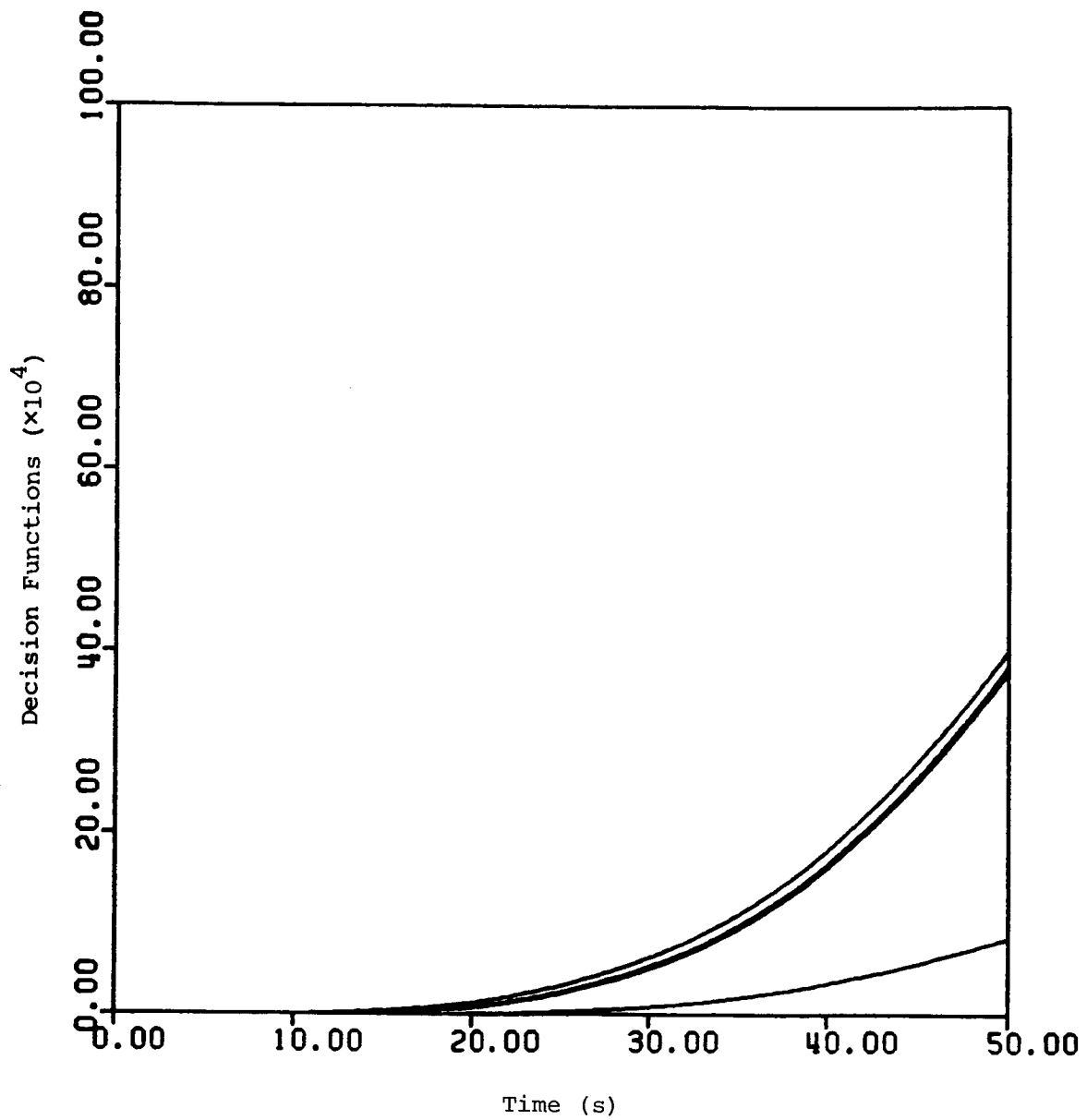


Figure 4.4 OSGLR decision functions for a -0.01745 rad (-1°) elevator bias failure which occurred at 10 seconds at the nominal cruise flight condition of 77.2 m/s (150 knots) and 304.8 m (1000 ft)

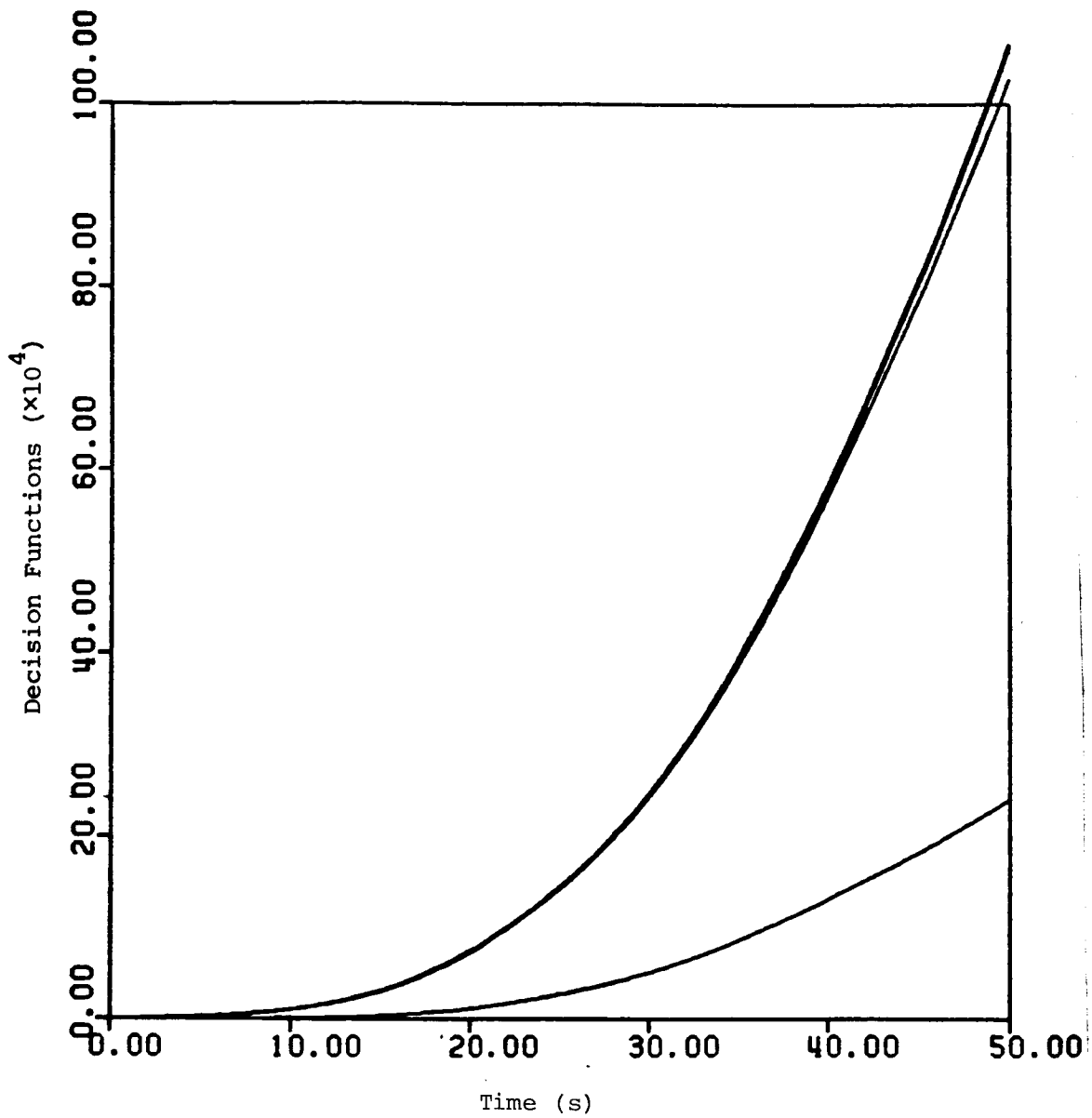


Figure 4.5 OSGLR decision functions for a no-failure case at an off-nominal cruise flight condition of 102.9 m/s (200 knots) and 1524 m (5000 ft)

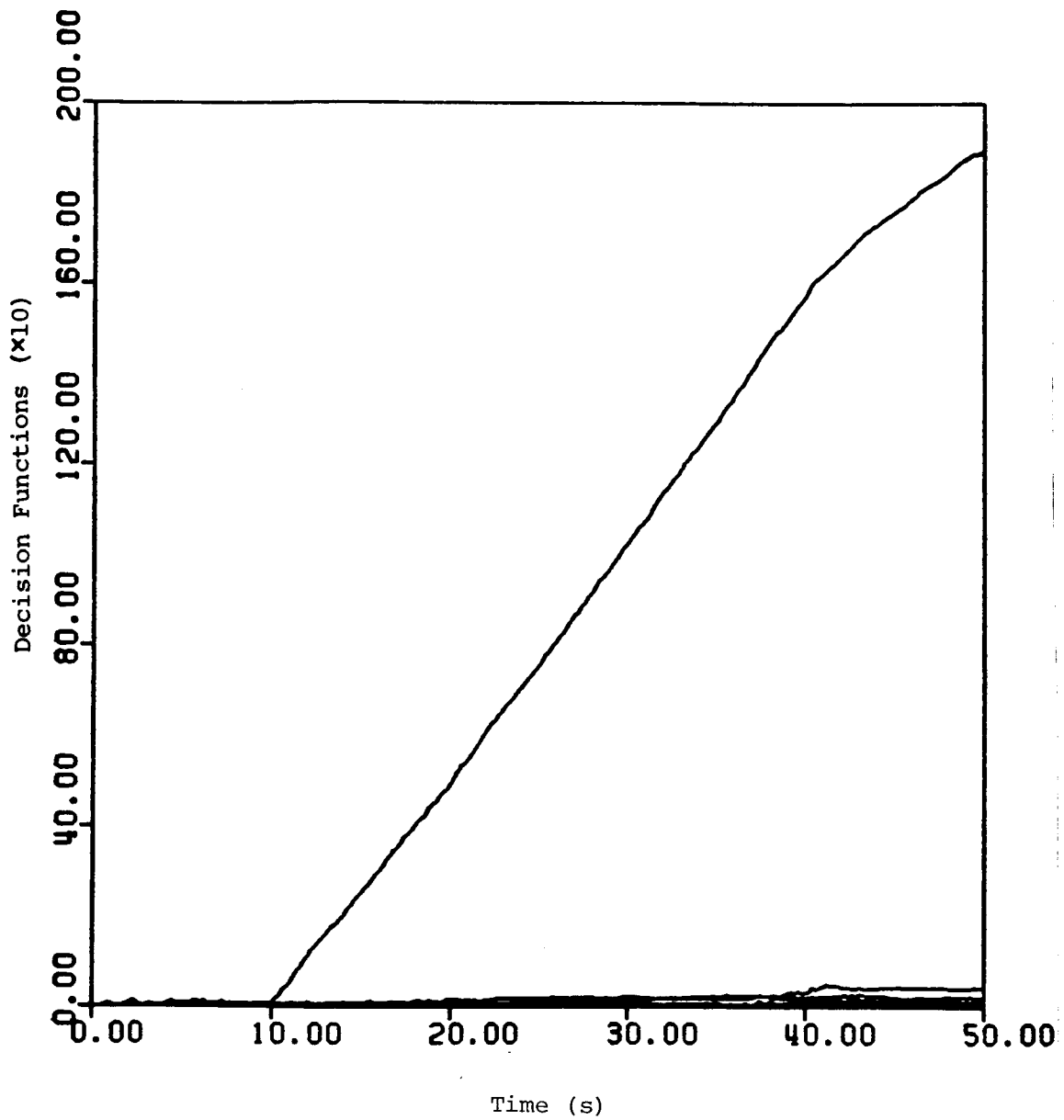


Figure 4.6 OSGLR decision functions for a -0.01745 rad (-1°) elevator bias failure at 10 seconds at the nominal cruise condition of 77.2 m/s and 304.8 m using a Kalman filter with process noise added

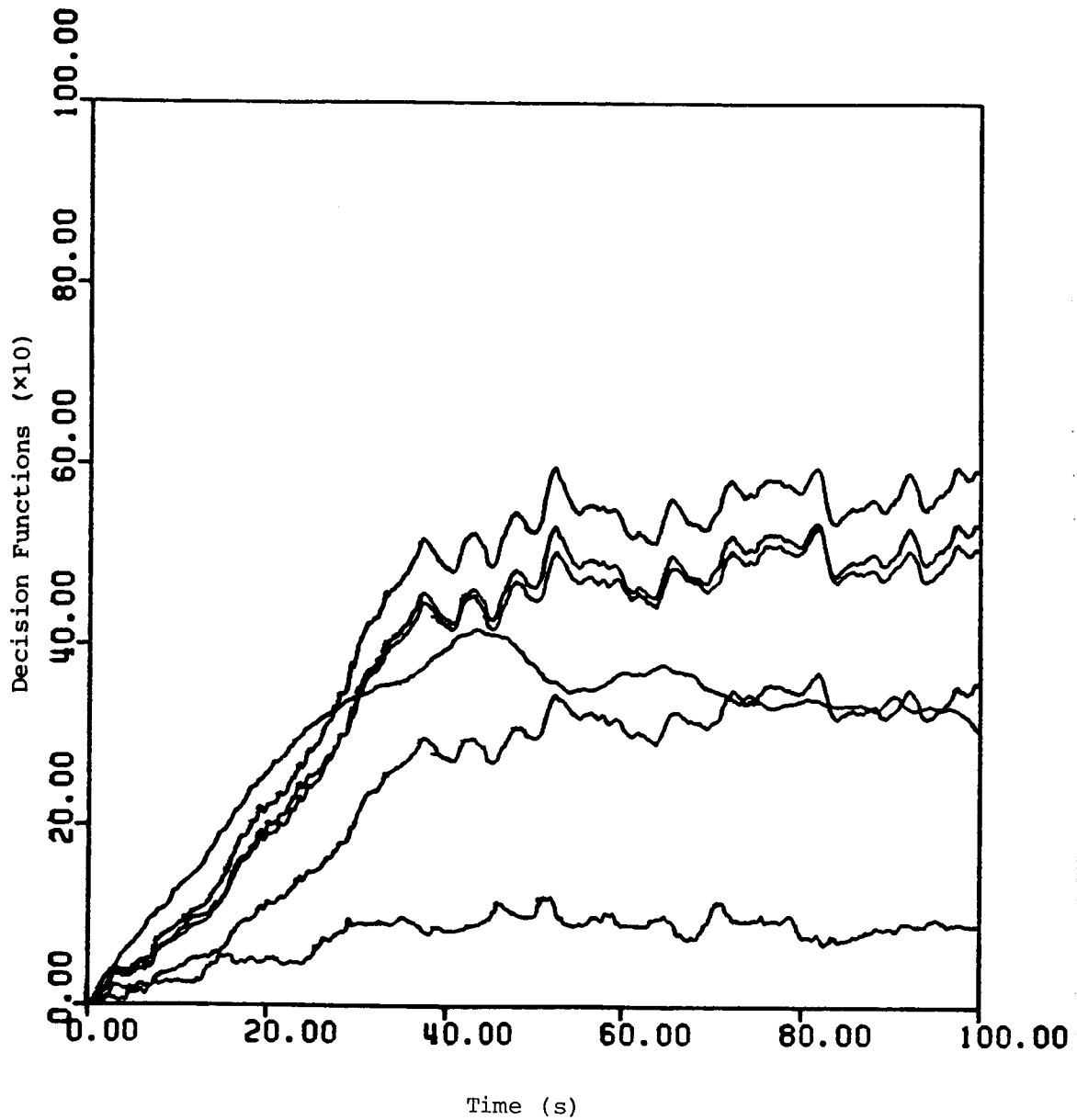


Figure 4.7 OSGLR decision functions for a no-failure case at an off-nominal cruise flight condition of 102.9 m/s and 1524.0 m using a Kalman filter with process noise added

basic idea of limited memory filtering is the more or less gradual elimination of old data, as it is no longer thought to be meaningful. One approximate method that can be used in the current application is the age-weighted filter (Reference 23). In this filter, discarding old measurement data is accomplished by weighting them according to when they occurred. In other words, the covariance of the measurement noise is increased for past measurements. For assumed constant measurement noise covariance R , one manner of accomplishing this is to set

$$R'_{k-m} = (e^{m\Delta t/\tau})R, \quad m = 0,1,2\dots \quad (4.7)$$

where R' is the new noise covariance and k denotes the current time in the filtering. Δt is the measurement (sampling) interval, and τ is a time constant associated with the length of time the model is considered valid.

A recursive filter can be constructed under these assumptions. The only difference between the resulting algorithm and the standard Kalman filter is the appearance of the age-weighting factor $s = e^{\Delta t/\tau}$ in the state covariance update equation:

$$P'_k(-) = s\phi_{k-1}P'_{k-1}(+)\phi_{k-1}^T + Q_{k-1} \quad (4.8)$$

Otherwise the age-weighted filter equations are the same as the Kalman filter equations (Eqs. 2.25-2.30 and Eq. 2.32). Compared with the original Kalman filter, the factor s , being greater than 1, leads to larger state and measurement covariances and, consequently, a larger filter update gain. The result is a faster tracking filter. Only the steady-state implementation of the age-weighted filter is tested in this report.

If the measurement noise covariance matrix is actually constant and the age-weighting is being used to produce a faster tracking filter

as in this report, the P_k' is not the state error covariance matrix $E[(\hat{x}_k - x_k)(\hat{x}_k - x_k)^T]$. The state error covariance matrix can be calculated using results for a filter of the form of the Kalman filter but with an arbitrary gain matrix. The measurement error covariance matrix is calculated by using the correct state error covariance matrix. For convenience, since the actual covariance matrices are not of interest, the covariance matrices including the effects of age-weighting will be referenced to the age-weighted filter state error and residual covariance matrices.

The (normal) OSGLR FDI scheme involves the use of a no-failure Kalman filter and what are essentially matched Kalman filters for the various control surface failure hypotheses driven by the residuals of the no-failure filter. (Recall that for each control surface there is basically an estimator for the coefficients of the failure signature function.) Implementing an age-weighting filter for only the first, no-failure filter has been found to result in little change in the size of the decision functions. Age-weighting should thus be implemented in the matched filters as well. These filters are implemented in "information form", a form equivalent to the more common form of the Kalman filter.

The change in the standard filter equations can be mapped into the information form equations. This results in changes in the propagation equations for the information vector and information matrix. In the matched filters,

$$\chi'(k+1) = \frac{1}{s} A_{\phi} \chi'(k) + G^T(k+1)M^{-1}(k+1)\underline{y}(k+1) \quad (4.9)$$

$$S'(k+1) = \frac{1}{s} A_{\phi} S'(k)A_{\phi}^T + G^T(k+1)M^{-1}(k+1)G(k+1) \quad (4.10)$$

Here,

- A_{ϕ} is the single-step transition matrix for the coefficients, a , being estimated;
- G is the residual influence matrix for the system;
- γ is the residual of the no-failure filter; and
- M is the residual covariance of the incoming measurements γ including the effect of age-weighting.

As with the age-weighted filter, only the steady-state implementation of matched filters with age-weighting will be tested in this report.

The effect of age-weighting on the OSGLR algorithm can be seen from Figures 4.8 and 4.9. The decision functions for the off-nominal, no-failure test case and the -0.01745 rad (-1° deg) elevator bias failure (occurring at 10 s) test case with age-weighting time constant of 15 s are shown in Figures 4.8 and 4.9, respectively. The largest value of the decision functions for the off-nominal test case is reduced by age-weighting from 1,100,000 (at 50 s and increasing) to 45,000 for this age-weighting time constant of 15 s. The major benefit of age-weighting is to limit the decision functions caused by modeling errors. Otherwise, false alarms would be certain to occur. However, age-weighting also reduces and limits the decision functions caused by failures. The largest value of the decision functions for the -0.01745 rad (-1 deg) elevator bias failure test case was reduced by age-weighting from 400,000 (at 50 s and increasing) to 40,000 (and increasing at 50 s although more slowly) for the time constant of 15 s.

The effect of age weighting ultimately depends on the age-weighting time constant chosen. As the time constant is decreased, past information will be discarded sooner and the size of the decision functions caused by both modeling errors and failures will decrease. However, in order to allow the state estimates to converge, the age-weighting time constant should be larger than the time constant associated with the smallest closed-loop filter eigenvalue. With no age-weighting, the

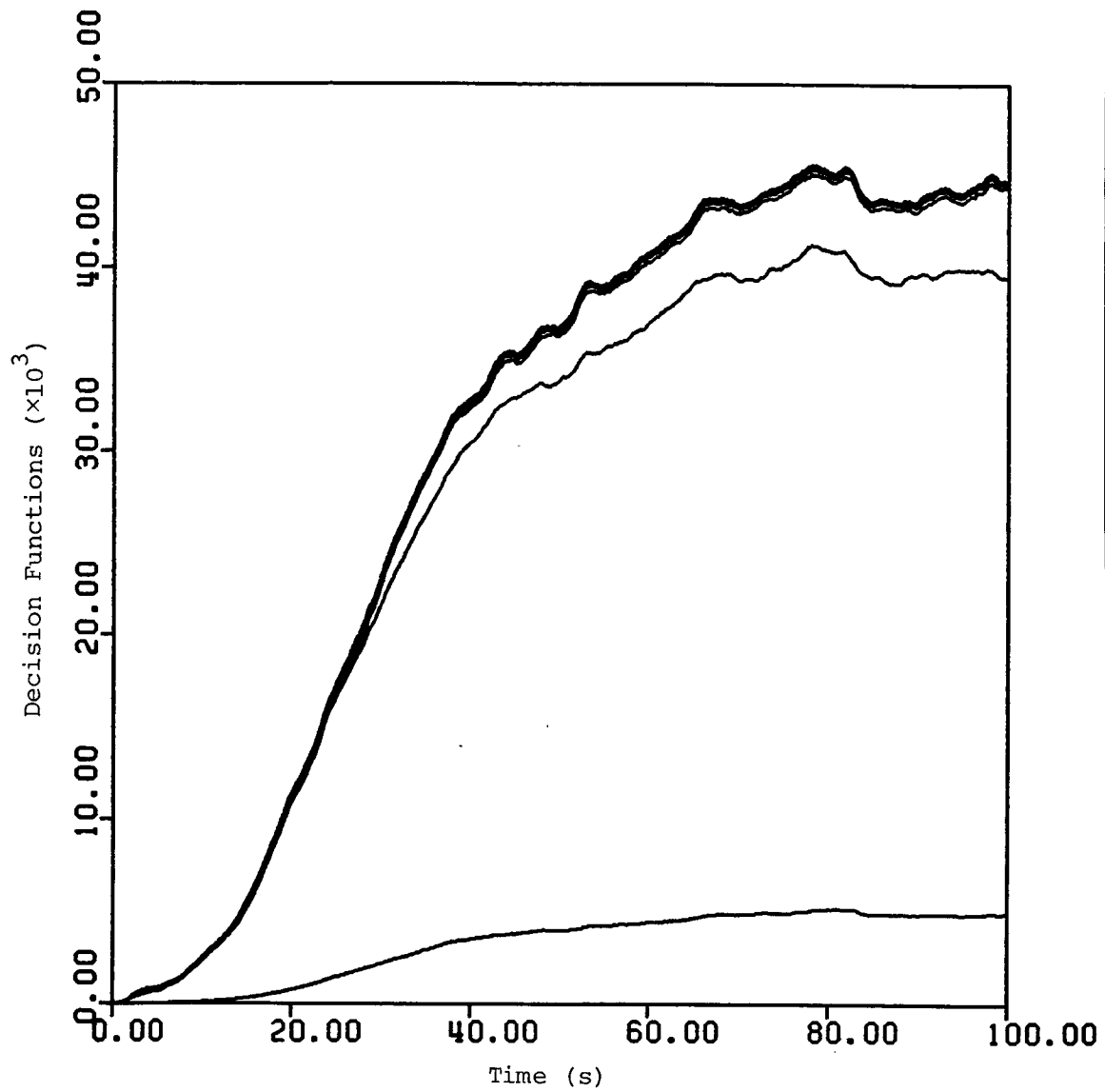


Figure 4.8 Decision functions produced by an age-weighted OSGLR algorithm

- no failures
- off-nominal cruise flight condition of 102.9 m/s and 1524.0 m
- age-weighting time constant of 15 s

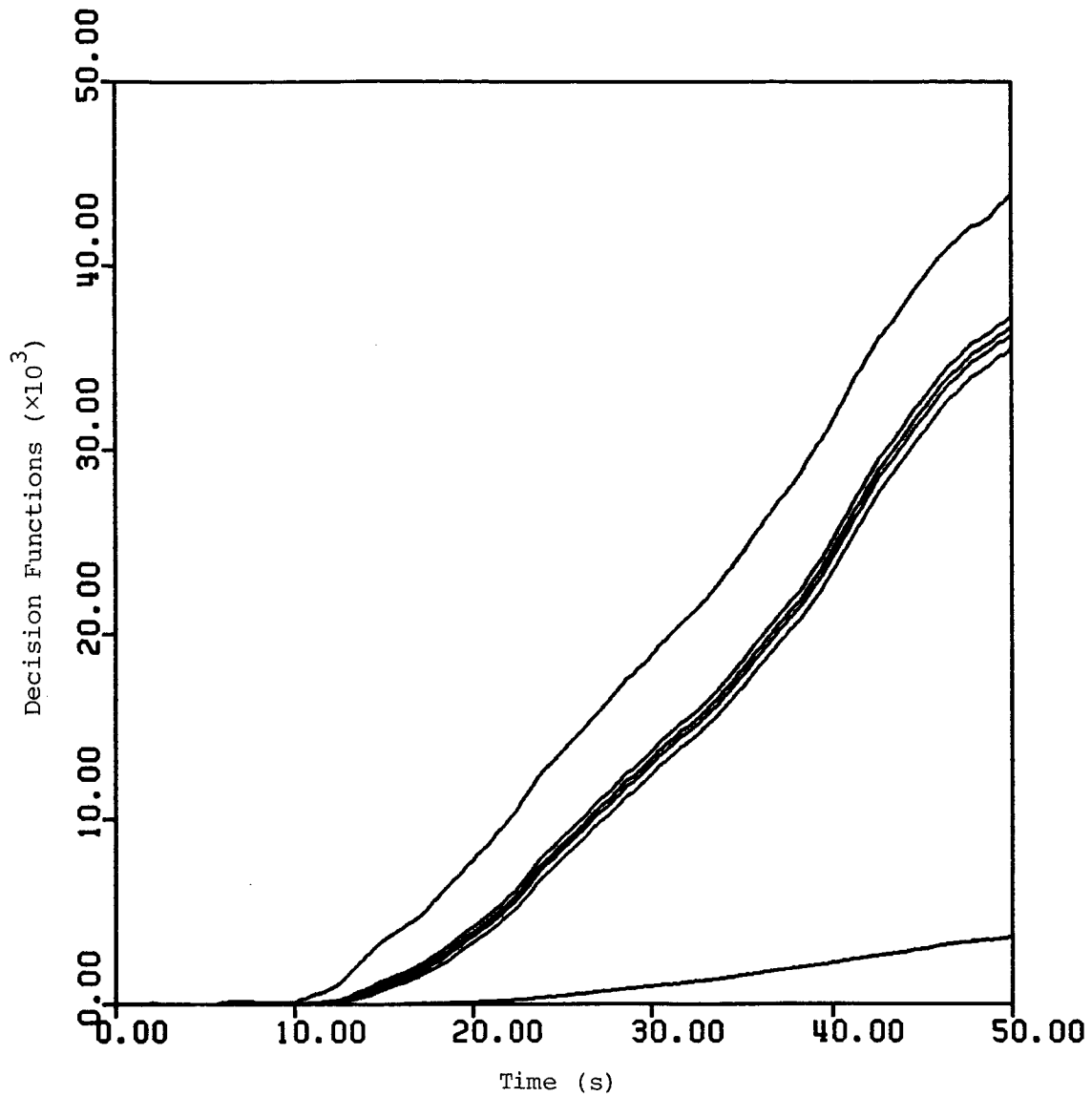


Figure 4.9 Decision functions produced by an age-weighted OSGLR algorithm

- -0.01745 rad (-1°) elevator bias failure at 10 s
- nominal flight condition of 77.2 m/s and 304.8 m
- age-weighting time constant of 15 s

largest filter time constant is 1.4 s. Small age-weighting time constants may also cause difficulty in the convergence of the higher order basis function coefficient estimates. Figure 4.10 shows the estimated rudder basis function coefficients for a 0.001745 rad/s (0.1°/s) rudder ramp failure starting at the beginning of the test case. The age-weighting time constant is 3 s. The first four coefficients converge reasonably well, whereas the last two, although they remain fairly well behaved, have more difficulty. Still, the convergence of the basis function coefficients was adequate for this case.

The 3 s age-weighting time constant was investigated in addition to the 15 s time constant already considered. The decision functions for the off-nominal, no-failure test case and the -0.01745 rad (-1.0 deg) elevator bias failure test case with age-weighting time constant of 3 s are shown in Figures 4.11 and 4.12. The 3 s time constant reduces the largest value of the decision functions for the off-nominal test case from 45,000 for the 15 s time constant to 1600. Likewise, the maximum magnitude of the decision functions for the -1 deg elevator bias failure test case was reduced from 45,000 (and increasing) to 3500. Based on these two test cases, the 3 s time constant produces the greatest reduction in the decision function caused by mismodeling while causing the least reduction in the decision functions resulting from a failure. But an age-weighted time constant this small will make detecting failures of limited time duration difficult as the OSGLR algorithm will forget that a failure had occurred. These failures may not be significant though. Therefore, in the interest of keeping the decision functions as insensitive to modeling errors as possible, the 3 s age-weighting time constant will be used from henceforth.

4.5 Summary and Conclusions

Several options for accommodating modeling errors in failure detection and isolation have been discussed. These included dynamic thresholds, dynamic decision regions, model error estimation, and robust

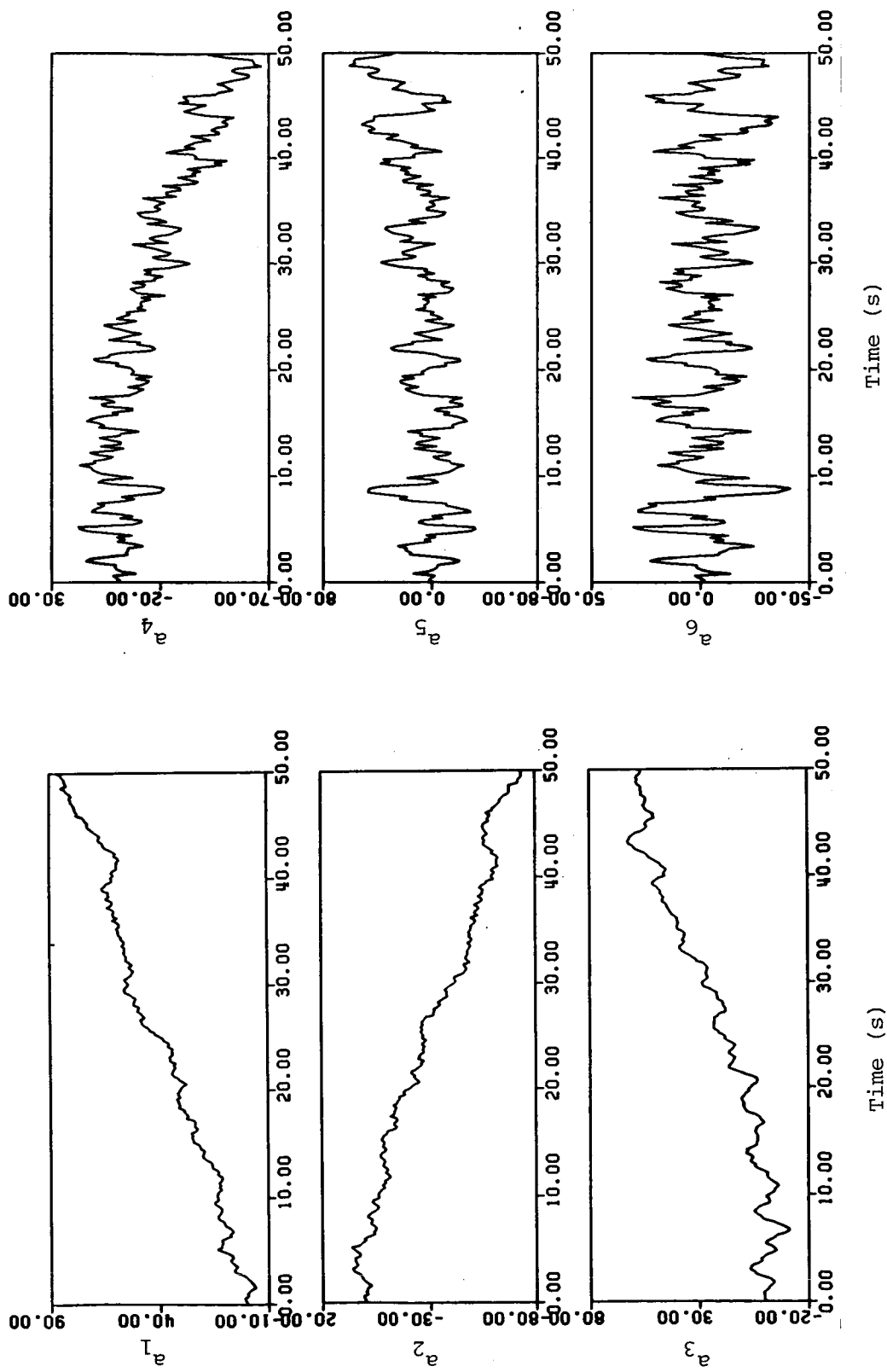


Figure 4.10 Estimated rudder basis function coefficients for a 0.001745 rad/s (0.1° deg/s) rudder ramp failure starting at t=0 produced by an age-weighted OSGLR algorithm with age-weighting time constant of 3 seconds

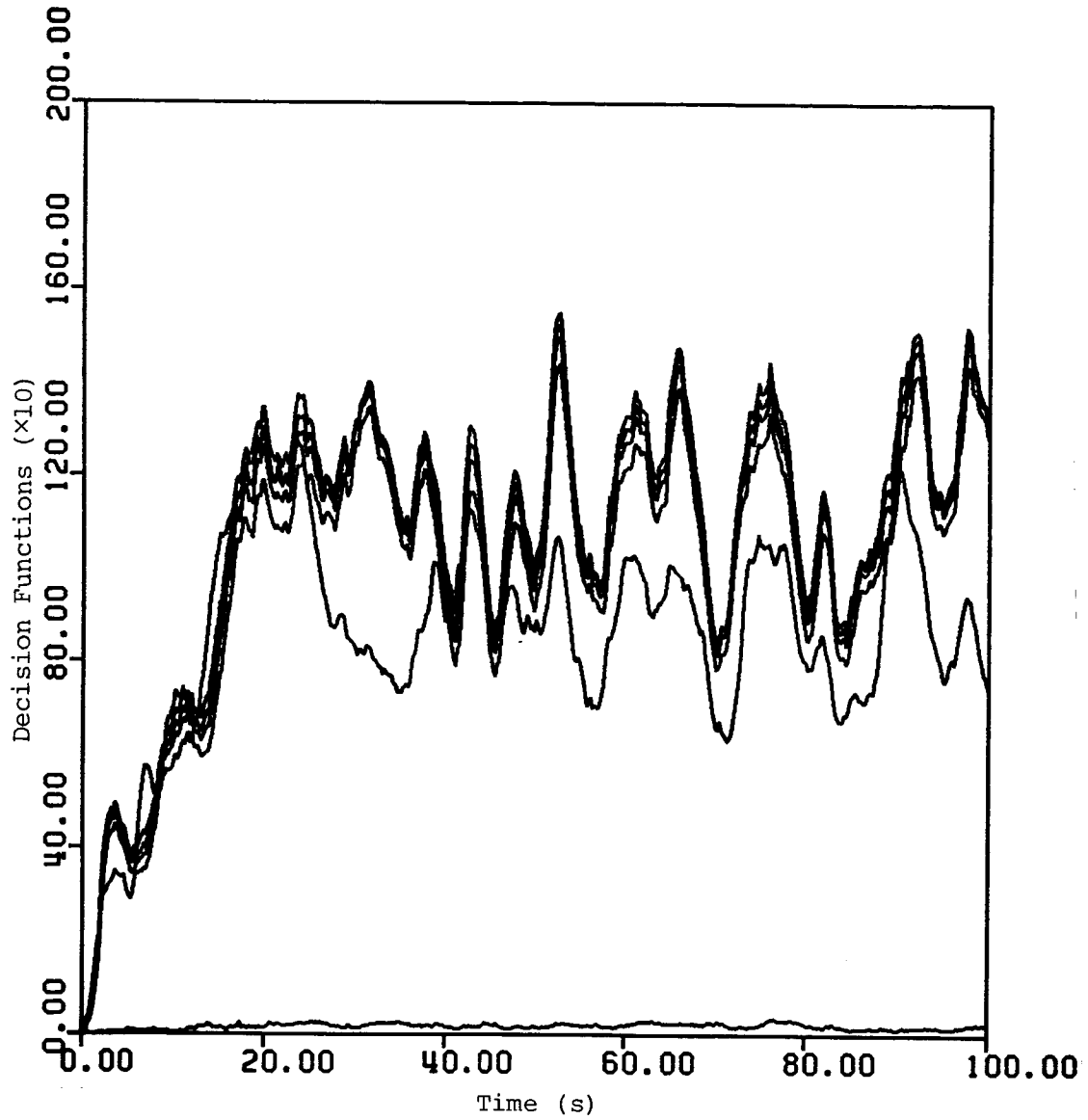


Figure 4.11 Decision functions produced by an age-weighted OSGLR algorithm

- no failures
- off-nominal cruise flight condition of 102.9 m/s and 1524 m
- age-weighting time constant of 3 s

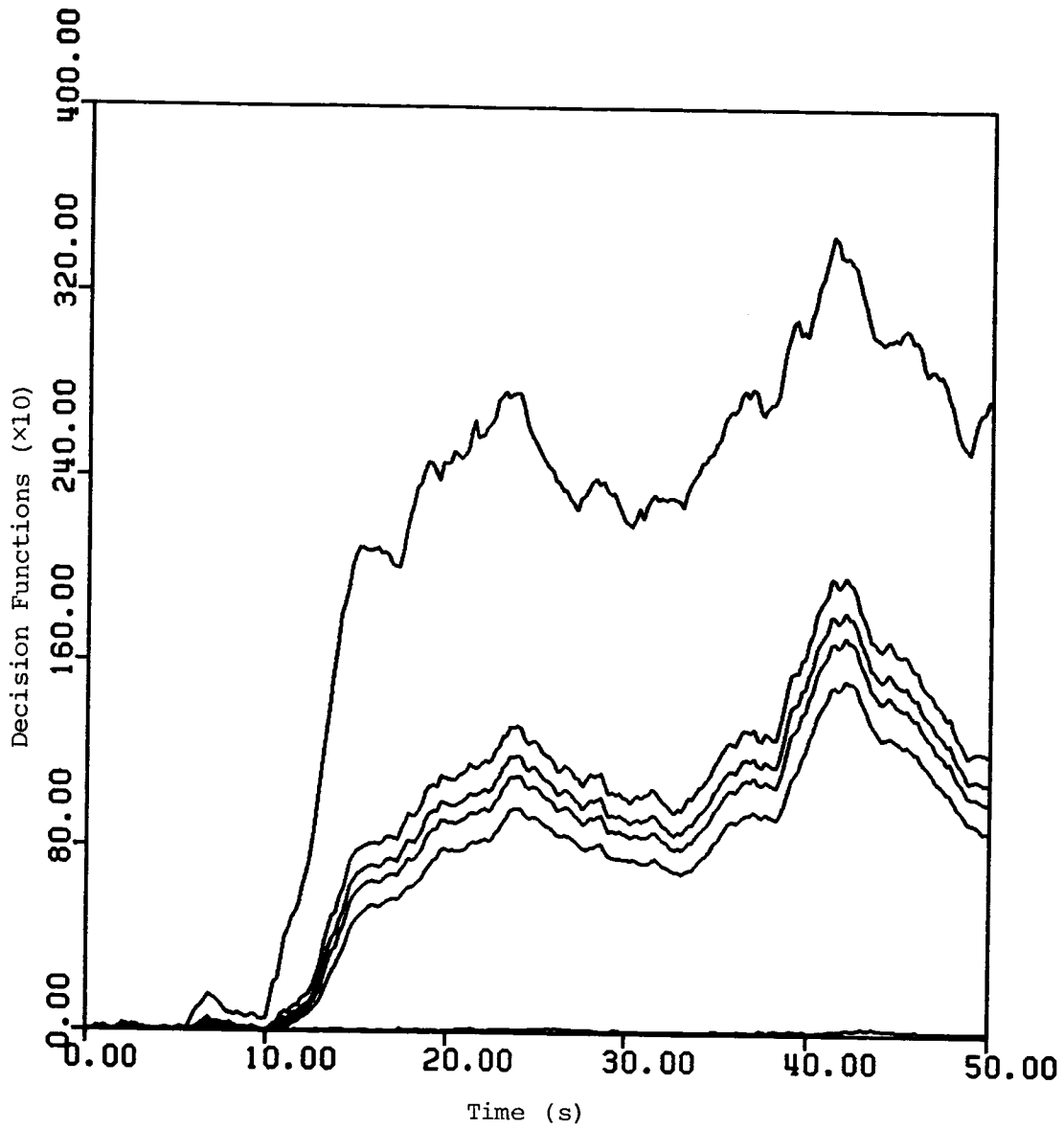


Figure 4.12 Decision functions produced by an age-weighted OSGLR algorithm

- -0.01745 rad (-1°) elevator bias failure at 10 s
- nominal cruise flight condition of 77.2 m/s and 304.8 m
- age-weighting time constant of 3 s

residual generation. Using dynamic thresholds is a simple approach to reducing false alarms caused by modeling errors. However, since modeling errors will, in general, cause the decision functions to grow in an unlimited manner, this approach would not give satisfactory performance alone. Also, there is no convenient systematic approach for selecting the dynamic thresholds. The dynamic decision region approach alters the information matrix used to weight the information vector in calculating the decision function to better reflect the uncertainties associated with modeling errors. Similar to the dynamic threshold approach, this approach alone could not reduce the effects of mismodeling satisfactorily. In addition, the procedure suggested to design these dynamic decision regions may as in the case of the C-130 aircraft, require significant effort. Model error estimation probably would be the most difficult and computationally burdensome of the four approaches. Two ideas were presented to improve the robustness of the filter used to generate residuals for the OSGLR algorithm. The first was to add process noise in certain directions (e.g., specific states). While adding process noise worked well for the few cases tested, the selection of the noise is an iterative process and may only be valid for that particular linear system model. The second idea, age-weighted filter, was found to be simple, general, and very effective. Age-weighted filtering allows the consideration of only the more recent information for estimating aircraft state and the basis function coefficients. Consequently, modeling errors due to linearization or aircraft maneuvering do not cause the filters to diverge.

Age-weighted filtering, because of its simplicity and effectiveness, will be used to reduce the effects of modeling errors. The age-weighting time constant will be 3 s.

SECTION 5

DETAILED EVALUATION OF THE OSGLR ALGORITHM USING A SINGLE CRUISE LINEAR MODEL

5.1 Introduction

In the preliminary evaluation described in Section 2, the steady-state implementation of the OSGLR algorithm was tested at a nominal and an off-nominal cruise flight condition. Furthermore, only a few failure cases at the nominal cruise flight condition were tested. This section further examines the flight regime in the neighborhood of the nominal cruise flight condition 77.2 m/s (150 knots) at 304.8 m (1000 ft). The effects of sensor errors, off-nominal flight conditions including maneuvers, different turbulence intensity levels, steady winds, and nonzero flap deflections are considered.¹ Also, a number of bias failures are tested. Based on these results, the magnitude of bias failures that can be detected and the detection times (for this nominal flight condition) can be determined for a particular threshold.

In this and the following section, DF_i is the decision function whose failure hypothesis is that the i th control surface has failed. The control surfaces are defined in Table 5.1

¹ A summary of the test cases is presented in Appendix A for easy reference and comparison of the test cases presented in this section and in sections 4 and 6.

Table 5-1. C-130 control surface definition

Input	Control Surface
1	elevator
2	right aileron
3	left aileron
4	rudder
5	right flap
6	left flap

5.2 Sensor Errors and Dynamics

Misalignment, scale factor error, and quantization were added to the acceleration and angular rate measurements. Biases were added to the acceleration, angular rate, and attitude measurements. Sensor models including first-order lag filter dynamics were included for all the measurements except for the altitude rate.

The altitude rate measurement was eliminated because a sensor model was not readily available. The performance of the OSGLR algorithm was not affected in detecting and isolating elevator, right aileron, and right flap failures. However, eliminating the altitude rate measurement reduced the ability of the algorithm to isolate a 0.01745 rad (1 deg) rudder bias failure. Larger rudder failures, such as a 0.0349 rad (2 deg) bias failure, still could be easily isolated. Therefore, the elimination of the altitude measurement caused only a minor degradation in performance.

The OSGLR algorithm was tested with the sensor noise, errors, and dynamics shown in Table 5.2; the effect on the performance was too small to be evident. All the results presented in this report were produced with these effects of sensor noise, errors, and dynamics included.

Table 5.2 Sensor errors

Measurement	Standard Deviation	Misalignment (rad)	Scale Factor (percent)	Quantization	Bias	Time Constant of lag filters (s)
Airspeed	3.35 m/s (11 ft/s)	-	-	-	-	.03
Normal Acceleration	.3 m/s ² (.98 ft/s ²)	.00183	.0114	.011 m/s (.036 ft/s)	-.001319 m/s (-.402E-03 ft/s)	.000375
Lateral Acceleration	.3 m/s ² (.98 ft/s ²)	.00157	.087	.011 m/s (.036 ft/s)	-.00107 m/s (-.326E-03 ft/s)	.000375
Roll Rate	.0024 rad/s (.1375 deg/s)	.00034267	.0129	.0024 rad/s	.353E-07 rad	1.0E-06
Pitch Rate	.0007 rad/s (.04 deg/s)	.00031145	.0084	.0007 rad/s	-.2236E-07 rad	1.0e-06
Yaw Rate	.0007 rad/s (.04 deg/s)	.00037026	.0176	.0007 rad/s	.1173E-07 rad	1.0E-06
Roll	.01 radians (.573 degrees)	-	-	-	-	.02
Pitch	.01 radians (.573 degrees)	-	-	-	-	.02
Yaw	.01 radians (.573 degrees)	-	-	-	-	.02
Altitude	3.05 m (10 ft)	-	-	-	-	.03

5.3 Off-Nominal, No-Failure Flight Conditions

The steady-state implementation of the OSGLR algorithm based on the 77.2 m/s (150 knot) linear model was tested for a variety of maneuvering and other off-nominal flight conditions to determine their effects on the performance of the algorithm. This testing served to determine the range of flight conditions for which the 77.2 m/s (150 knot) linear model is valid for the purposes of FDI. Light and thunderstorm turbulence and steady wind conditions were also tested.

5.3.1 Maneuvering Test Case

The first test case considered was a combination of cruise flight conditions and turning, acceleration, and climb maneuvers as described in Table 5.3. This test case will be referred to as the maneuvering test case. The aircraft begins cruising at 77.2 m/s (150 knots), then turns at 0.0524 rad/s (3 deg/s), returns to level flight, accelerates with full thrust, climbs at first with nominal thrust level and later full thrust, and finally turns slowly while climbing at full thrust. The decision functions for this test case are shown in Figure 5.1. The decision functions increase slightly as the aircraft rolls to begin the turn and again as the aircraft rolls to level flight. As full thrust is applied and the aircraft accelerates at an approximately constant altitude, the decision functions increase significantly. The decision functions decrease and become small again with the thrust level returning to the nominal value and the velocity decreasing with the aircraft climbing. In order to maintain the climb, the thrust level is increased and the decision functions increase significantly once again.

As thrust level, or alternatively thrust, is an actual input to the system, incorporating thrust level or thrust into the linear model as an input might reduce the decision functions at off-nominal thrust levels. Thrust was found to be more effective than thrust level. Thrust is actually a nonlinear function of both thrust level and velocity. With thrust level as the input, some of the velocity dependence of thrust

Table 5.3 Maneuvering test case

<u>Time(s)</u>	<u>Maneuver</u>
0-20	Nominal cruise condition 77.2 m/s (150 knots) at 304.8 m (1000 ft), no flaps, 55% thrust level
20-25	Roll to 0.4363 rad (25 degrees)
20-55	Turn at approximately 0.0524 rad/s (3 deg/s)
50-55	Roll back to level flight
55-60	Nominal cruise condition
60-100	Thrust level increased to 100% causing the velocity to increase from 77.2 m/s (150 knots) to 102.9 m/s (200 knots)
100-125	Thrust level decreased to nominal value
105-165	Climb at an average rate of 6.7 m/s (22 ft/s)
125-165	Thrust level increased to 100%
145-165	Roll and turn slightly in addition to the climb

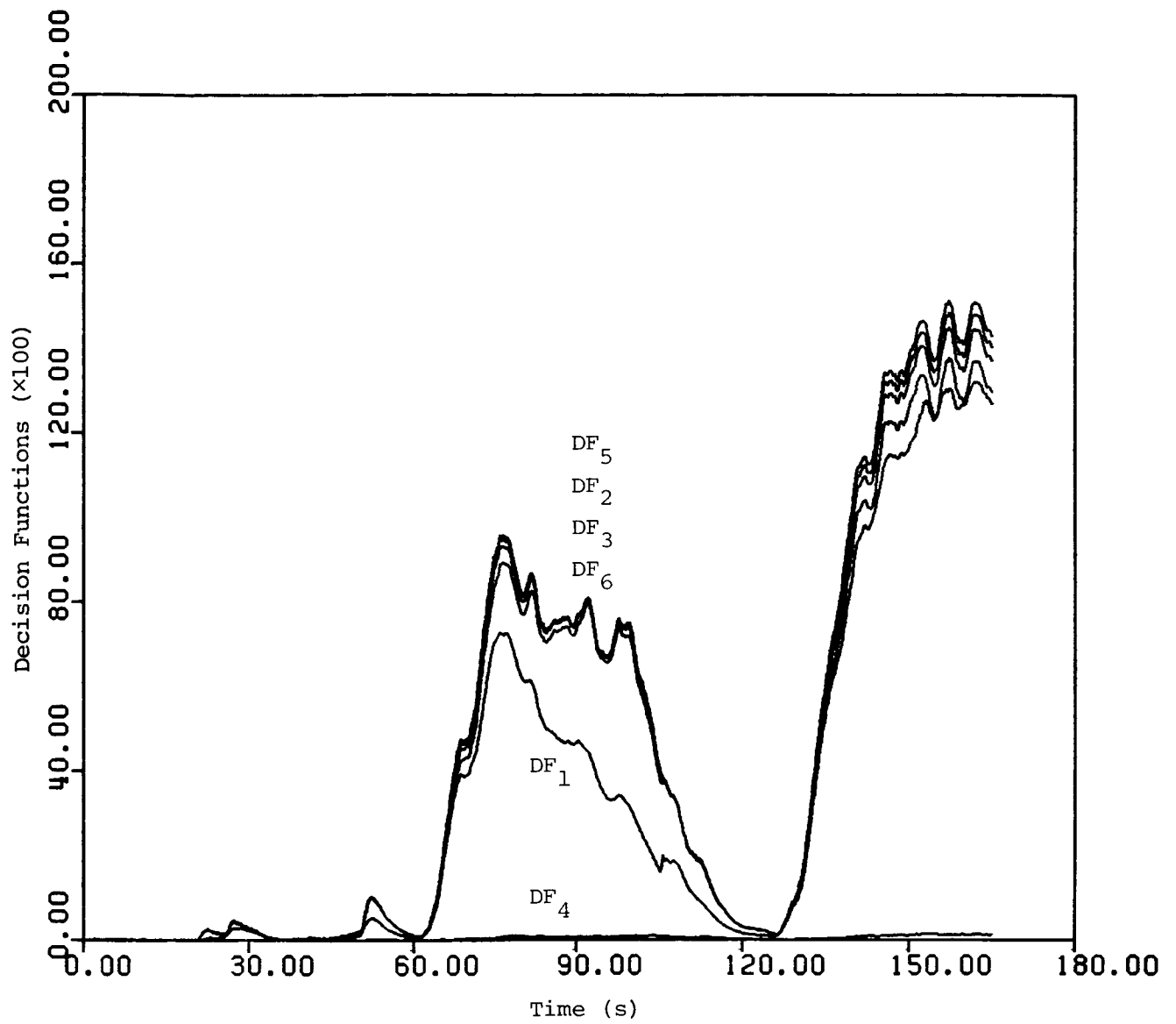


Figure 5.1 Decision functions for the maneuvering test case

could be accounted for in the linear model. Still, less mismodeling will result with thrust as the input. (Thrust was added to the linear model simply by adding another column to the B and D matrices.)

The decision functions for the maneuvering test case with thrust incorporated as an input are shown in Figure 5.2. The decision functions during the periods of off-nominal thrust levels are significantly decreased. The largest decision functions are now during the acceleration at constant altitude portion of the test case rather than the climb with 100% thrust portion. The decision functions during the acceleration at constant altitude portion increase as the velocity and therefore dynamic pressure increases. As the thrust level begins to decrease to the nominal value at 100 s, the decision functions also decrease. The increased thrust level during the climb portion of the trajectory does not cause any difficulty. The probable reason for this is that the dynamic pressure is close to the nominal dynamic pressure. Based on this test, the largest no-failure decision functions occur when both the dynamic pressure and the thrust are significantly off-nominal.

All further results use thrust as an input.

5.3.2 Turning Test Case

A longer turning maneuver, where the aircraft rolls and begins a 0.0524 rad/s (3 deg/s) right turn at 5 s, was also considered. At 65 s, the aircraft returns to level flight having turned 190 deg. The aircraft then turns left starting at 75 s, returning to level flight at 130 s. The decision functions, shown in Figure 5.3, are small with the two largest spikes occurring when the aircraft first rolls to turn right and when the aircraft returns to level flight after the left turn. These spikes appear to correspond to off-nominal aileron activity required to roll the aircraft.

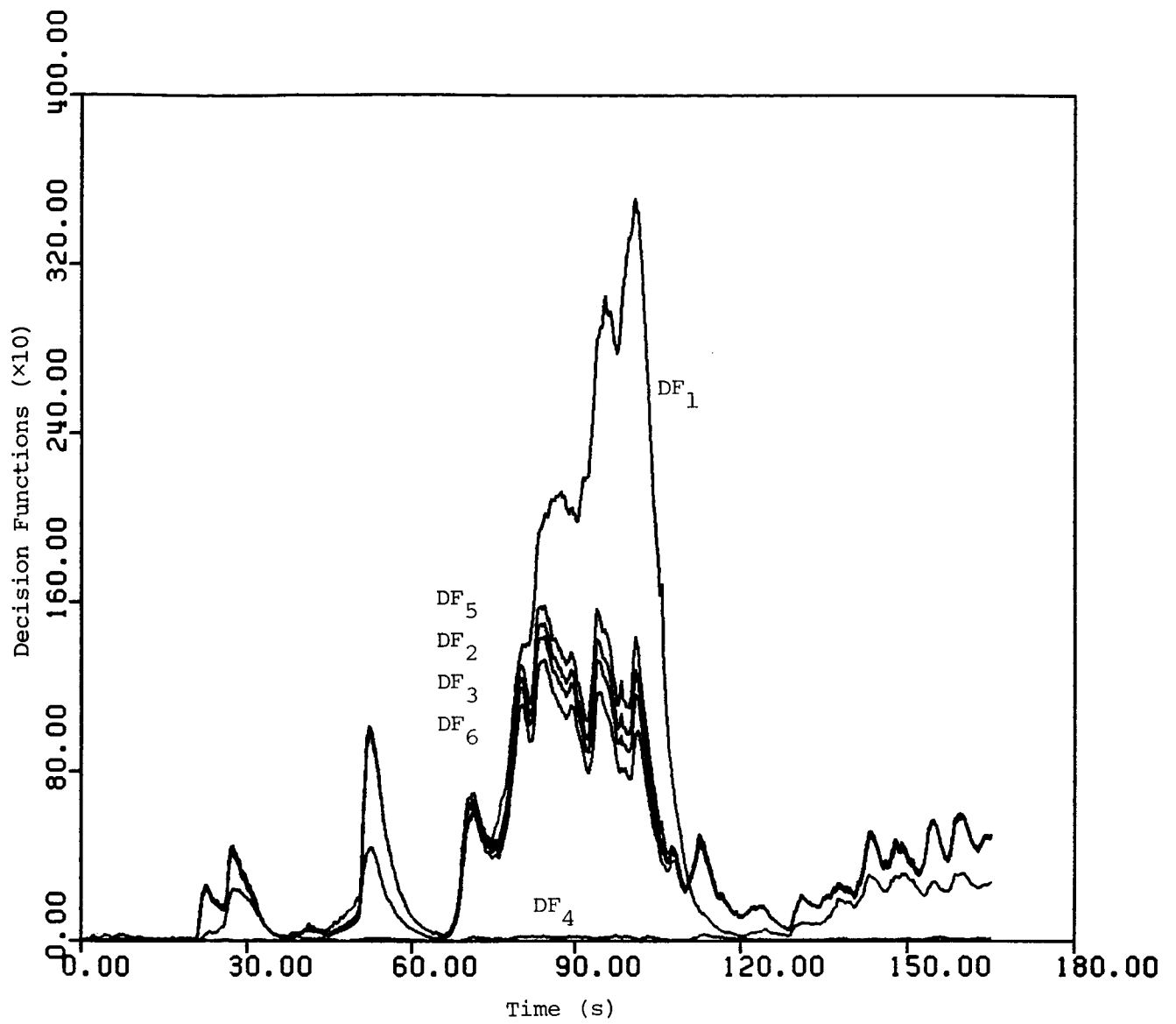


Figure 5.2 Decision functions for the maneuvering test case with thrust as an input

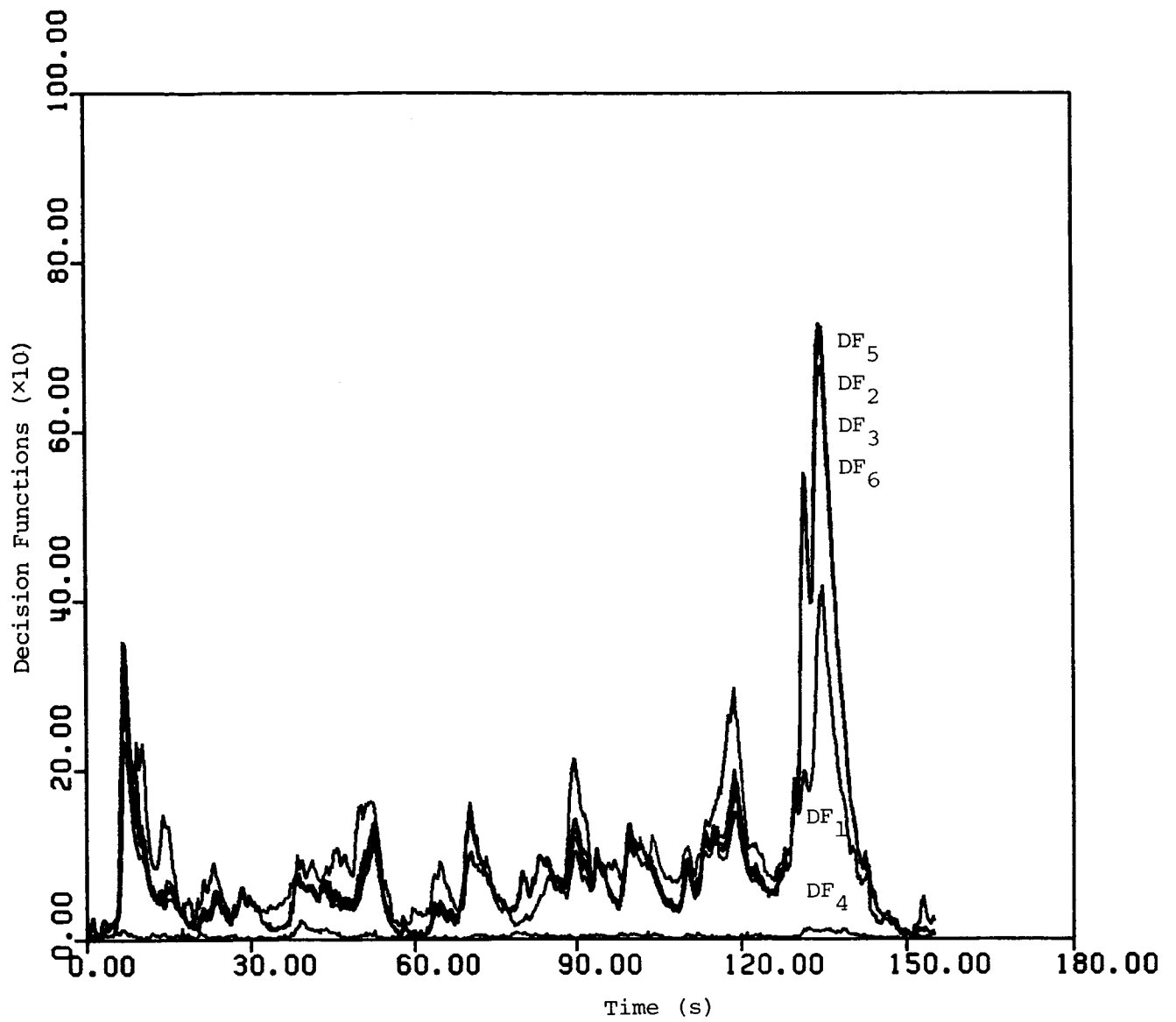


Figure 5.3 Decision functions with the aircraft turning right for 3.32 rad (190 deg) and then left for 3.14 rad (180 deg)

5.3.3 Maximum Rate-of-Climb Test Case

In the maneuvering test case, the climbing rate of the aircraft is significant but less than the maximum possible. In order to determine the largest decision functions that could be produced by a sustained climbing maneuver, the algorithm was tested with the aircraft climbing at an average rate of 10 m/s (33 ft/s) which is approximately the maximum rate of climb. At the beginning of the test case, the aircraft is flying at the nominal cruise condition. Five seconds into the flight, the thrust level is increased to 100% with the climb initiated at 15s. The decision functions (Figure 5.4) are larger than in the climbing portion maneuvering test case but only 800 larger than the largest decision function produced by the maneuvering test case.

5.3.4 Accelerating Test Cases

A number of accelerating cases were tested with the most severe case being the acceleration from 51.44 m/s (100 knots) to 102.9 m/s (200 knots) test case. The decision functions for this test case are shown in Figure 5.5. The largest decision functions are at the beginning of the test case. Initially, the airspeed of the aircraft is 51.44 m/s (100 knots) but the airspeed drops a few seconds later to 33.44 m/s (65 knots). This airspeed drop is caused partly by a large turbulence level at the beginning of the simulation run and also because the control surfaces are being moved to control the aircraft. The result of this airspeed drop is that the actual dynamic pressure a few seconds after the beginning of the test case is only 20% of the nominal dynamic pressure of the 77.2 m/s (150 knot) linear model. The linear model is clearly not valid in the neighborhood of 51.44 m/s (100 knots). The thrust level was increased to 100% starting at 10 s, causing the airspeed to increase. As the actual dynamic pressure approaches the nominal dynamic pressure, decision functions decrease. At 41 s, the airspeed is approximately 77.2 m/s (150 knots) which is the nominal airspeed of the linear model and the decision functions are very small in this region. They increase again as

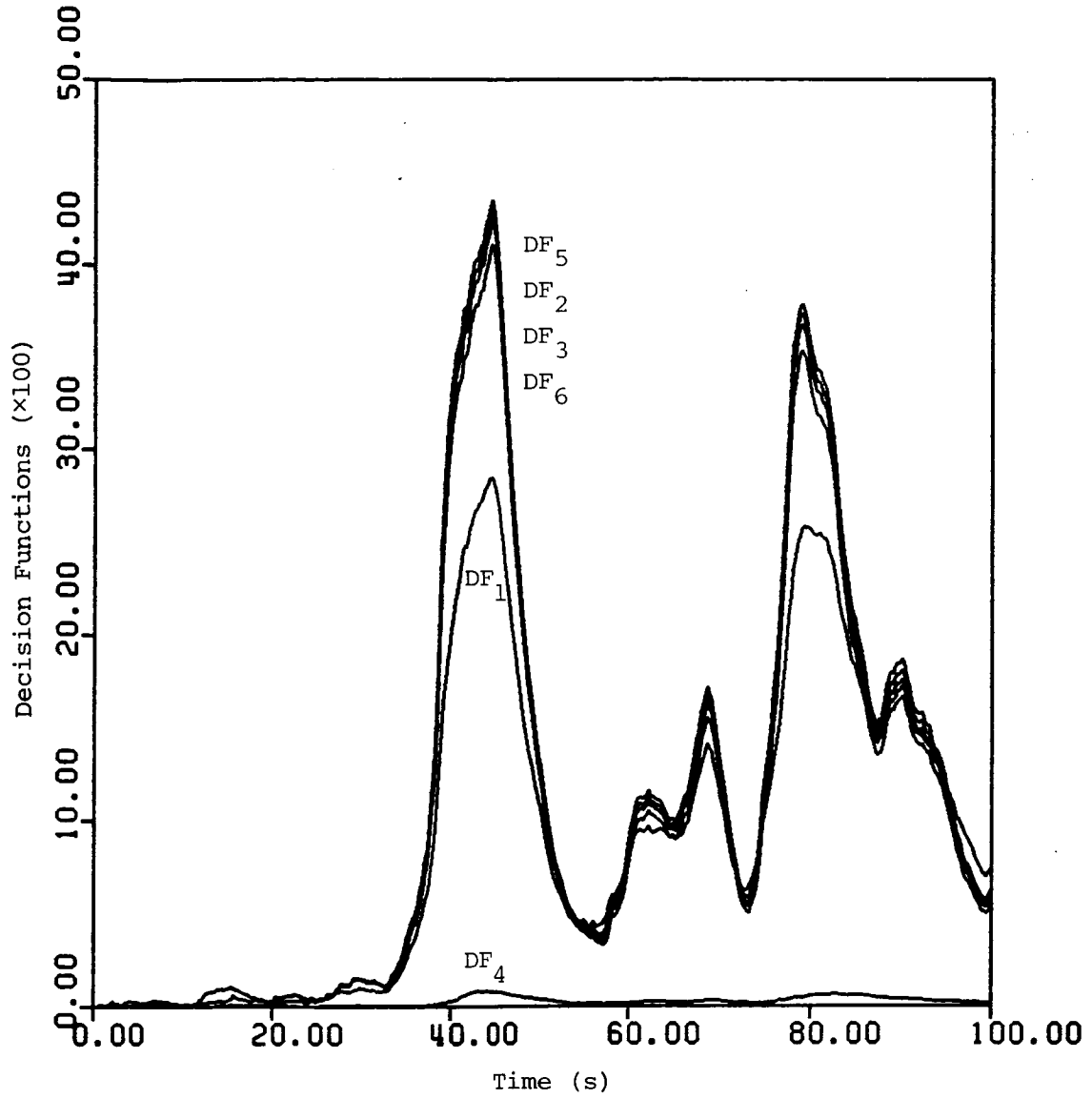


Figure 5.4 Decision functions for the maximum rate-of-climb test case

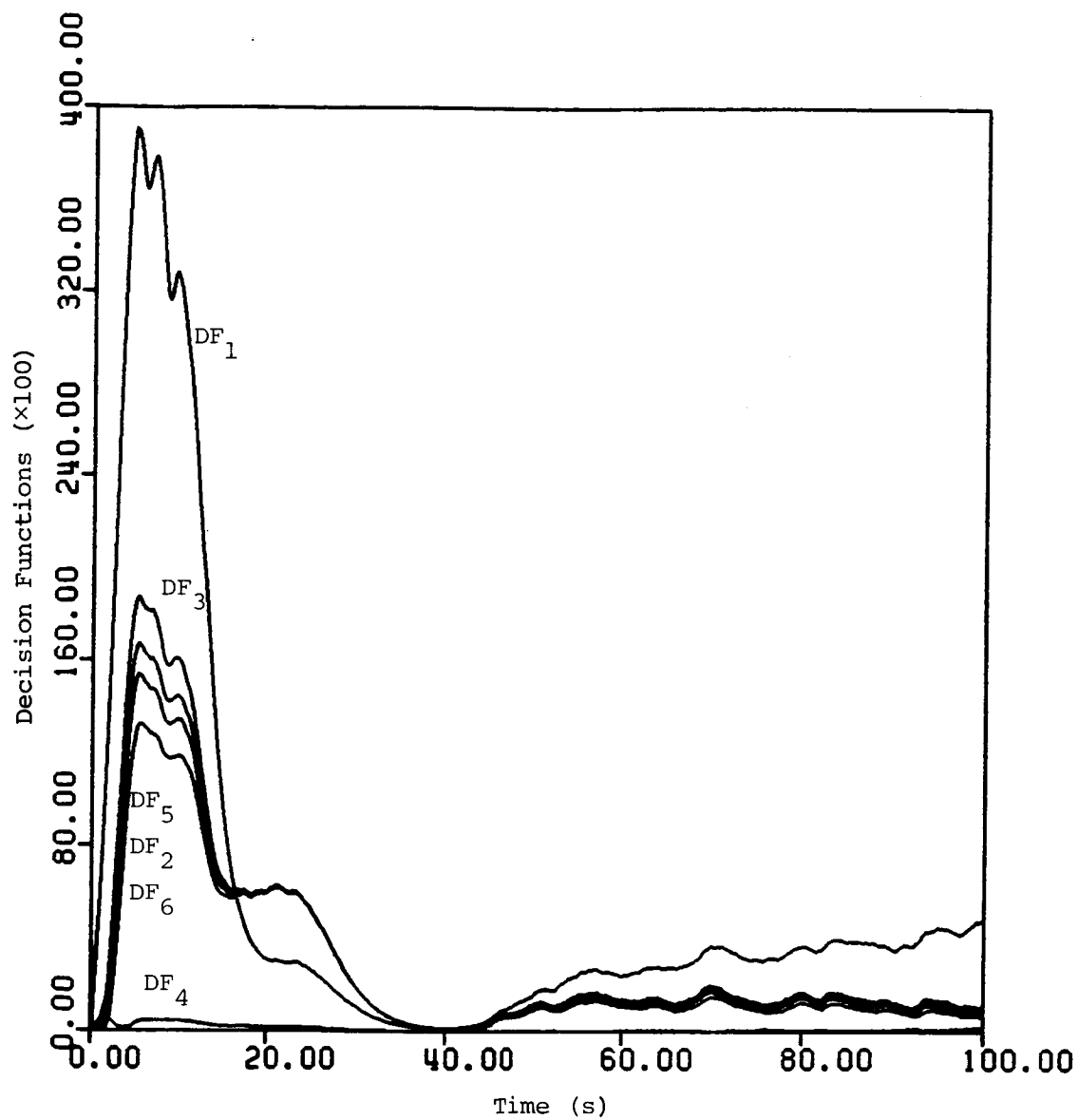


Figure 5.5 Decision functions for the acceleration from 51.44 m/s (100 knots) to 102.9 m/s (200 knots) test case

the velocity increases to 102.9 m/s (200 knots). Based on this test case, there appears to be more mismodeling at low dynamic pressures than at high dynamic pressures.

5.3.5 Decelerating and Descending Test Cases

To investigate decelerating flight, the aircraft was started at an airspeed of 102.9 m/s (200 knots) with a thrust level of 30%. (The thrust level required to maintain 102.9 m/s airspeed at 304.8 m (1000 ft) is 80%.) The altitude of 304.8 m (1000 ft) was approximately maintained. The airspeed at the end of the simulation run is approximately 51 m/s (100 knots). The decision functions, shown in Figure 5.6, are small until the airspeed drops below 61 m/s (118.5 knots). As in the maneuvering test case, the 150 knot linear model is not adequate for airspeeds in the neighborhood of 51 m/s (100 knots).

Decision functions for a descending test case are shown in Figure 5.7. The aircraft has an initial airspeed of 103 m/s at an altitude of 1524 m (5000 ft) with a thrust level of 20%. The aircraft descends to an altitude of 762 m (2500 ft) at the end of the test case. The final airspeed is approximately 77 m/s (150 knots). The decision functions are small with the larger magnitudes occurring in the first 35 s where the dynamic pressure is the most off-nominal.

5.3.6 Non-Zero Flap Deflections

In addition to maneuvers, the OSGLR algorithm was tested with the flaps extended 50, 75, and 100%. In each of the test cases, the flaps were extended starting at 5 s, and reached 50% to 100% in 5 to 15 s. The decision functions for the 50% test case shown in Figure 5.8 are small. However, the decision functions for the 75% test case, shown in Figure 5.9 are large. The decision functions for the 100% test case are approximately four times larger than those of the 75% case. One explanation for the large decision functions is that large deflections of the flaps

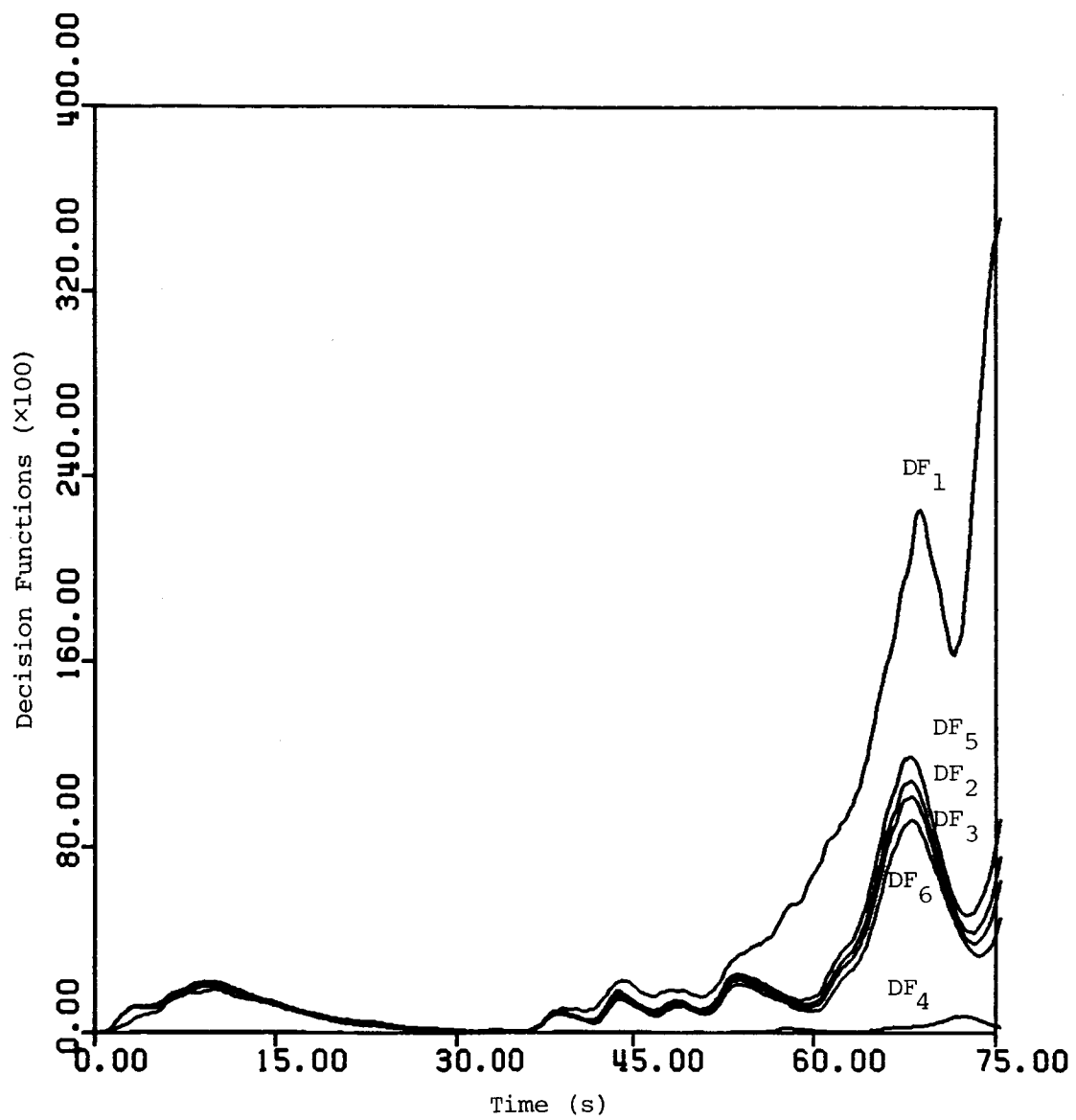


Figure 5.6 Decision functions for the decelerating at constant altitude from 102.9 m/s to 51 m/s test case

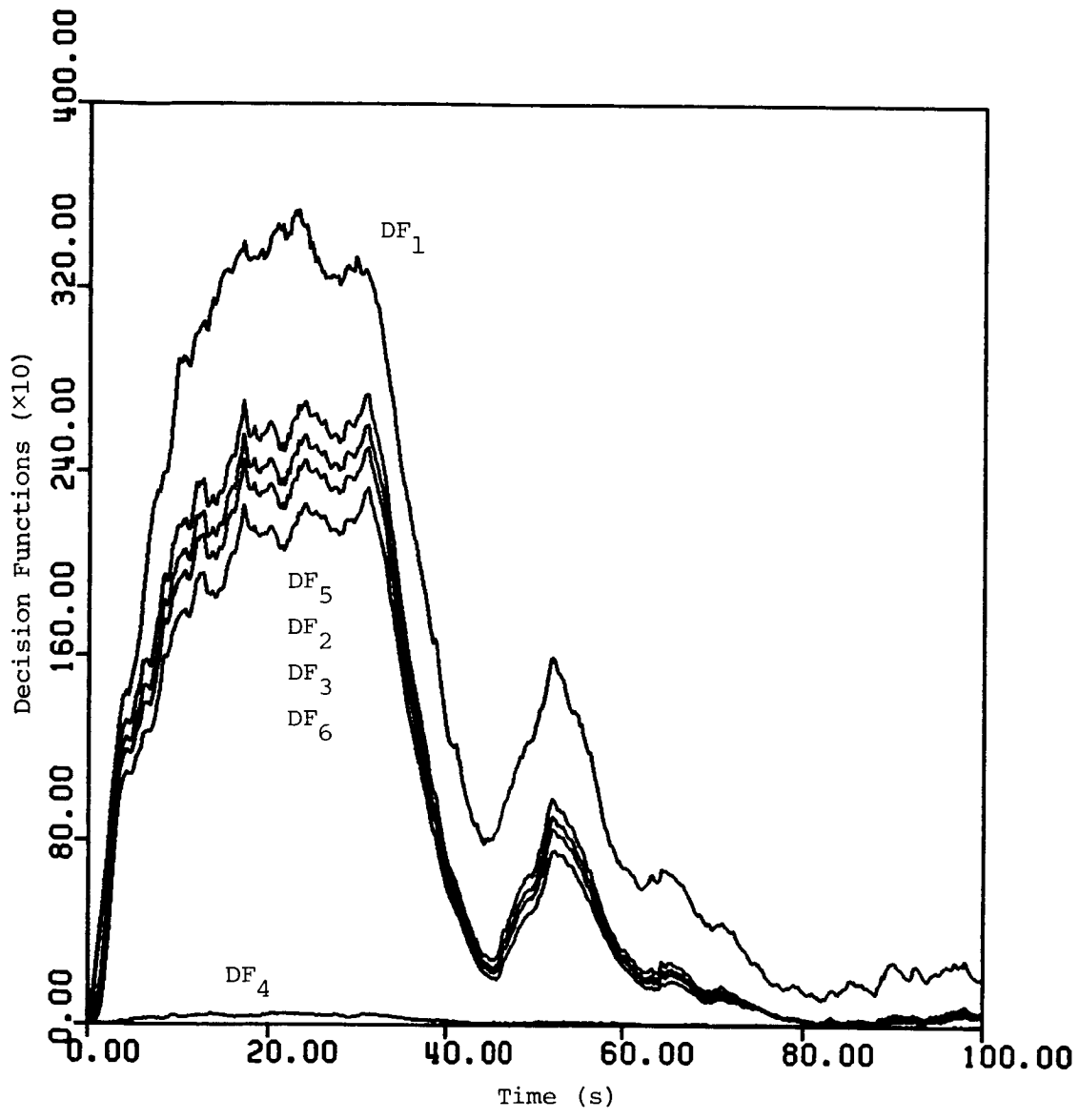


Figure 5.7 Decision functions for the descending from 1524 m (5000 ft) test case

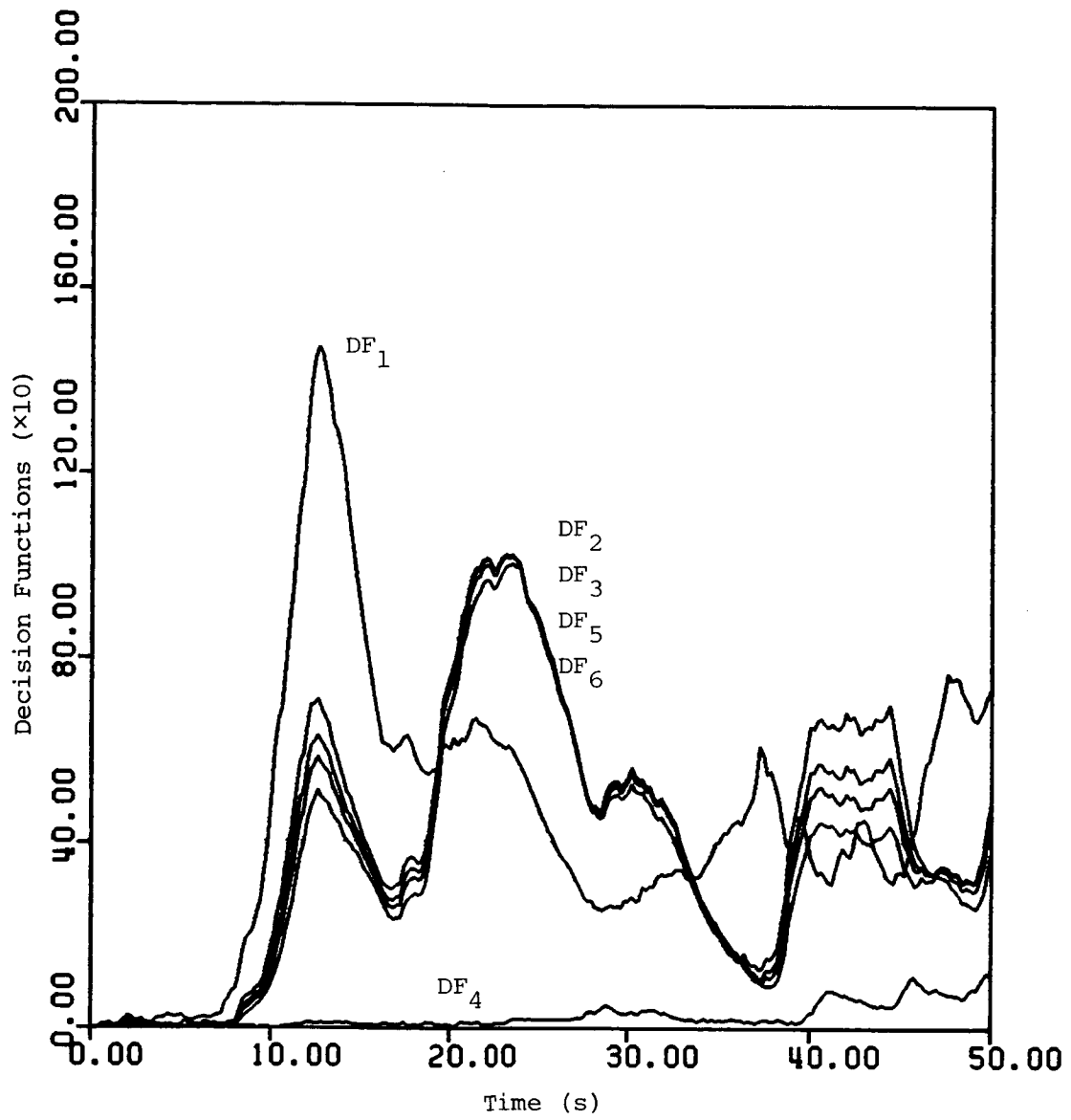


Figure 5.8 Decision functions for the 50% flap deflection test case

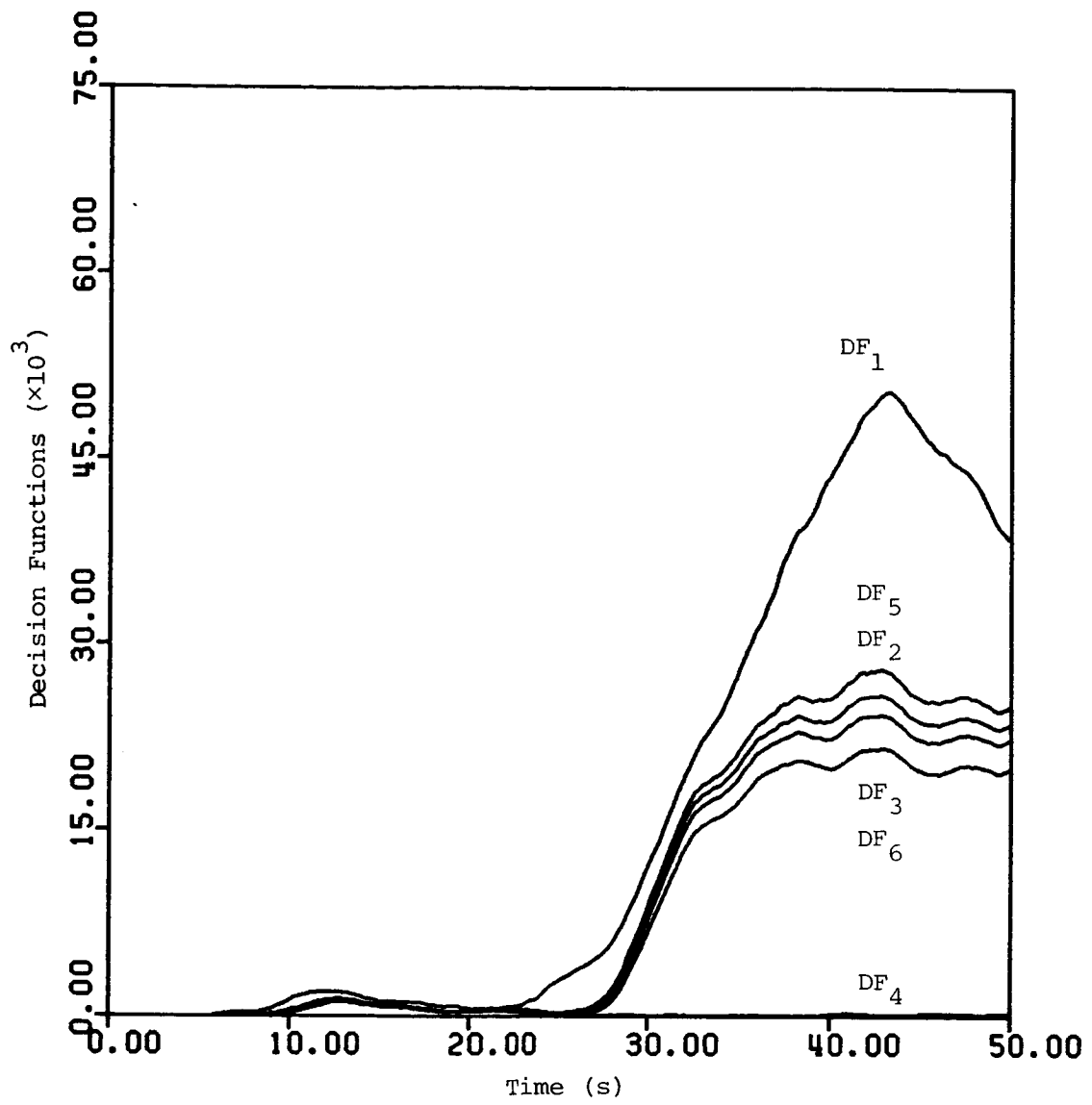


Figure 5.9 Decision functions for the 75% flap deflection test case

causes significant changes in the dynamics. Also, large flap deflections cause a significant decrease in the airspeed and therefore dynamic pressure.

5.3.7 Off-Nominal Turbulence and Steady Winds

The nominal turbulence used to test the OSGLR algorithm is the Dryden model with clear air scales and intensity of 1.98 m/s (6.5 ft/s) (Reference 12). As the turbulence model is incorporated into the linear model of the system, the nominal turbulence does not cause significant no-failure decision functions. To determine the effect of off-nominal turbulence, light turbulence of intensity 0.3 m/s (1 ft/s) and thunderstorm turbulence of intensity 6.4 m/s (21 ft/s) were tested. The decision functions for the maneuvering test case with light turbulence, shown in Figure 5.10, are slightly smaller than with the nominal turbulence intensity. The decision functions for the aircraft cruising at the nominal flight condition in thunderstorm turbulence are shown in Figure 5.11. The validity of this test case is questionable for the first 20 s as the turbulence causes the angle of attack to exceed the largest angle of attack for which the aerodynamic forces are modeled. (The simulation needs a pilot to control the aircraft adequately in thunderstorm turbulence.) In general, the decision functions due to thunderstorm turbulence are significant. One approach to reduce the effect of thunderstorm turbulence might be to develop the age-weighted filter gain and the OSGLR influence and information matrices for the thunderstorm case and schedule these matrices as a function of turbulence level. A simpler approach would be to use a higher nominal turbulence level. This approach should be adequate if detection and isolation at lower turbulence levels is not significantly degraded.

The effect of steady winds on the performance of the algorithm was determined by testing a number of wind conditions. The steady winds tested were headwinds, crosswinds, and a direction in between. These horizontal winds were all 10.3 m/s (20 knots). A downwind of 2.57 m/s

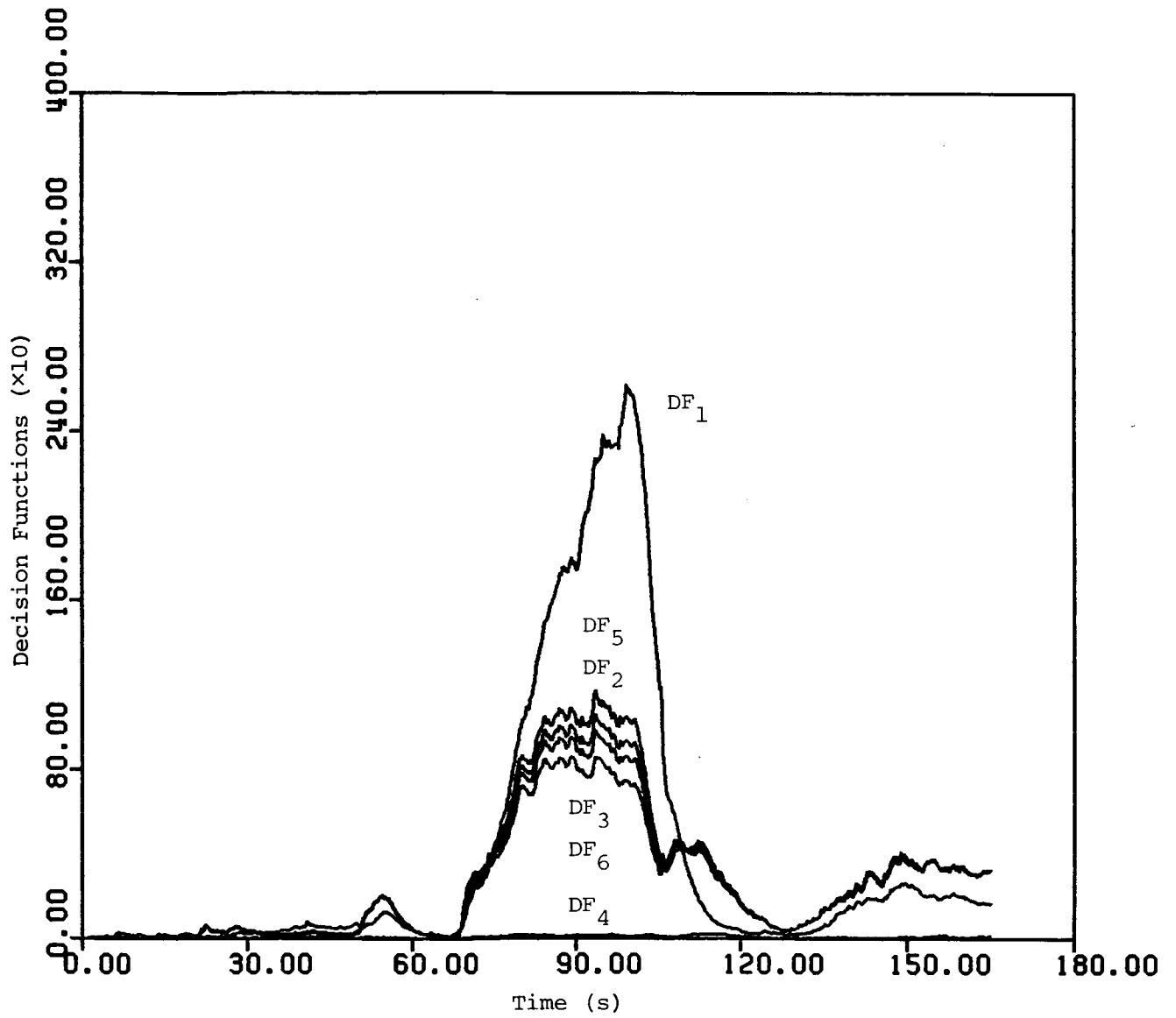


Figure 5.10 Decision functions for the maneuvering test case with light turbulence

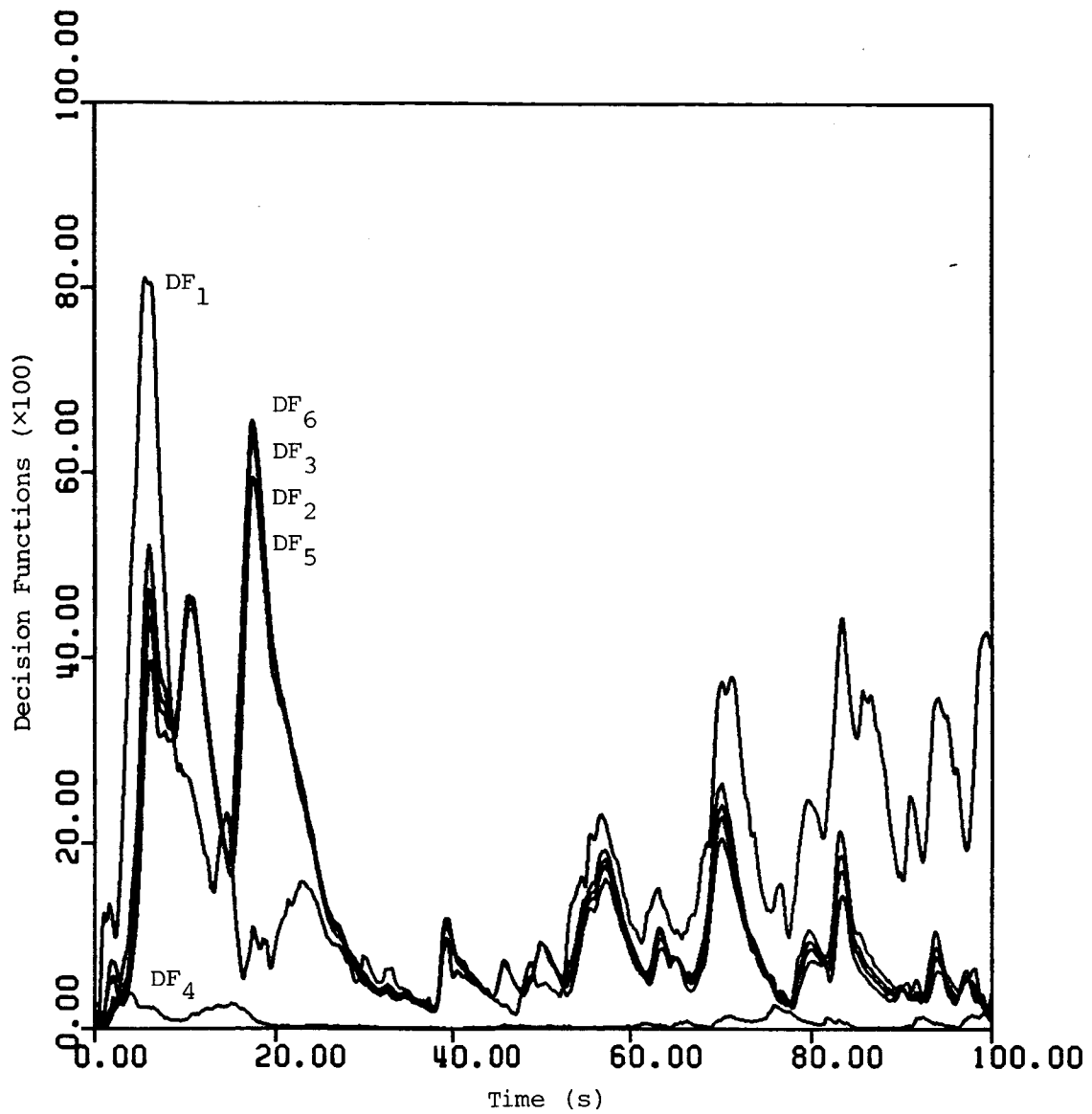


Figure 5.11 Decision functions for the aircraft flying at the nominal cruise flight condition in thunderstorm turbulence

(5 knots) was also tested. The crosswind test case produced the largest decision functions (Figure 5.12). The large decision functions in the first ten seconds of the test case are caused by the aircraft responding to the crosswind. In response to the crosswind, the thrust was increased momentarily and the ailerons and rudder were used to control the aircraft. After the initial transient, steady winds do not result in increased decision functions.

5.4 Failures

Elevator, right aileron, rudder, and right flap bias failures are considered in this section. With two exceptions, all the failures occur with the aircraft flying at the nominal cruise flight condition of 77.2 m/s (150 knots) at 304.8 m (1000 ft). The exceptions are elevator bias failures with the aircraft flying at two off-nominal airspeeds, 64.3 m/s (125 knots) and 90.0 m/s (175 knots). All the failures occurred 10 s into the simulation run.

A representative failure test case for each of the surfaces tested as well as the two off-nominal flight condition test cases will be presented. In lieu of the individual failure cases, results for the nominal flight condition failure test cases are then summarized, for each surface tested, in terms of the maximum decision function as a function of the time from the occurrence of the failure and the failure magnitude. The ability to isolate a failure of each of the surfaces tested is similarly examined.

5.4.1 Elevator Failure Test Case

The decision functions for the -0.0873 rad (-5 deg) elevator bias failure with the aircraft at the nominal cruise flight condition are shown in Figure 5.13. The growth of the decision functions is limited by the age-weighting, as in the off-nominal, no-failure cases. The failure

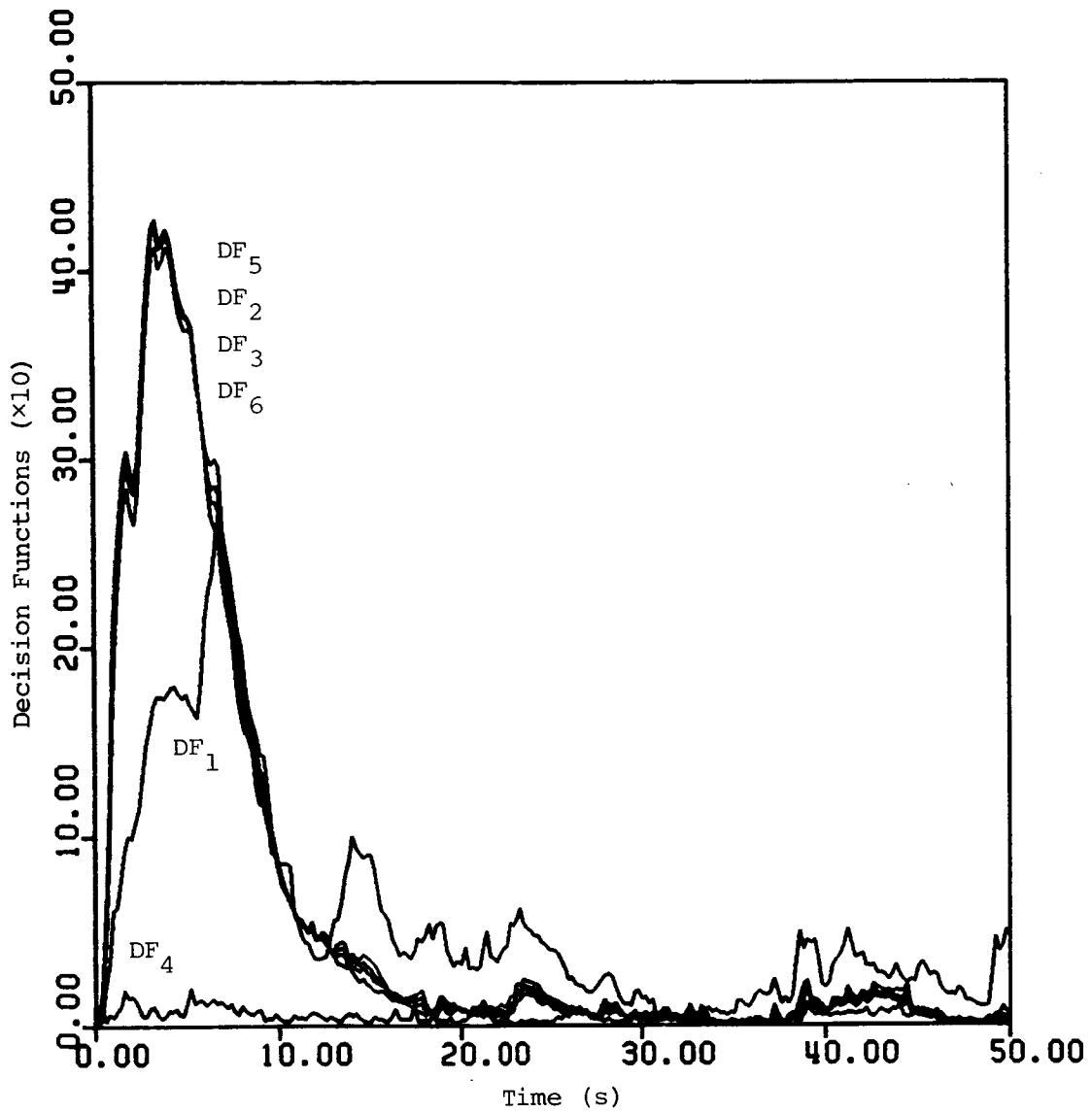


Figure 5.12 Decision functions for a 10.3 m/s (20 knots) crosswind test case

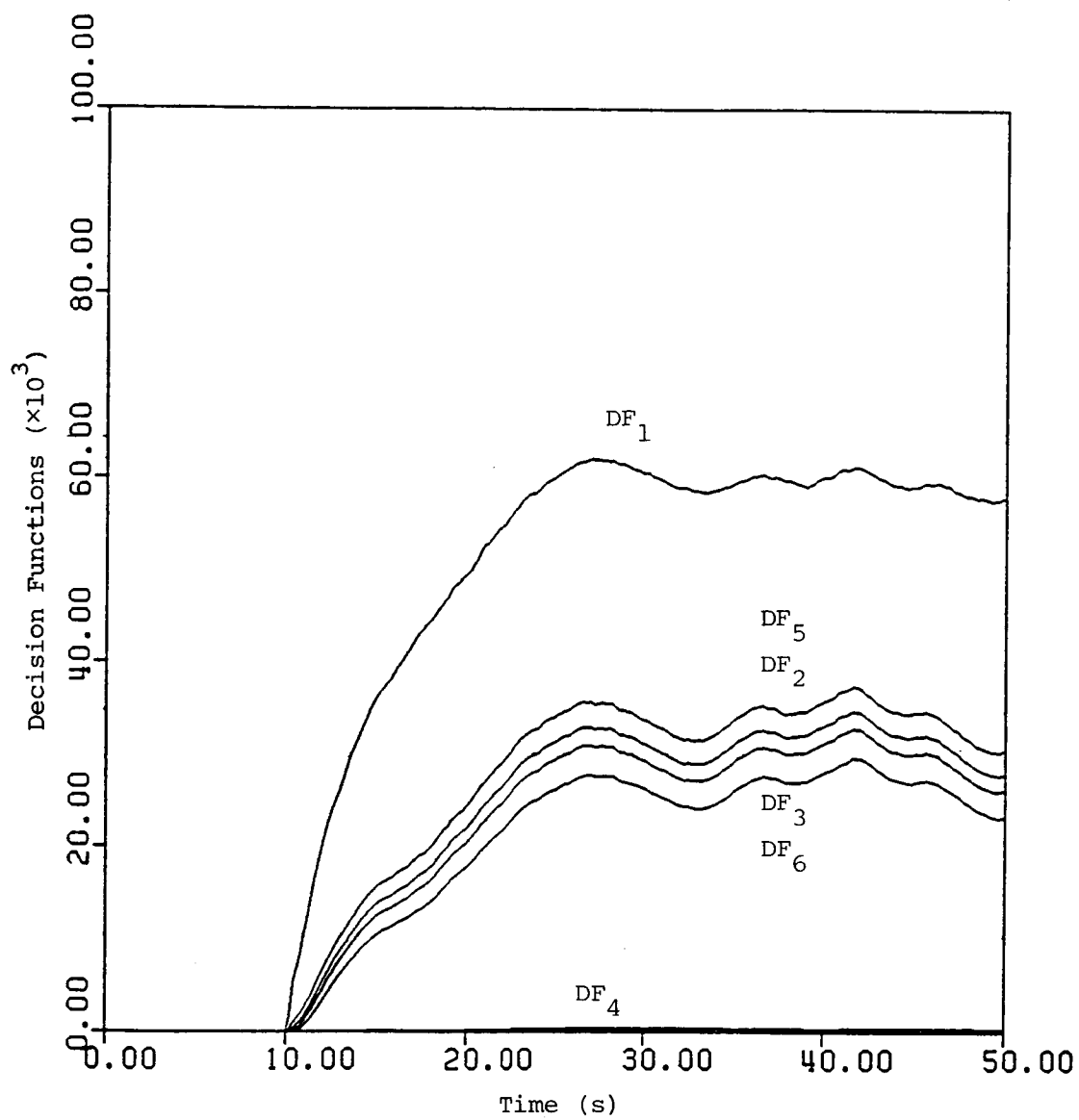


Figure 5.13 Decision functions for a -0.0873 rad (-5 deg) elevator bias failure

is easily detected if the detection threshold is less than 60,000. The failure can be detected in approximately 2 s if the threshold is less than 20,000. Four of the isolation decision functions, DF_{ij} , are shown in Figure 5.14 where DF_{ij} is defined to be

$$DF_{ij} = DF_i - DF_j$$

Isolation decision function DF_{14} , not shown in Figure 5.14, would have been even larger than those shown. Isolating this failure is straightforward.

5.4.2 Off-Nominal Elevator Failure Test Cases

The decision functions for the same failure with the aircraft flying at an airspeed of 64.3 m/s (125 knots) at the time of the failure are shown in Figure 5.15. The decision functions rise more slowly than for the same magnitude failure occurring with the aircraft flying at the nominal cruise flight condition. The effect of the failure is less because the dynamic pressure for this case is less than the nominal flight condition. Still, a detection threshold that could detect a failure of the same magnitude at the nominal airspeed could detect this failure. At approximately 35 s, the decision functions peak and decrease afterwards. This decrease is caused by a decrease in the airspeed. In Section 5.3, the OSGLR algorithm based on the 77.2 m/s (150 knot) linear model produced large no-failure decision functions at low speeds in the neighborhood of 100 knots. Apparently, the 77.2 m/s (150 knot) linear model does not model the aircraft well at these low speeds. Also, as just mentioned, a decrease in dynamic pressure will reduce the effect of the failure.

The decision functions for the -0.0873 rad (-5 deg) elevator bias failure with the aircraft flying with an airspeed of 90.0 m/s (175 knots) are shown in Figure 5.16. The decision functions rise more quickly than

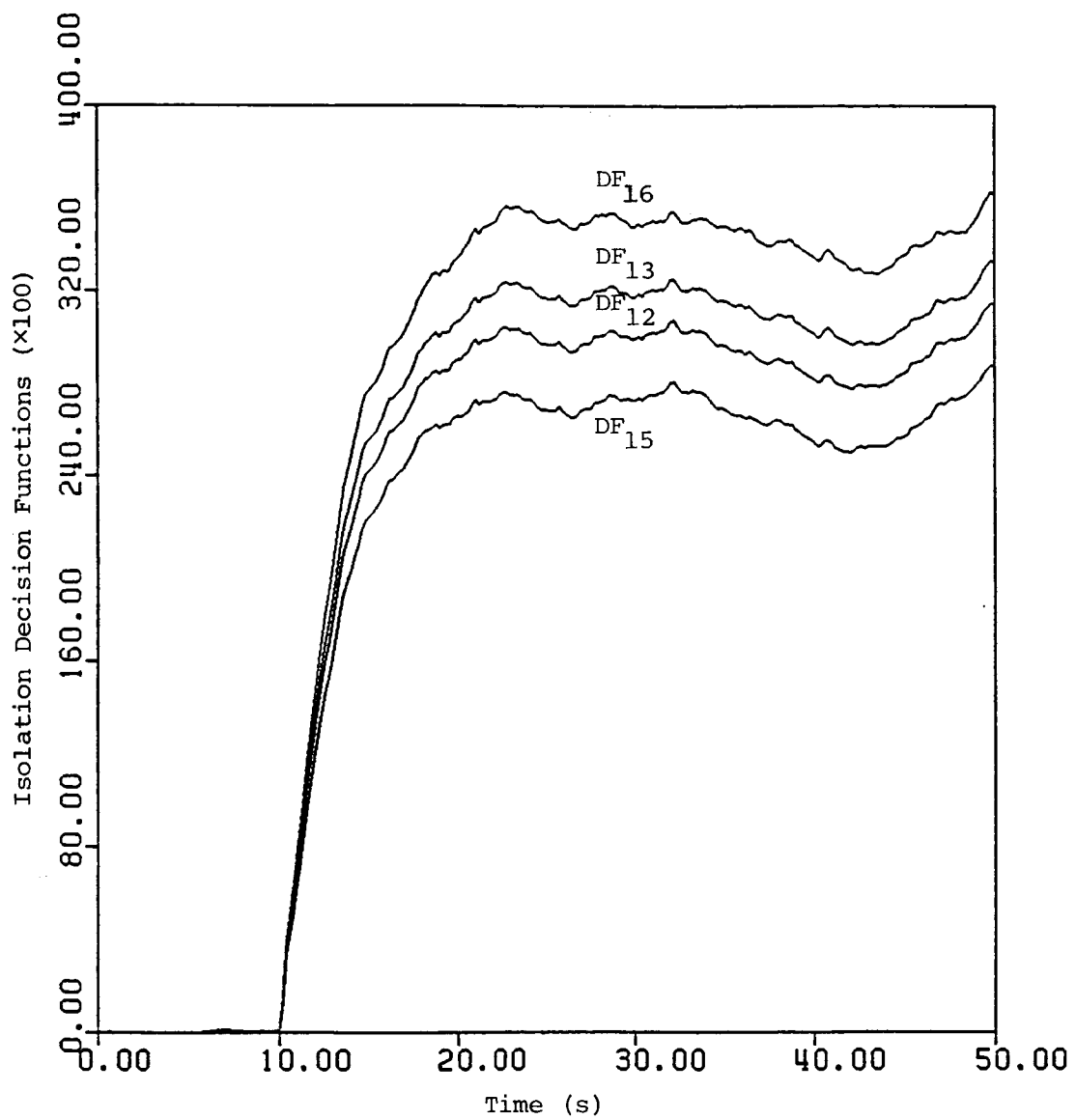


Figure 5.14 Isolation decision functions for a -0.0873 rad (-5 deg) elevator bias failure

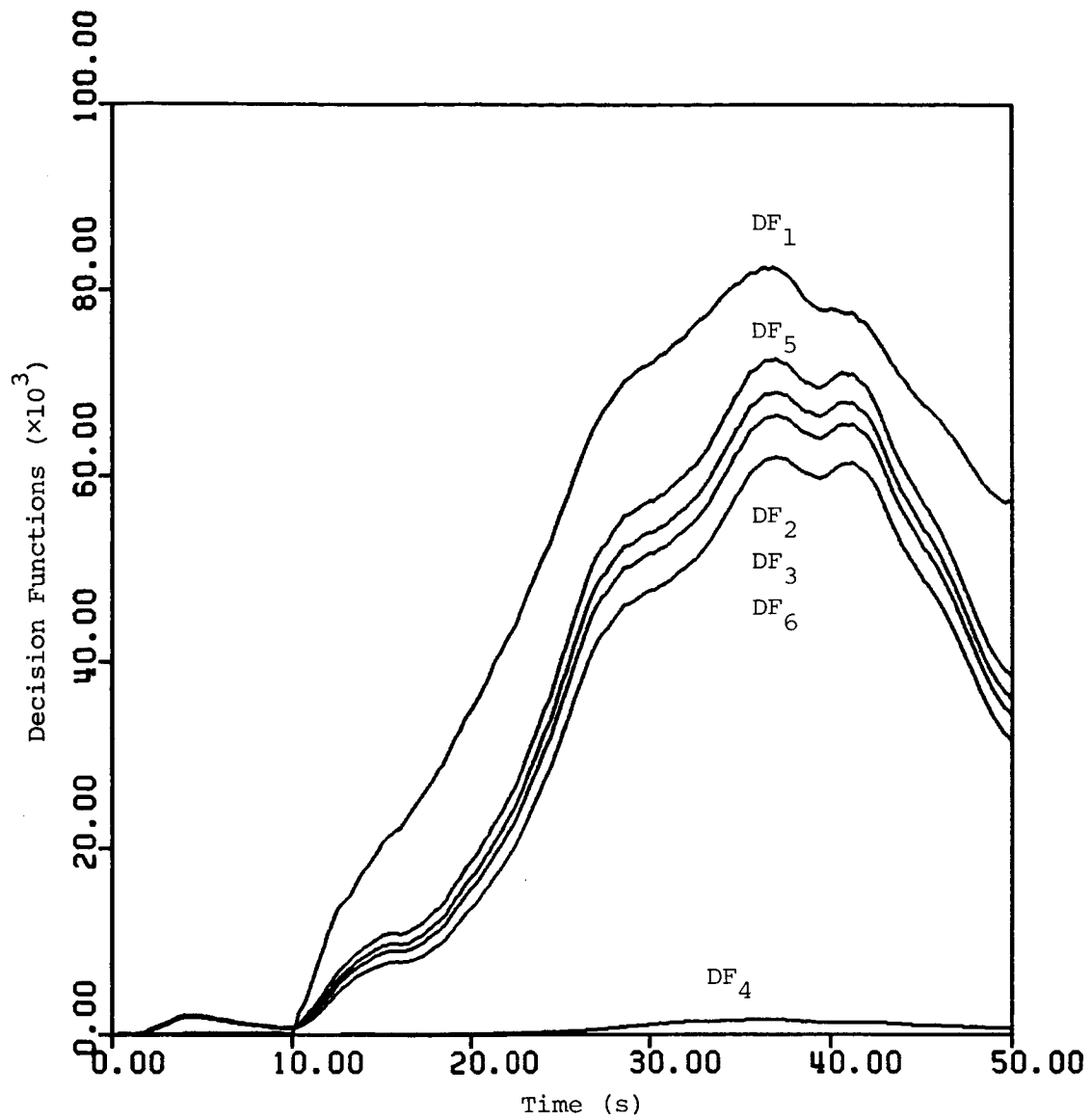


Figure 5.15 Decision functions for a -0.0873 rad (-5 deg) elevator bias failure with the aircraft flying at an off-nominal cruise airspeed of 64.3 m/s (125 knots) at the time of failure

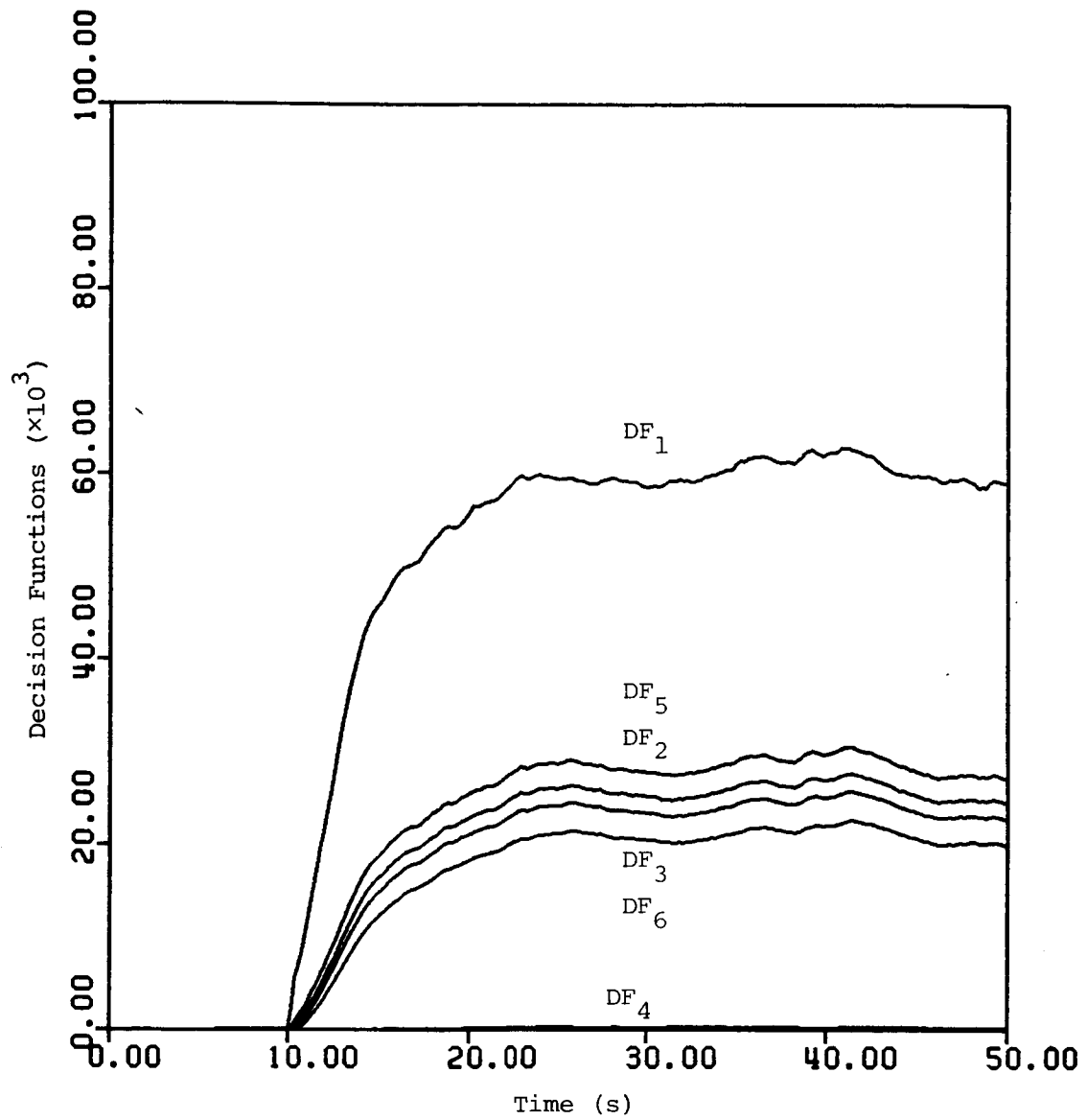


Figure 5.16 Decision functions for a -0.0873 rad (-5 deg) elevator bias failure with the aircraft flying at an off-nominal cruise airspeed of 90 m/s (175 knots) at the time of failure

the nominal flight condition -0.0873 rad (-5 deg) elevator bias failure test case. Again, this is to be expected because of the higher dynamic pressure. The steady-state magnitude of the elevator decision function is approximately the same as for the nominal flight condition failure test case.

5.4.3 Right Aileron Failure Test Case

The decision functions for a 0.0873 rad (5 deg) right aileron bias failure at the nominal cruise flight condition test case are shown in Figure 5.17. The wing surface decision functions (DF_2 , DF_3 , DF_5 , DF_6) become large quickly. As with the -0.0873 rad (-5 deg) elevator bias failure at the nominal flight condition test case, a detection threshold of 20,000 would allow detection of a failure within 2 s. Isolating the failure to the right aileron surface is more difficult. The isolation decision functions DF_{23} , DF_{25} , and DF_{26} are shown in Figure 5.18. If an isolation threshold of 100 was realistic, this failure could be correctly isolated. However, testing of right aileron failures in a variety of flight conditions would be required to determine if this isolation threshold is realistic.

5.4.4 Rudder Failure Test Case

The decision functions for a -0.0873 rad (-5 deg) rudder bias failure are shown in Figure 5.19. For the same magnitude failure, the decision functions produced by a rudder failure are much smaller than produced by the other surfaces. Apparently, the rudder has less effect on the motion of the aircraft than the other surfaces. If the same detection threshold was used for each of the decision functions, this rudder failure could not be detected. Based on the no-failure results presented in Section 5.3, the smallest detection threshold that could be possibly selected would be 5000. This assumes the aircraft is flying near the nominal flight condition, the aircraft is not flying in thunder-storm turbulence, the flaps are not deflected and the maneuvers presented

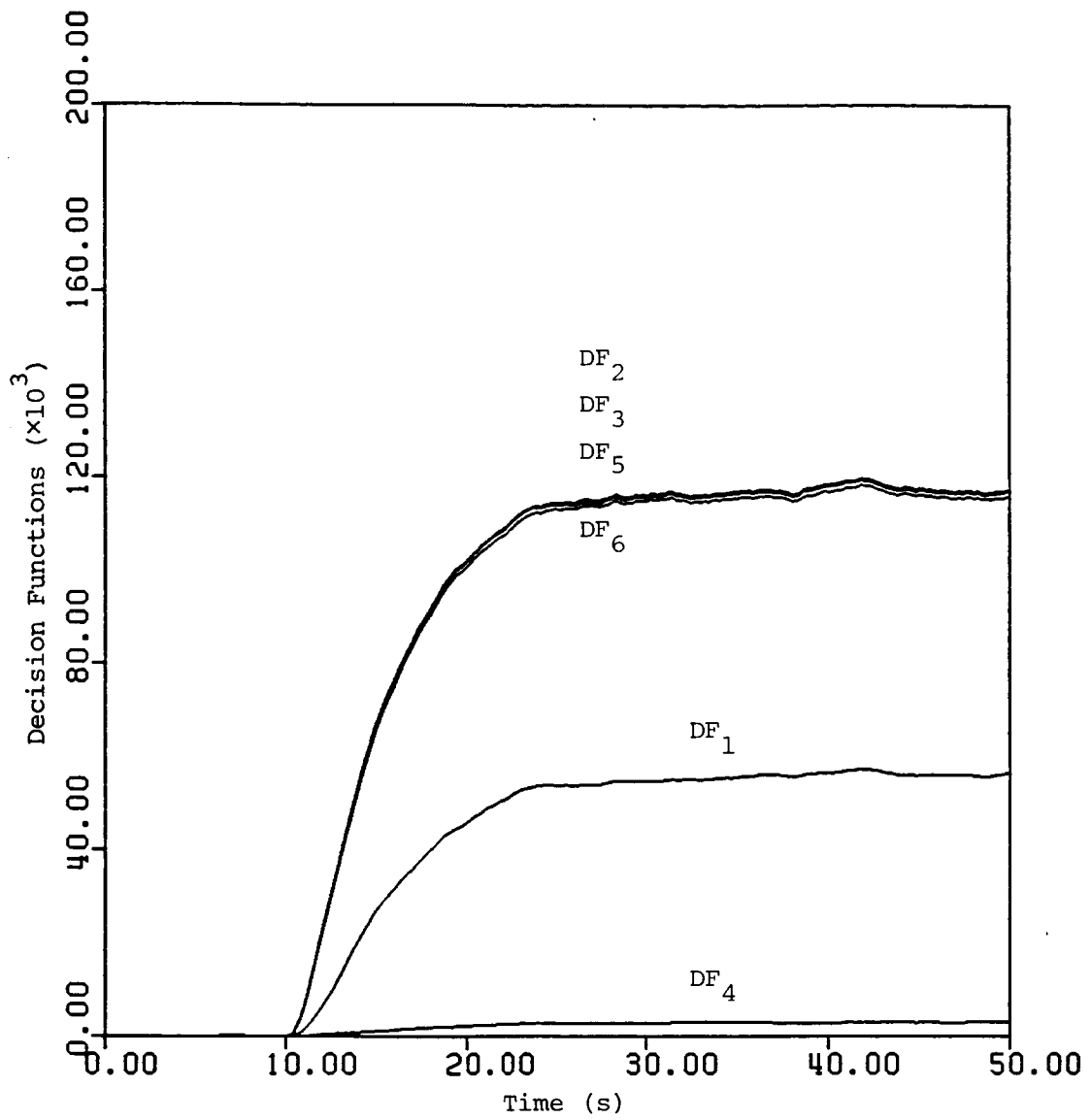


Figure 5.17 Decision functions for a 0.0873 rad (5 deg) right aileron bias failure

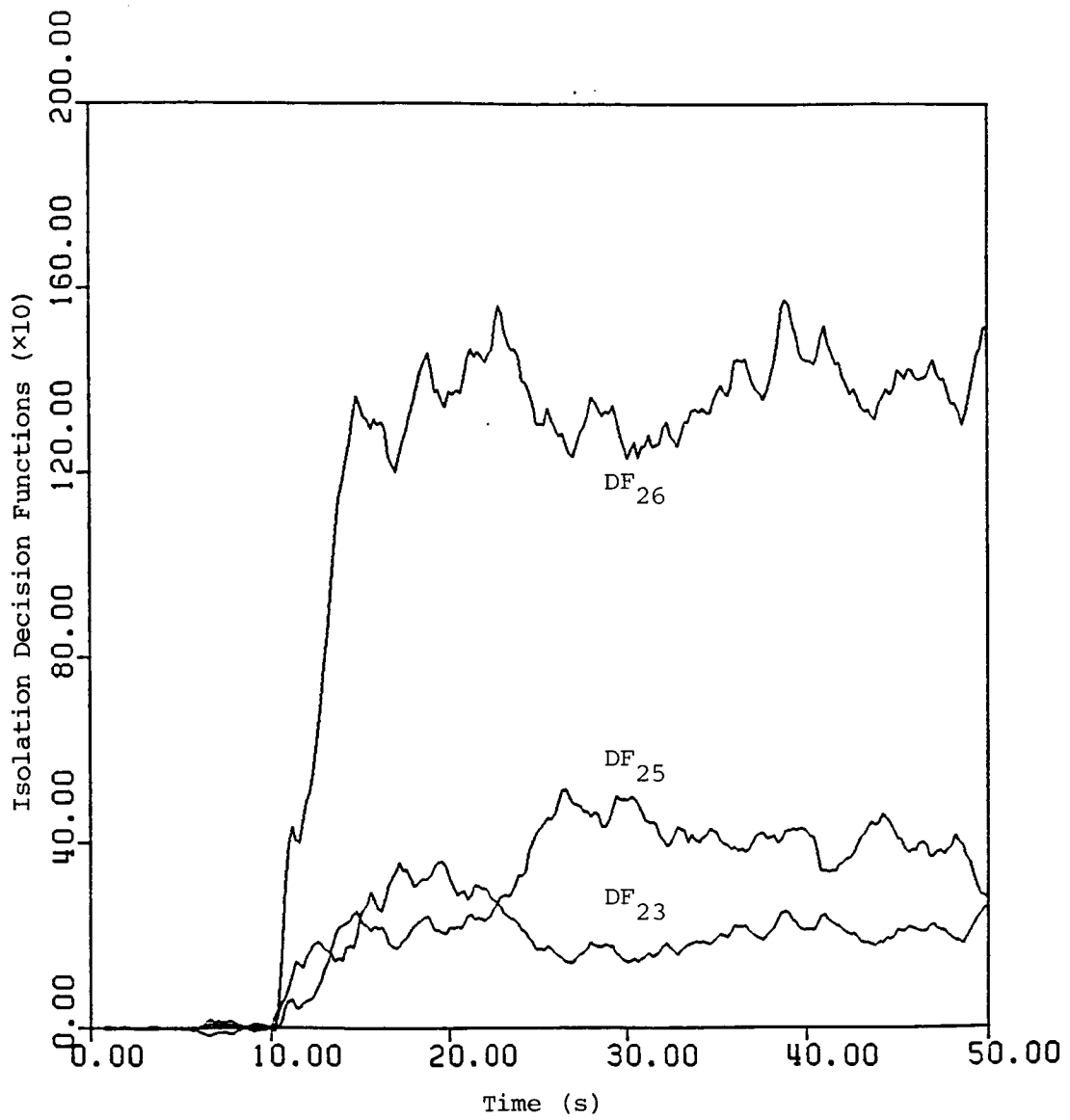


Figure 5.18 Isolation decision functions for a 0.0873 rad (5 deg) right aileron bias failure

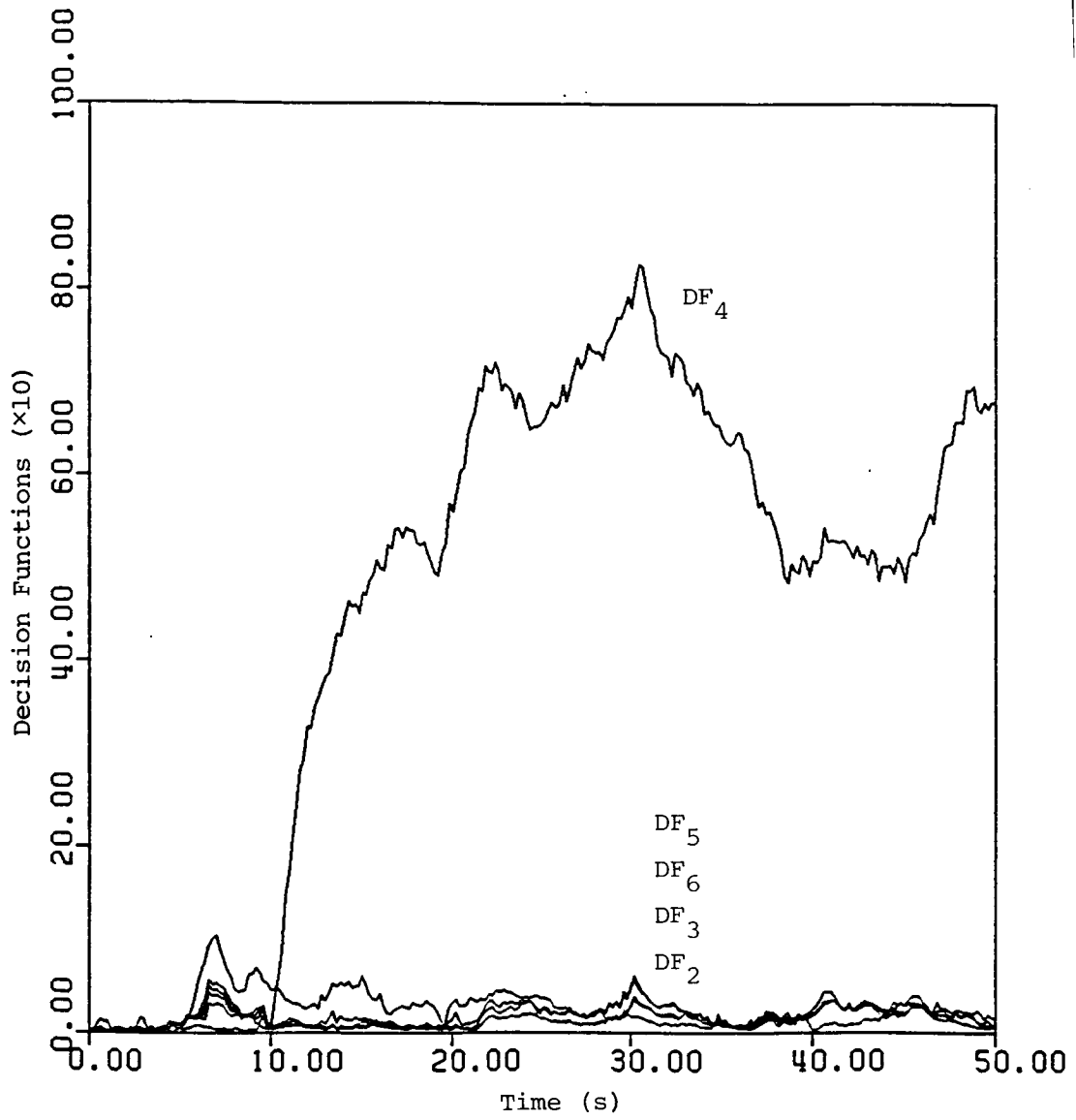


Figure 5.19 Decision functions for a -0.0873 rad (-5 deg) rudder bias failure

were the most severe normally attempted by commercial aircraft. However, in the no-failure test cases presented in Section 5.3, the rudder decision function is always small. The rudder decision function, excluding the times the airspeed was in the neighborhood of 51.44 m/s (100 knots), is less than 200 except for the large flap deflection and the thunderstorm turbulence test cases. With some compensation for thunderstorm turbulence and large flap deflections, a detection threshold of 400 for only the rudder decision function might be possible. If so, this rudder failure could be detected in approximately 3 s.

Isolation of this rudder failure is easy since the other decision functions are all less than 100. However, in general, isolation would have to be based simply on the magnitude of the rudder decision function since the decision functions of the other surfaces may be larger due to modeling errors. One approach would be to simultaneously detect and isolate a rudder failure when the rudder decision function reaches the rudder detection threshold. Since failures of other control surfaces also produce large rudder decision functions, a rudder failure should not be declared if another failure has already been detected.

5.4.5 Right Flap Failure Test Case

The decision functions for a 5% right flap failure test case are shown in Figure 5.20. For a detection threshold of 20,000, this failure would be detectable in 12 s. The failure would not be detectable for higher thresholds. As with the right aileron test case, isolating this failure to the correct wing surface may not be possible. Isolation decision functions DF_{52} , DF_{53} , and DF_{56} are shown in Figure 5.21. If an isolation threshold of a 100 was realistic, this failure could be isolated at the same time the failure was detected. Again, failure test cases at off-nominal flight conditions and wind conditions are required to determine realistic isolation thresholds.

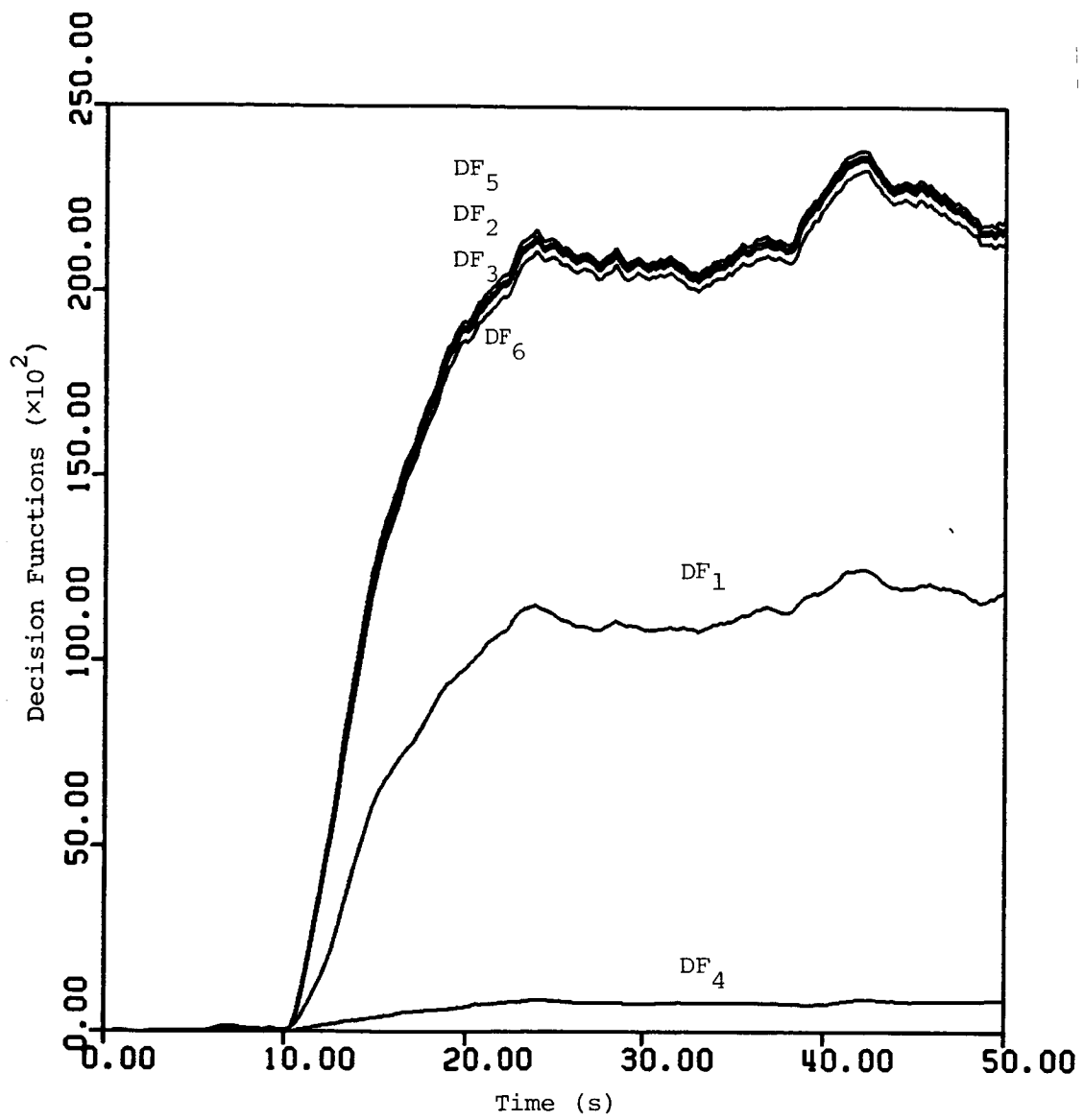


Figure 5.20 Decision functions for a 5% right flap bias failure

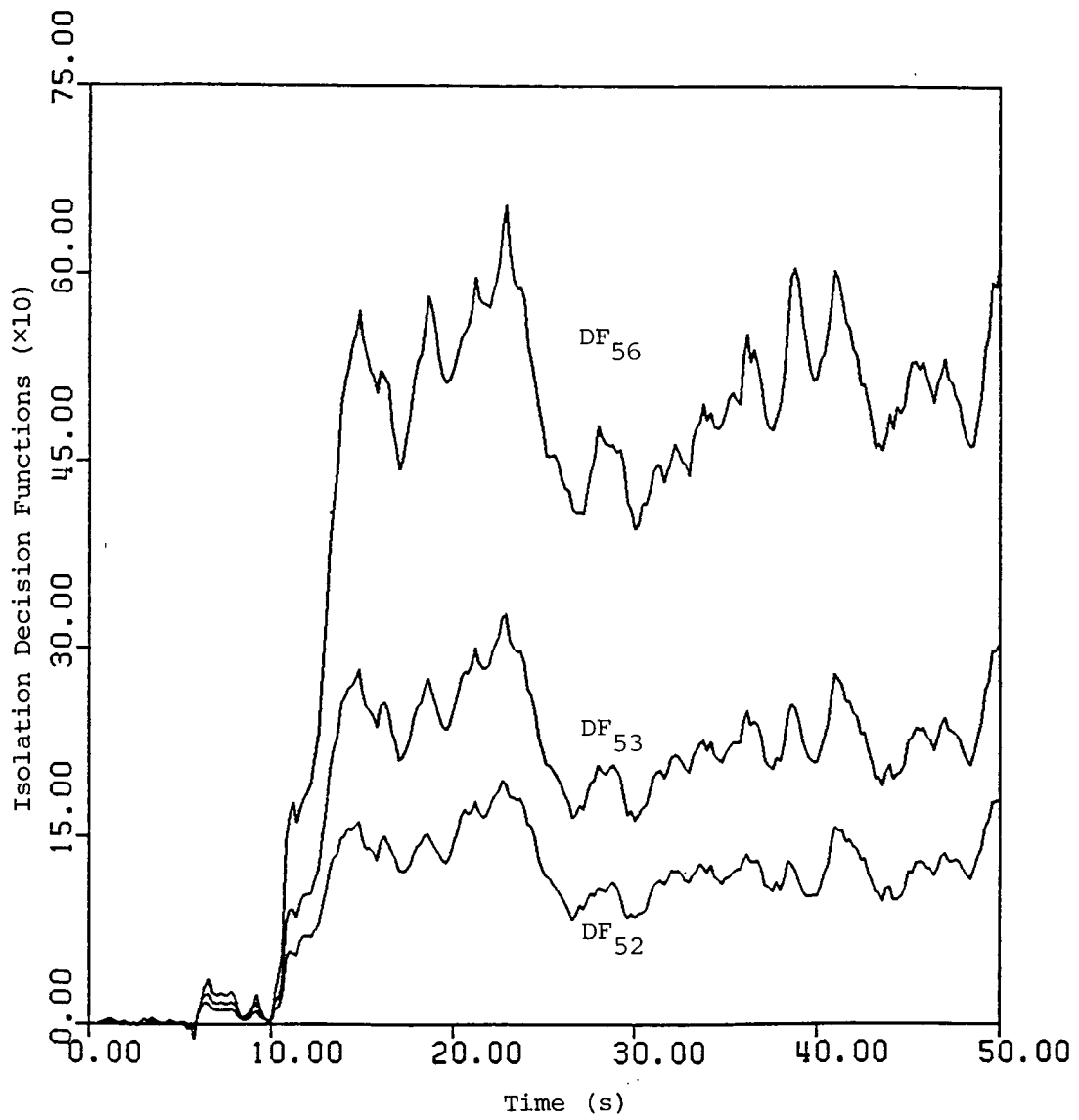


Figure 5.21 Isolation decision functions for a 5% right flap bias failure

5.4.6 Largest Failure Decision Functions as a Function of Time and Failure Magnitude

The purpose of testing the OSGLR algorithm with a number of failure cases is to determine, for a given detection threshold, the size of the failures that can be detected and the time required for detection. A number of bias failures with the aircraft flying at the nominal flight condition were used to test the algorithm. The results were then plotted for each surface to readily answer the two questions raised. The largest values of the decision functions as a function of the size of the bias failure are plotted for each surface tested in Figures 5.22 - 5.25. Each figure contains five curves where each curve is for a particular time after the failure onset. For example, one curve describes the largest value of the decision functions 1 s after the failure. The symbols and their corresponding times after the failure onset are defined in Table 5.4. The symbols correspond to actual test results. Considering the decision functions for only the first 15 s following a bias failure is sufficient because the decision functions, in most cases, grow slowly if at all after this. Since only a few bias failure cases for each surface were tested, the curves are approximate.

In addition, the elevator and rudder plots only considers negative bias failures, and the right aileron plot only considers positive bias failures. Yet, one might expect the plots to be approximately the same for failures with opposite signs but the same magnitude.

First consider elevator, right aileron, and right flap failures. Excluding the 75% and full flap deflection and the acceleration from 51.44 m/s (100 knots) test cases, the largest value of the decision functions for the off-nominal flight conditions have been less than 10,000. Therefore, selecting a threshold of 20,000 might be reasonable at least for some flight regimes. Based on Figure 5.22, -0.0524 rad (-3 deg) elevator bias failures should be detectable with a 20,000 threshold. Similarly, 0.0436 rad (2.5 deg) right aileron and 5% right flap bias failures should be detectable. These bias failures would take 10 to 15 s

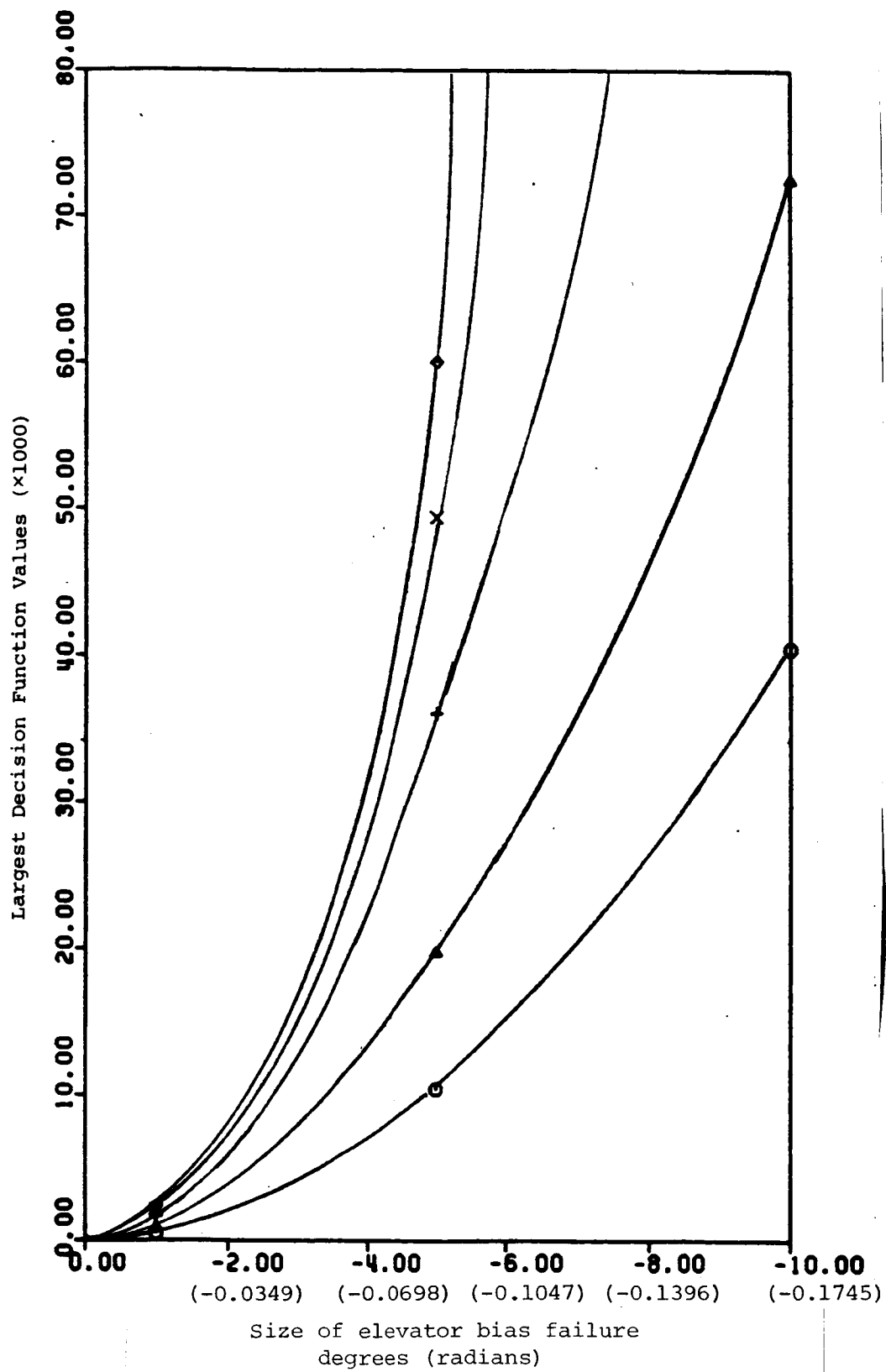


Figure 5.22 The largest decision function values produced by elevator bias failures

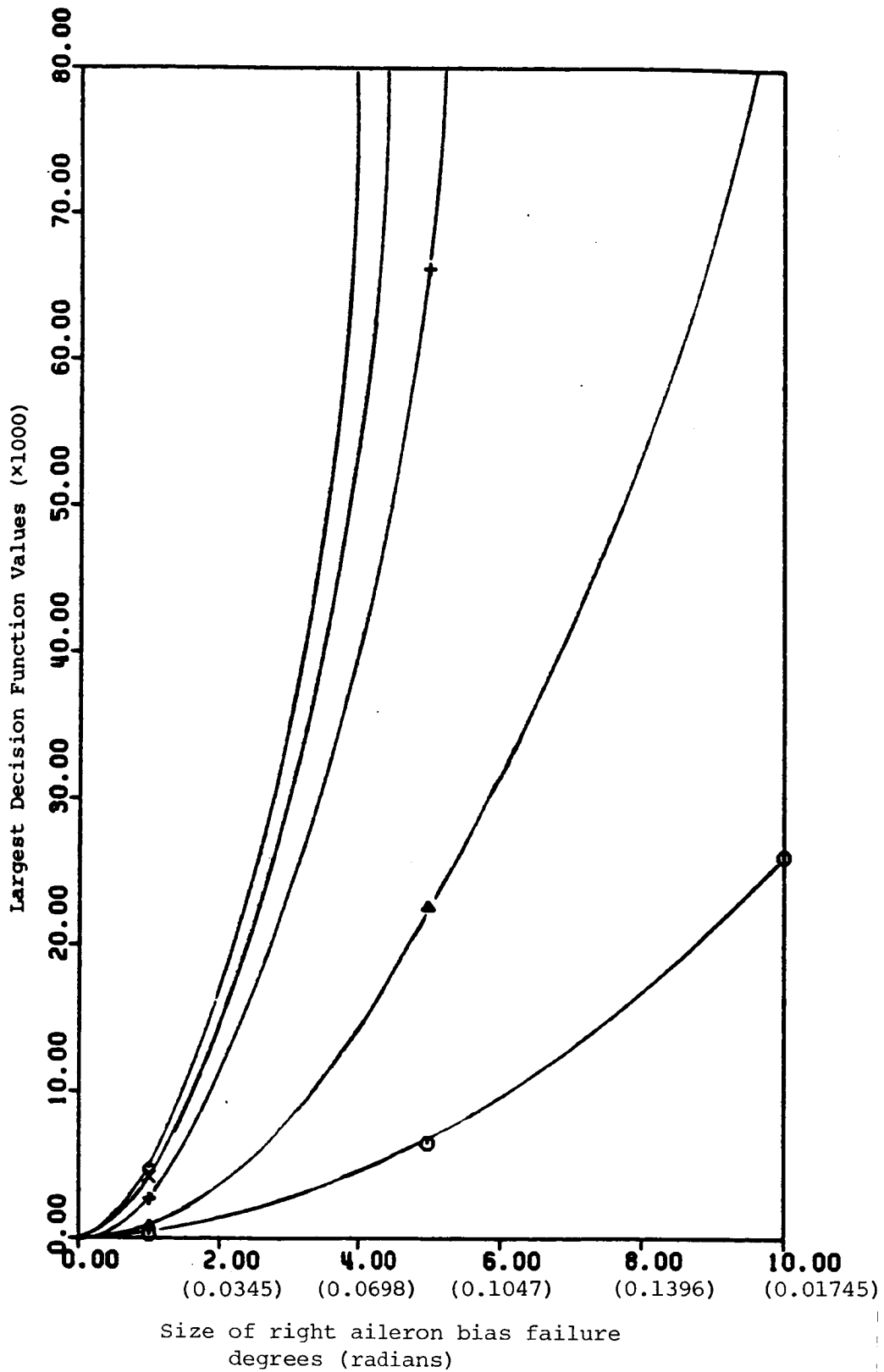


Figure 5.23 The largest decision function values produced by right aileron bias failures

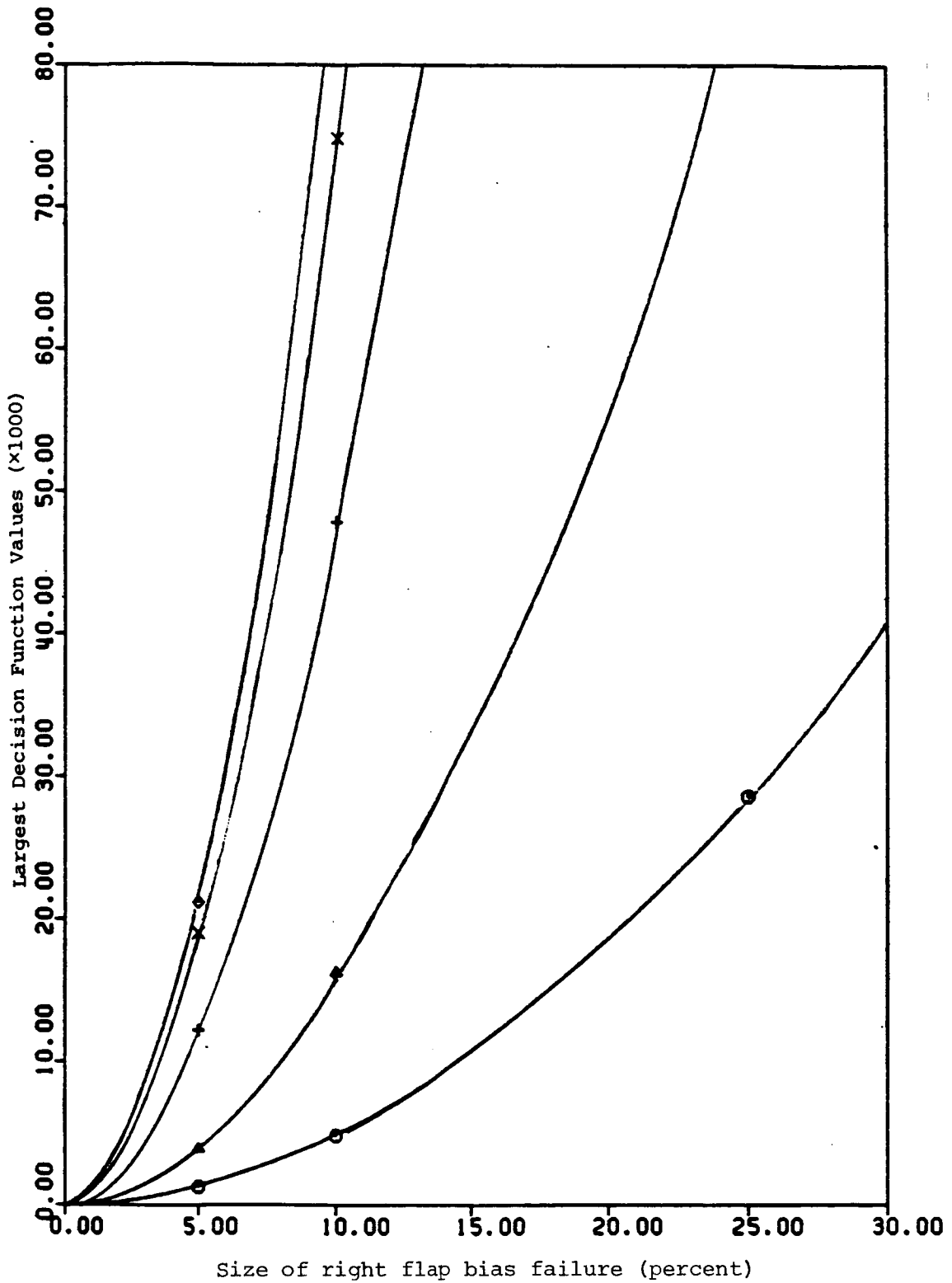


Figure 5.24 The largest decision function values produced by right flap bias failures

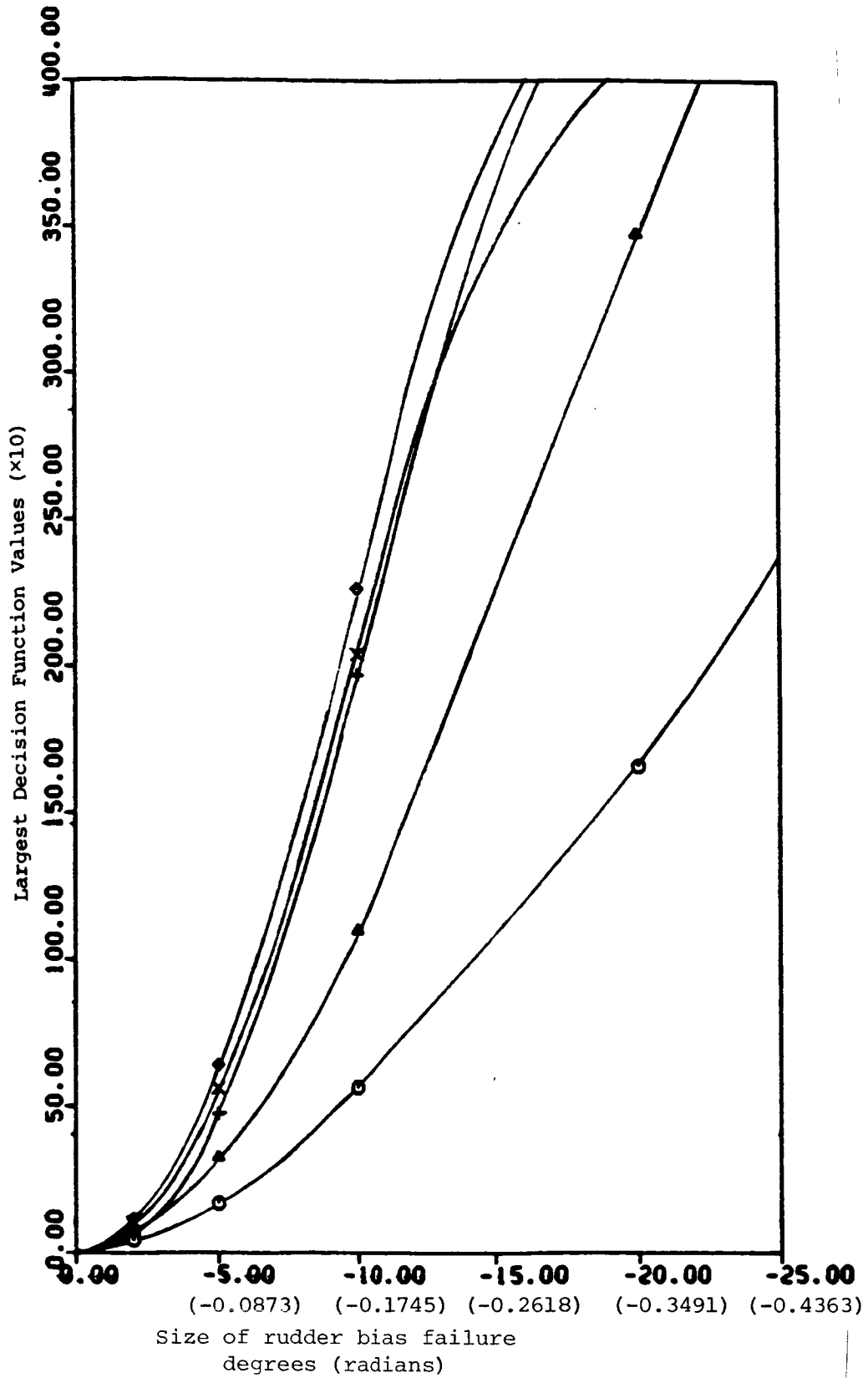


Figure 5.25 The largest decision function values produced by rudder bias failures

Table 5.4 Symbols for time after onset of bias failure

Symbol	Time After Onset of Bias Failure
⊙	1 sec
▲	2 sec
+	5 sec
×	10 sec
◆	15 sec

to detect. However, -0.1222 rad (-7 deg) elevator, 0.1571 rad (9 deg) right aileron, and 21% right flap bias failures, should be detectable in approximately 1 s. Ignoring thunderstorm turbulence, a threshold of 10,000 would be reasonable. With this threshold, a -0.0873 rad (-5 deg) elevator bias failure, a 0.1134 rad (6.5 deg) right aileron bias failure, and a 15% right flap bias failure could be detected in 1s.

In the rudder bias failure test case discussion, a separate detection threshold for the rudder decision function of 400 was motivated. This threshold may be reasonable for some operating envelope about the nominal flight condition that excludes thunderstorm turbulence and large flap deflections. With this threshold, a -0.07 rad (-4 deg) bias failure should be detected in approximately 15 s and a -0.1396 rad (-8 deg) bias failure in approximately 1 s.

As detection thresholds will be selected to minimize false alarms, the size of the decision functions produced by off-nominal, no-failure flight conditions will determine the thresholds. Since these plots approximately define the detection performance for a given detection threshold, they help determine the off-nominal flight conditions for which the decision functions need to be reduced to achieve acceptable performance.

While these figures are only for bias failures, they still might be of use to estimate the detectability of other failures whose failure modes can be reasonably approximated by a bias failure. For example, a failure that ramps at 0.01745 rad/s (1 deg/s) to a bias failure of 0.0873 rad (5 deg) will produce larger decision functions than a 0.0873 rad (5 deg) failure that occurs 5 s after the ramp-to-a-bias failure.

It should be emphasized that Figures 5.22 - 5.25 are only valid in a neighborhood of the nominal airspeed of 77.2 m/s (150 knots). At lower airspeeds, the decision functions are likely to be smaller for the same magnitude failure as less aerodynamic forces are produced for the same deflection. Similarly, the decision functions are likely to be larger for the same magnitude failure at higher airspeeds.

Similar plots of the smallest failure isolation decision functions as a function of the time after failure and the failure magnitude can be used to determine the isolation performance. In Figure 5.26, the minimum of the isolation decision functions DF_{12}' , DF_{13}' , DF_{14}' , DF_{15}' , and DF_{16}' are plotted for two elevator bias magnitudes of -0.01745 rad (-1 deg) and -0.0873 rad (-5 deg). Approximate curves for the minimum of these isolation decision functions for five times after the failure onset are also shown in the figure. No effort was made to define what might be reasonable isolation thresholds. Yet, even small failures on the order of 0.045 rad (2.58 deg) should be easily and quickly isolated.

The minimum of the isolation decision functions DF_{21}' , DF_{23}' , DF_{24}' , DF_{25}' , and DF_{26}' are plotted for the right aileron bias failure test cases in Figure 5.27. Even for a small isolation threshold of 100, only 0.07 rad (4 deg) and larger bias failures that can be isolated. The OSGLR algorithm might be able to quickly isolate large right aileron failures if an isolation threshold of 500 was reasonable.

The minimum of the isolation decision functions for the right flap bias failure test case DF_{51}' , DF_{52}' , DF_{53}' , DF_{54}' , and DF_{56}' are plotted in Figure 5.28. While larger than the minimum of the isolation decision functions for the right aileron failures, an isolation threshold of less than 400 would be required to isolate 10% and smaller bias failures.

No figure for the rudder bias failure test cases is shown because there might be circumstances where a rudder failure would be detected and isolated even though the decision functions for the other surfaces are larger due to an off-nominal flight condition. The detection and isolation of a rudder failure would be based simply on the rudder decision function unless another failure has already been detected.

5.5 Summary and Conclusions

The OSGLR algorithm, based upon the linear model developed for the nominal cruise flight condition of 77.2 m/s (150 knots) at 304.8 m

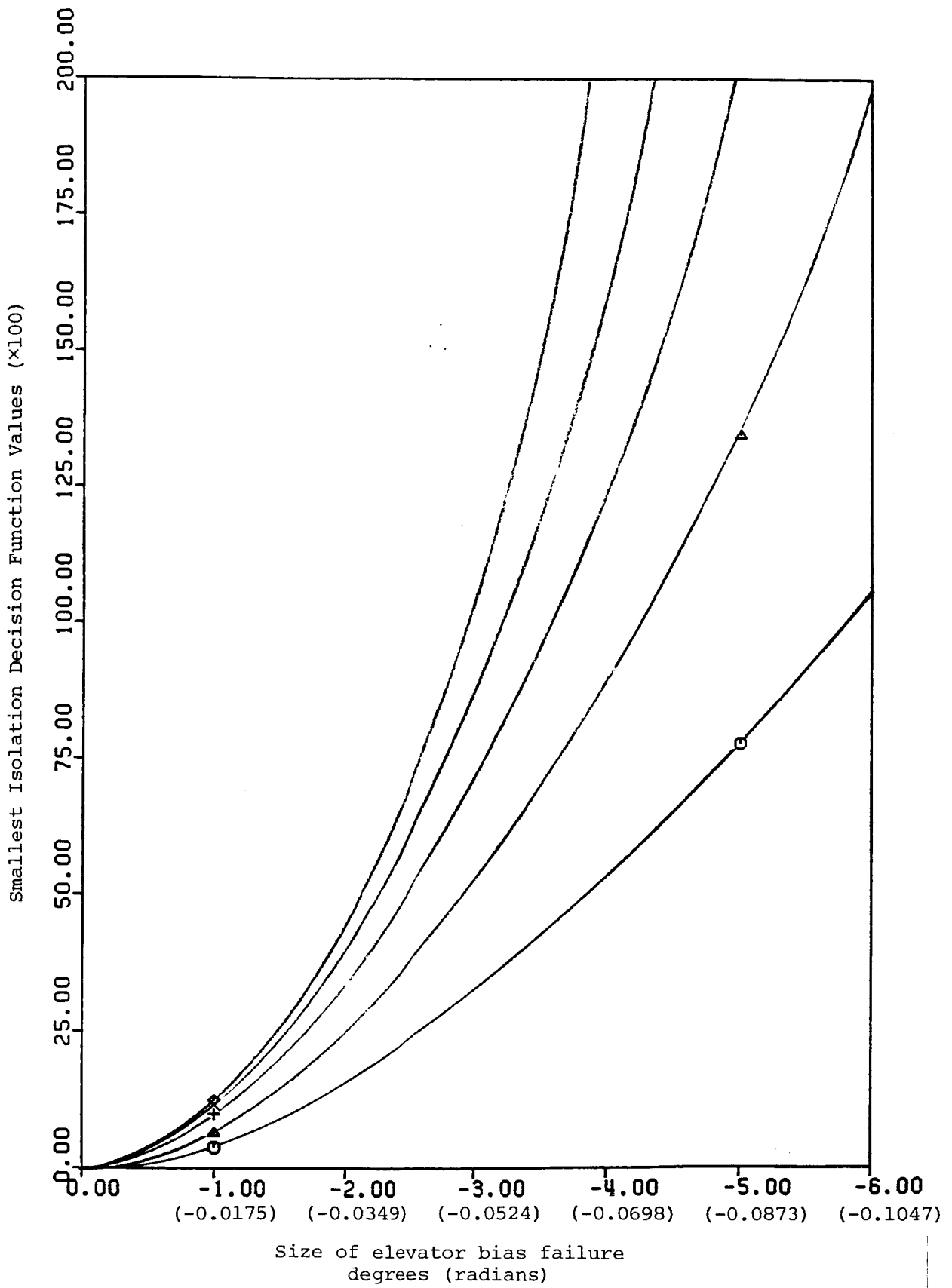


Figure 5.26 The smallest of the isolation decision functions DF_{1i} ($i \neq 1$) produced by elevator bias failures

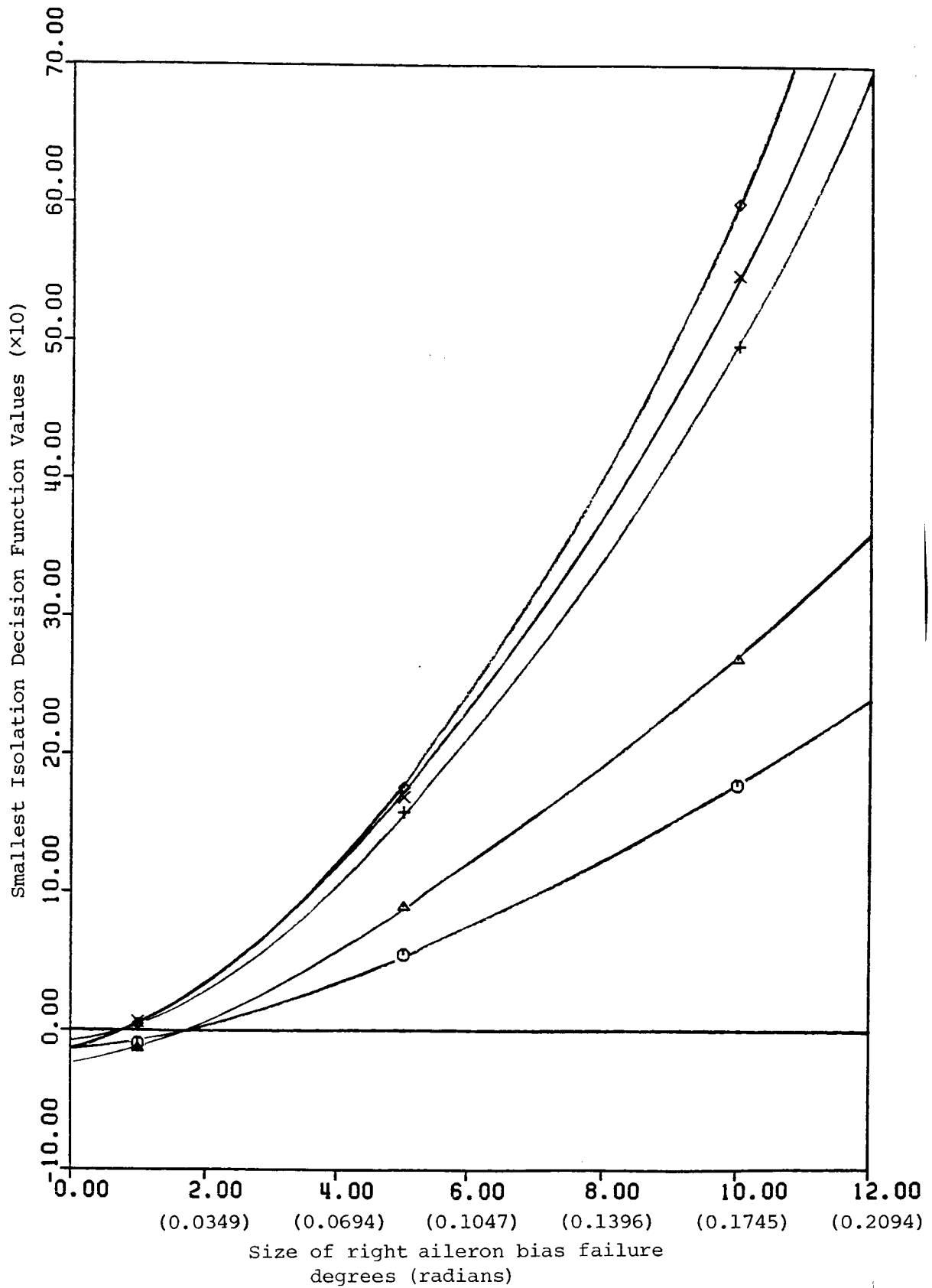


Figure 5.27 The smallest of the isolation decision functions DF_{2i} ($i \neq 2$) produced by right aileron bias failures

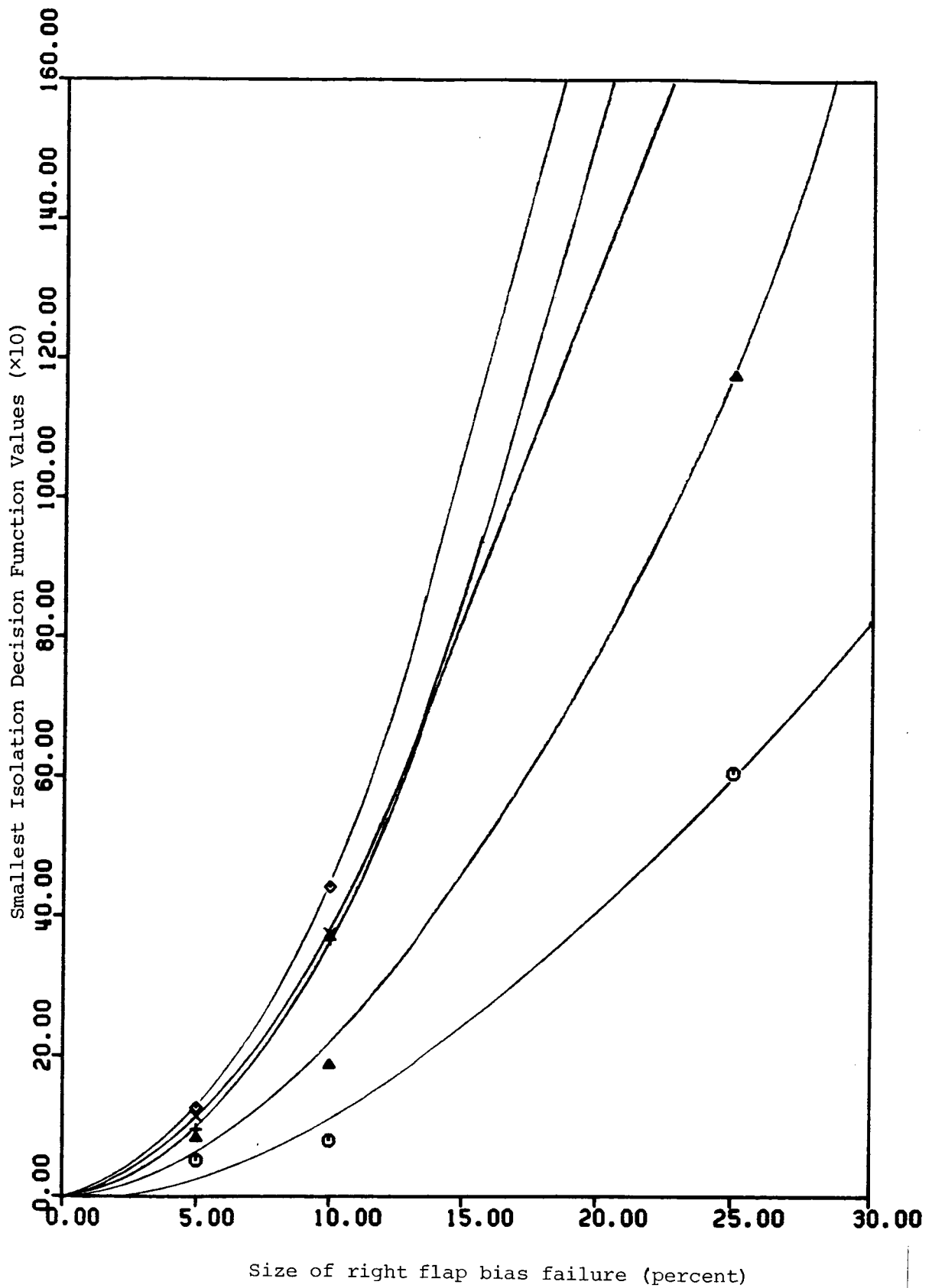


Figure 5.28 The smallest of the isolation decision functions DF_{5i} ($i \neq 5$) produced by right flap bias failures

(1000 ft), was tested with sensor errors and dynamics at a number of off-nominal flight conditions. These off-nominal flight conditions included maneuvers, nonzero flap deflections, off-nominal turbulence intensity levels, and steady winds. Also, a number of bias failures were tested. Based on these tests, the following conclusion have been made.

- o Sensor errors and dynamics have a negligible effect on the performance of the OSGLR algorithm.
- o Including thrust as an input to the linear model reduces the mismodeling caused by off-nominal thrust.
- o Mismodeling increases as the actual dynamic pressure diverges from the nominal dynamic pressure.
- o The 77.2 m/s (150 knot) linear model is not valid for large (75% and greater) flap deflections. The decision functions produced by these flap deflections were 50,000 and larger. The same linear model also had difficulty in the neighborhood of 51.44 m/s (100 knots) and slower. In one case, the decision functions produced in this low airspeed environment were almost 40,000. Setting thresholds to accommodate these large decision functions would result in fair to poor FDI performance. For example, a threshold of 60,000 could detect a -0.1571 rad (-9 deg) elevator bias failure, a 0.1396 rad (8 deg) right aileron bias failure, and a 20% right flap bias failure in 2 s. Yet, flap deflection greater than 75% would still produce false alarms with this threshold.
- o The cruise linear model was adequate for maneuvering flight. Ignoring airspeeds in the neighborhood of 51.44 m/s (100 knots) for which the linear model is not valid, the largest decision function produced by maneuvering flight was 4500 for the maximum rate-of-climb test case. Therefore, a threshold of 10,000 in the neighborhood of 77.2 m/s (150 knots) and excluding larger flap deflections should provide excellent false alarm

performance. With this threshold, a -0.0873 rad (-5 deg) elevator bias failure, a 0.1134 rad (6.5 deg) right aileron bias failure, and a 15% right flap bias failure could be detected in 1s. A -0.0611 rad (-3.5 deg) elevator bias failure, a 0.0611 rad (3.5 deg) right aileron bias failure, and an 8% right flap failure could be detected in 2s.

- o Light turbulence of intensity 0.3 m/s (1 ft/s) and steady winds did not significantly effect the performance of the OSGLR algorithm. Thunderstorm turbulence of intensity of 6.4 m/s (21 ft/s) may possibly cause decision functions on the order of $6,000$ to $8,000$ when the aircraft is flying at the nominal cruise flight condition. Thunderstorm turbulence combined with maneuvers will most likely produce decision functions greater than $10,000$. Some compensation for thunderstorm turbulence may be desirable.
- o A separate detection threshold is required for the rudder decision function. A rudder failure produces a rudder decision function several orders of magnitude smaller than the same magnitude elevator and aileron failures. Therefore, if the same detection threshold used for the other surface was also used for the rudder, rudder failures would not be detectable. Fortunately, the rudder decision function is much smaller than the other decision functions in the off-nominal, no-failure cases tested. A detection threshold of 400 for the rudder decision function appears reasonable if low airspeeds in the neighborhood of 51.44 m/s (100 knots), large flap deflections, and thunderstorm turbulence are excluded. With this threshold, -0.1396 rad (-8 deg) rudder bias failure can be detected in 1 s, a -0.1047 rad (-6 deg) bias failure in 2 s and a -0.0648 rad (-4 deg) in 10 to 15 s.

- o Isolation of elevator failures should be straightforward. It may be possible to isolate large aileron and flap failures with the OSGLR algorithm. Failure test cases at off-nominal flight conditions are required to define adequate isolation thresholds for the ailerons and the flaps. Rudder failures should be simultaneously detected and isolated when the rudder decision function reaches the rudder detection threshold unless another failure has already been detected.

The next section will examine reducing the decision function produced at off-nominal dynamic pressures and nonzero flap deflections.

SECTION 6

SCHEDULING

6.1 Introduction

Airspeeds of 51.44 m/s (100 knots) and less and flap deflections of 75% and greater were shown in Section 5 to produce large no-failure decision functions with an OSGLR algorithm based on the 77.2 m/s (150 knots) cruise linear model. The large decision functions are due to the fact that the 77.2 m/s cruise linear model does not adequately characterize these off-nominal flight conditions. The scheduling of the linear models of the aircraft, the steady-state age-weighted filter gain and covariance matrices, and the steady-state OSGLR influence and information matrices is considered in this section as a means of reducing these mismodeling effects.¹ First, a simple approach of scheduling zero flap deflection linear models only is described and tested with no-failure cases. Scheduling for nonzero flap deflections is then examined. The effect of scheduling only the linear models on the detection of failures is also briefly investigated. Finally, the scheduling of the age-weighted filter and OSGLR matrices in addition to the linear models is discussed.

6.2 Scheduling of Zero Flap Deflection Linear Models

Mismodeling was found in Section 5 to increase as the dynamic pressure deviated more from the nominal value. Scheduling only the

¹ A summary of the test cases is presented in Appendix A for easy reference and comparison.

linear models used by the age-weighted filter as a function of dynamic pressure was investigated as a means of reducing this mismodeling. (See Appendix B for further details.) By reducing the effects of mismodeling as reflected in the residual of the age-weighted filter, the no-failure decision functions should also be reduced. A linear model is chosen for use to minimize the ratio

$$\frac{|\bar{q} - \bar{q}_{m_i}|}{\bar{q}_{m_i}}$$

where \bar{q} is the actual dynamic pressure and \bar{q}_{m_i} is the nominal dynamic pressure of the i th linear model.

Three linear models corresponding to cruise flight conditions at 304.8 m (1000 ft) for airspeeds of 51.44 m/s (100 knots), 77.2 m/s (150 knots), and 102.9 m/s (200 knots) were developed to test this simple scheduling approach. Using these linear models, the scheduling approach was tested on the acceleration from 51.44 m/s test case. The decision functions for this test case with the age-weighted filter and OSGLR steady-state matrices corresponding to the 77.2 m/s linear model are shown in Figure 6.1. The decision functions for the same test case with no scheduling of the linear model are shown in Figure 5.5. The decision functions are reduced by the scheduling approach except in the neighborhood of 77.2 m/s (41 s) with the maximum decision function levels reduced from 39,000 to 11,500. One possible reason the decision functions are still large at the beginning of the test case is that the dynamic pressure drops 57% below the nominal value of the 51.44 m/s linear model in the first several seconds. (As mentioned earlier, this drop in dynamic pressure is caused mainly by a large turbulence level and also by the control surfaces moving to control the aircraft as the control system starts up). Another linear model with nominal airspeed less than 51.44

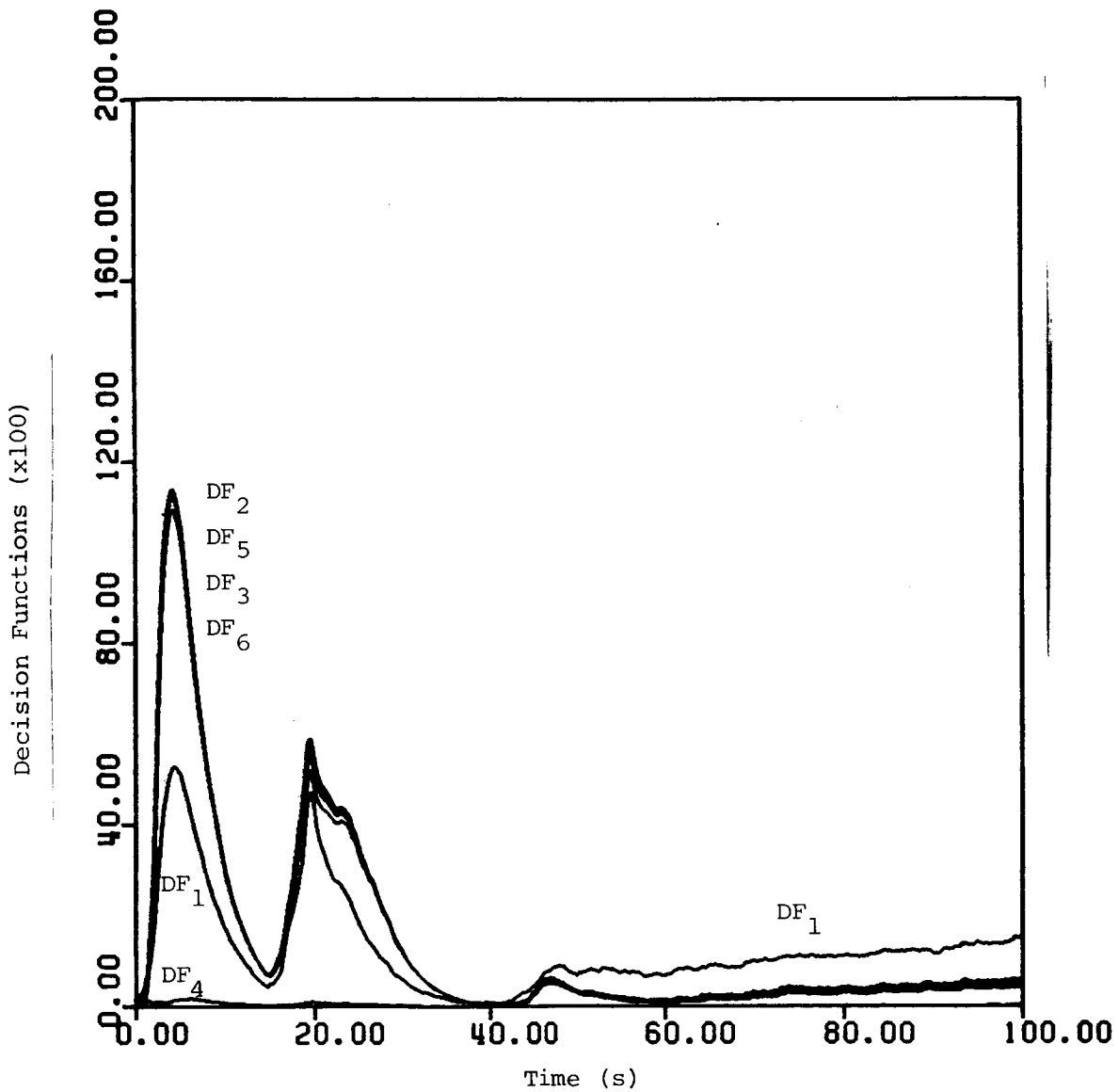


Figure 6.1 Decision functions produced by an age-weighted, scheduled OSGLR algorithm for the acceleration from 51.44 m/s test case

- 51.44, 77.2, 102.9 m/s linear models
- 77.2 m/s age-weighted filter and OSGLR steady-state matrices

m/s may reduce the decision functions at the beginning of the test case further.

Finding a steady-state cruise flight condition at low speeds about 40 m/s (77.75 knots) with no flap deflection was not possible as the angle of attack required exceeded the validity of the simulation. Instead, a linear model corresponding to a cruise flight condition of 46.3 m/s (90 knots) at 304.8 m (1000 ft) was developed and tested. Using the 46.3 m/s linear model as the fourth model with the age-weighted filter and OSGLR steady-state matrices corresponding to the 77.2 m/s linear model produced the decision functions shown in Figure 6.2. Even though the dynamic pressure for the 46.3 m/s model (1274.6 N/m^2 or 26.62 lbs/ft^2) was not significantly lower than the dynamic pressure for the 51.44 m/s model (1573.8 N/m^2 or 32.87 lbs/ft^2), adding the 46.3 m/s linear model was sufficient to reduce the decision functions from 11,500 to 3,500 during the first 15 s of the test case. The largest decision function levels are reached at approximately 20 s when the age-weighted filter switches from the 51.44 m/s linear model to the 77.2 m/s linear model.

Another reason that the decision functions are not reduced even more at low speeds is that the 51.44 m/s linear model does not as accurately describe the aircraft dynamics at its nominal flight condition as well as the 77.2 m/s linear model characterizes the 77.2 m/s cruise flight condition. The decision functions for a no-failure test case with the aircraft flying at 51.44 m/s and 304.8 m using the 51.44 m/s linear model and associated steady-state Kalman filter and OSGLR matrices (no age-weighting) are shown in Figure 6.3. These decision functions are significantly larger than the decision functions for a no-failure test case at 77.2 m/s with the 77.2 m/s linear model and associated Kalman filter and OSGLR steady-state matrices (no age-weighting) shown in Figure 6.4. Either the nonlinearities are much greater at slow airspeeds and high angles of attack or the linear model needs improvement to better describe the aircraft dynamics. Even with this large mismodeling, the

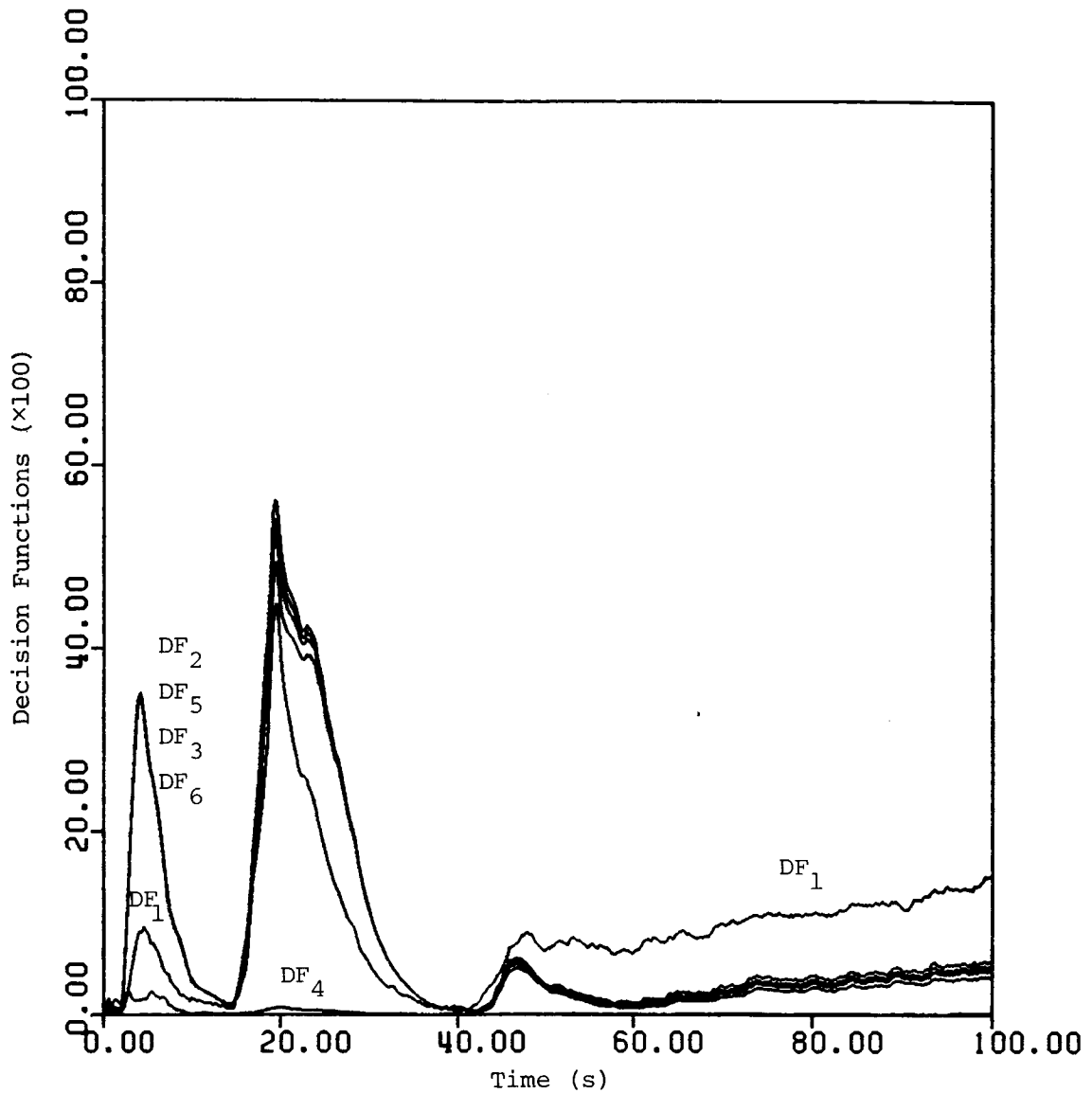


Figure 6.2 Decision functions produced by an age-weighted, scheduled OSGLR algorithm for an acceleration from 51.44 m/s test case

- 46.3, 51.44, 77.2, 102.9 m/s linear models
- 77.2 m/s age-weighted filter and OSGLR steady-state matrices

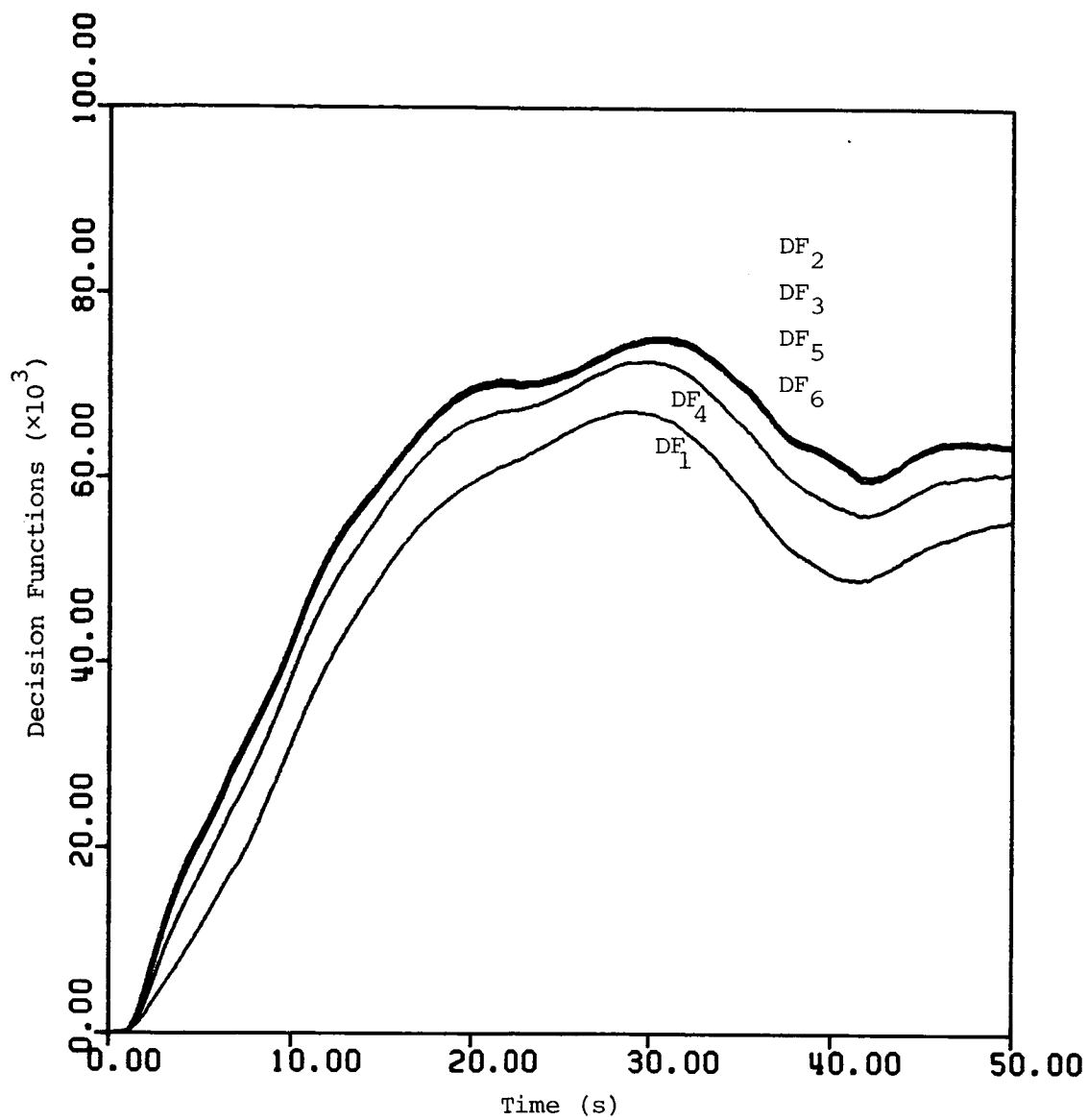


Figure 6.3 Decision functions for a 51.44 m/s, no-failure, cruise test case using the 51.44 m/s linear model and associated steady-state Kalman filter and OSGLR matrices (no age-weighting)

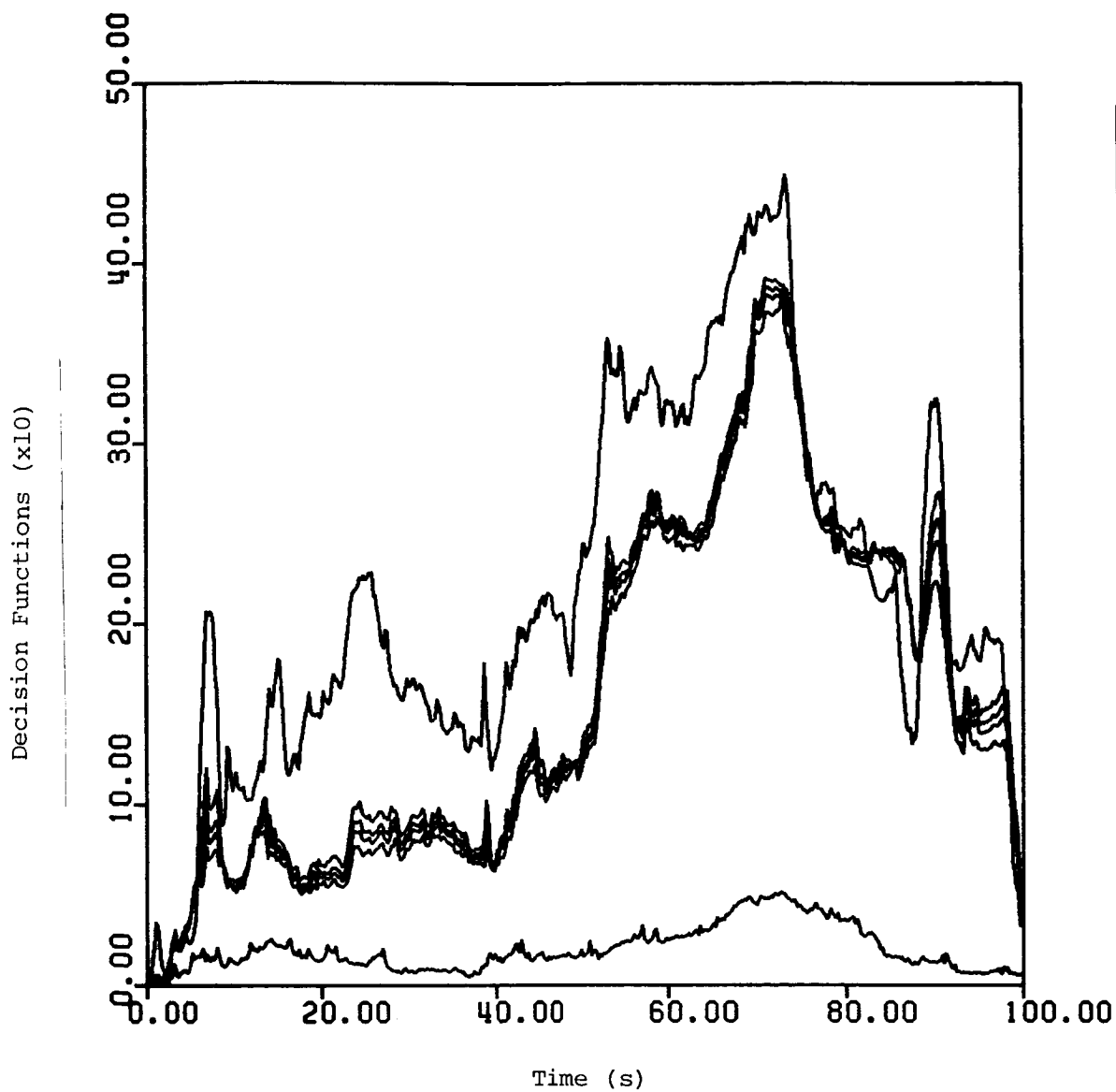


Figure 6.4 Decision functions for a 77.2 m/s cruise no-failure test case using the 77.2 m/s linear model and associated steady-state Kalman filter and OSGLR matrices (no age-weighting)

51.44 m/s model used with an age-weighting of time constant 3 s is adequate to reduce the effects of mismodeling for the acceleration from 51.44 m/s test case. Some effort was made to determine why the mismodeling is larger for the 51.44 m/s linear model in the limited time available but without success.

Despite the inadequacy of the 51.44 m/s linear model, scheduling of only the linear models used by the age-weighted filter was effective in reducing the decision functions at off-nominal dynamic pressures.

6.3 Nonzero Flap Deflections

Flap deflections of 75% and larger were shown in Section 5 to produce very large no-failure decision functions using only the 77.2 m/s linear model. The scheduling of zero-flap linear models as discussed in the previous subsection actually increases the no-failure decision functions. The decision functions for a 50% flap deflection test case with the scheduling of the 46.3, 51.44, 77.2, and 102.9 m/s linear models and the age-weighted filter and OSGLR steady-state matrices corresponding to the 77.2 m/s model are shown in Figure 6.5. The flaps are deflected approximately 10%/s, starting at 5 s, until the desired deflection is achieved. Extending the flaps causes the airspeed to drop. With the scheduling of the linear models used by the age-weighted filter as a function of dynamic pressure, linear models more accurate at low airspeeds than the 77.2 m/s model are used. Interestingly, as a result, the decision functions increase. The 77.2 m/s linear model, for some reason, is not as sensitive to the combination of the flaps extending and the airspeed dropping as the 51.44 m/s linear model is to the flaps extending. Similarly, scheduling with zero-flap deflection linear models does not help the 75% and 100% flap deflection test case. Scheduling based on flap deflection as well as dynamic pressure appears necessary.

Using linear models of 38.6, 51.44, and 77.2 m/s with a nominal flap deflection of 50% and age-weighted filter and OSGLR steady-state

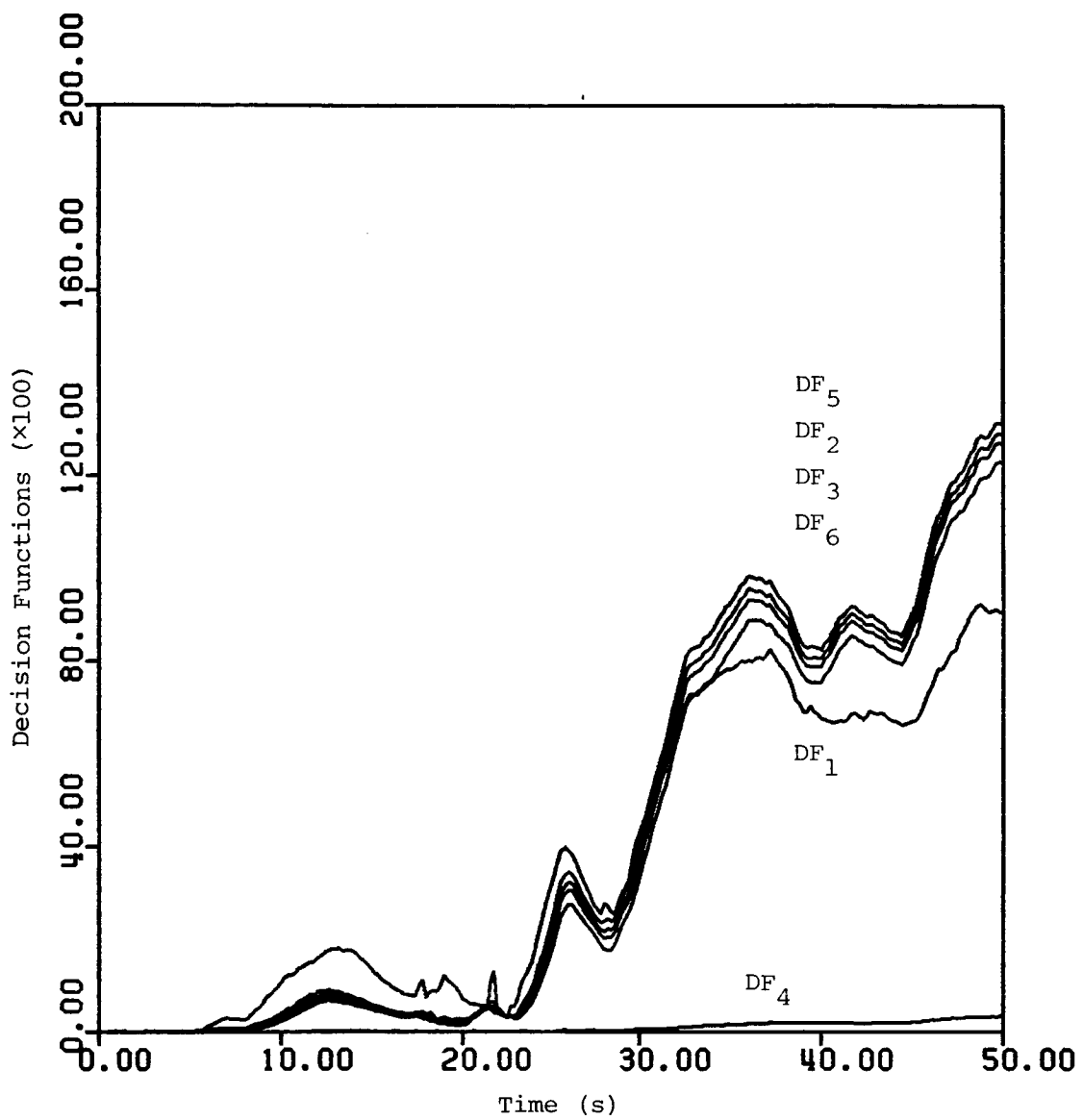


Figure 6.5 Decision functions produced by an age-weighted, scheduled OSGLR algorithm for a 50% flap deflection test case

- 46.3, 51.44, 77.2, 102.9 m/s linear models
- 77.2 m/s age-weighted filter and OSGLR steady-state matrices

matrices corresponding to the 77.2 m/s with 50% flap linear model significantly reduced the decision functions for the 50% and 75% test cases (Figures 6.6 and 6.7). The sudden increase in one of the decision functions in Figure 6.7 may be caused by a switch from the 77.2 m/s to the 51.44 m/s models. The decision functions for the 100% flap test case using the 50% flap linear models, however, were larger than with the zero-flap deflection linear models. Using linear models with 100% nominal flap deflection to reduce the decision functions for the 100% flap test was also briefly investigated without success (Figure 6.8). More effort is required, though, to determine why scheduling the 100% flap linear models was not adequate for the 100% flap test case. Also, the transition from zero to nonzero flap deflections still needs to be tested.

6.4 Failure Detection and Scheduling

The scheduling of linear models has been generally effective in reducing the effects of mismodeling on the no-failure decision functions. Detecting failures with the linear models scheduled is briefly considered here. Two failures at off-nominal flight conditions are presented. The first case is a -0.0873 rad (-5 deg) elevator failure at a cruise flight condition of 90.0 m/s (175 knots). The decision functions for this test case with the linear models scheduled and the 77.2 m/s Kalman filter and OSGLR steady-state matrices are shown in Figure 6.9. The failure causes a decrease in dynamic pressure and therefore a switch from the 102.9 m/s linear model to the 77.2 m/s linear model 5 s after the failure occurred. The change of linear models does not cause any noticeable change in the decision functions. However, this is not true for the second case.

The decision functions of a -0.0873 rad (-5 deg) elevator failure at a cruise flight condition of 64.3 m/s (125 knots) is shown in Figure 6.10. For the first five seconds following the failure, the decision functions increase. However, when the linear model used by the age-

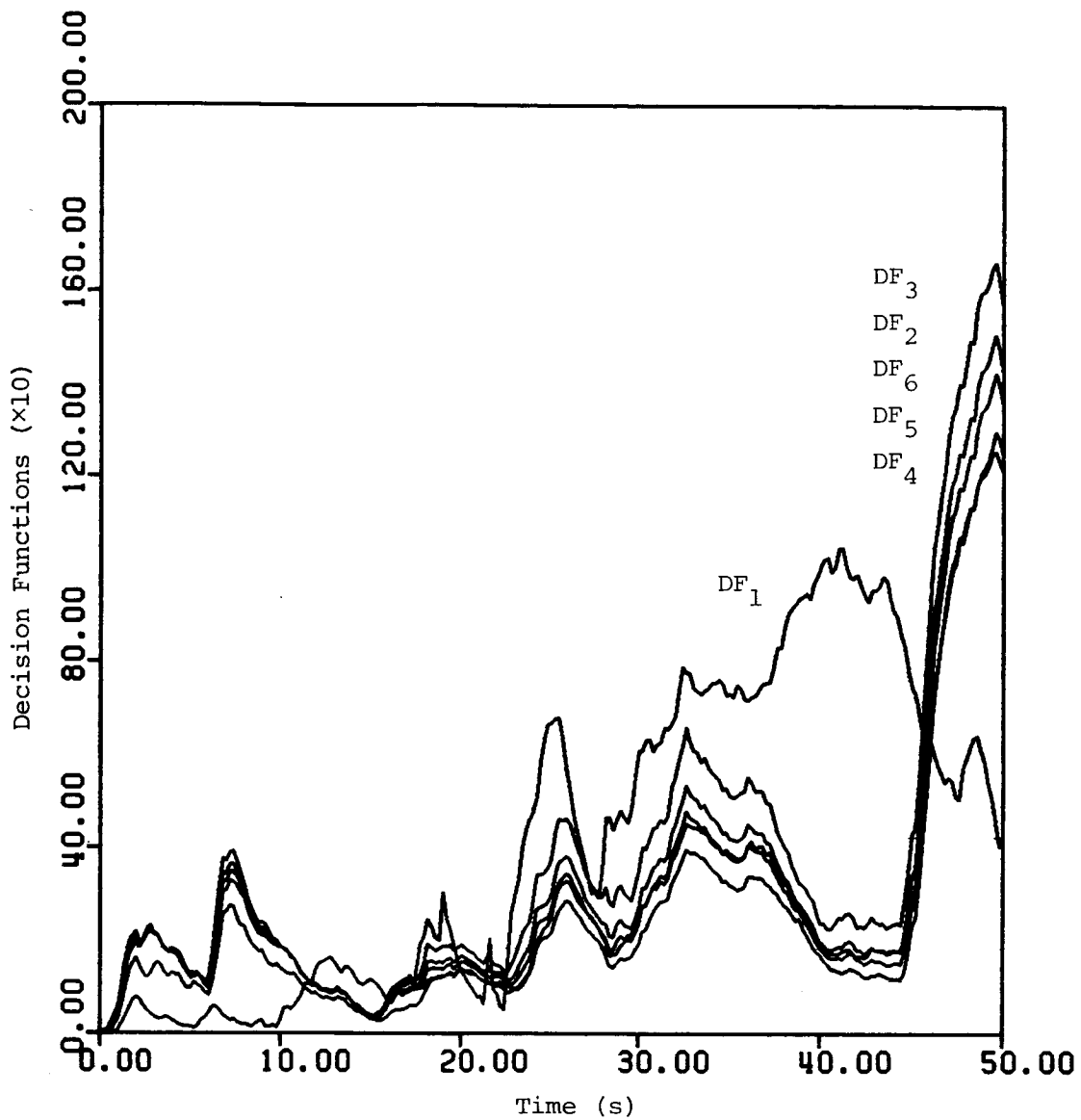


Figure 6.6 Decision functions produced by an age-weighted, scheduled OSGLR algorithm for a 50% flap deflection test case

- 38.6, 51.44, 77.2 m/s with 50% flap linear models
- 77.2 m/s with 50% flap age-weighted filter and OSGLR steady-state matrices

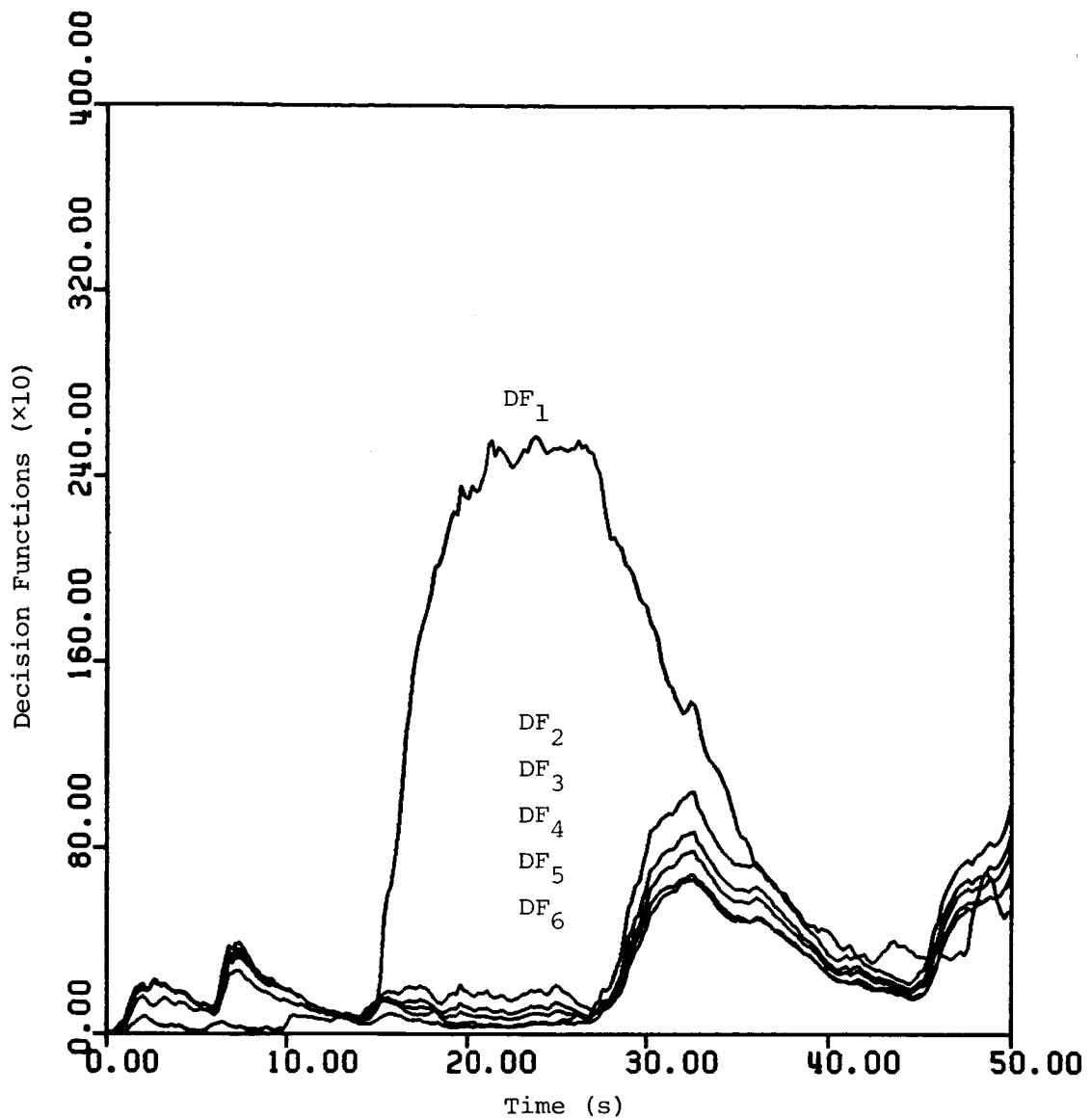


Figure 6.7 Decision functions produced by an age-weighted, scheduled OSGLR algorithm for a 75% flap deflection test case

- 38.6, 51.44, 77.2 m/s with 50% flap linear models
- 77.2 m/s with 50% flap age-weighted filter and OSGLR steady-state matrices

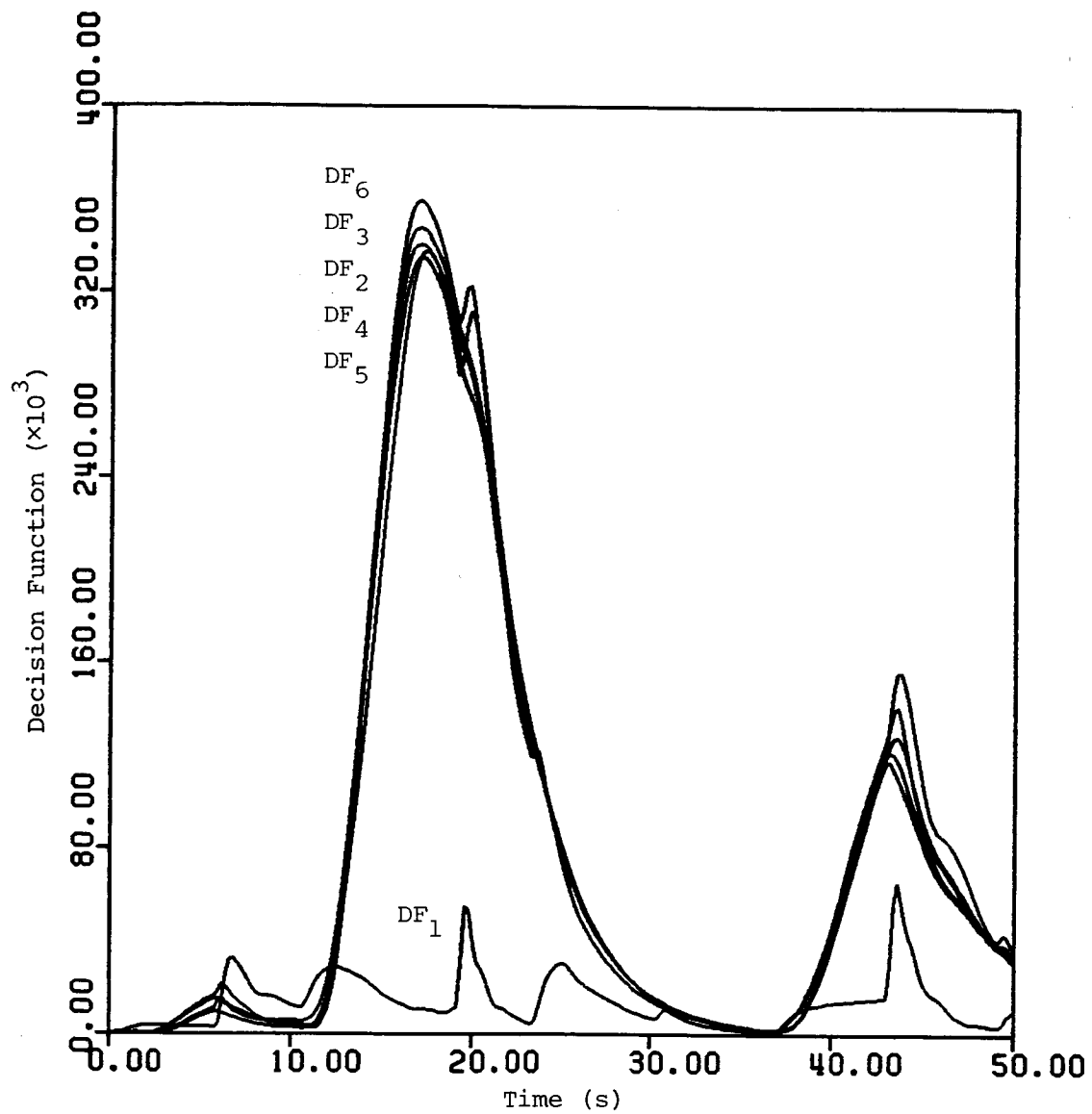


Figure 6.8 Decision functions produced by an age-weighted, scheduled OSGLR algorithm for a 100% flap deflection test case

- 100% flap deflection from the start of the test case
- 38.6, 51.44, 77.2 m/s with 100% flap linear models
- 77.2 m/s with 100% flap age-weighted filter and OSGLR steady-state matrices

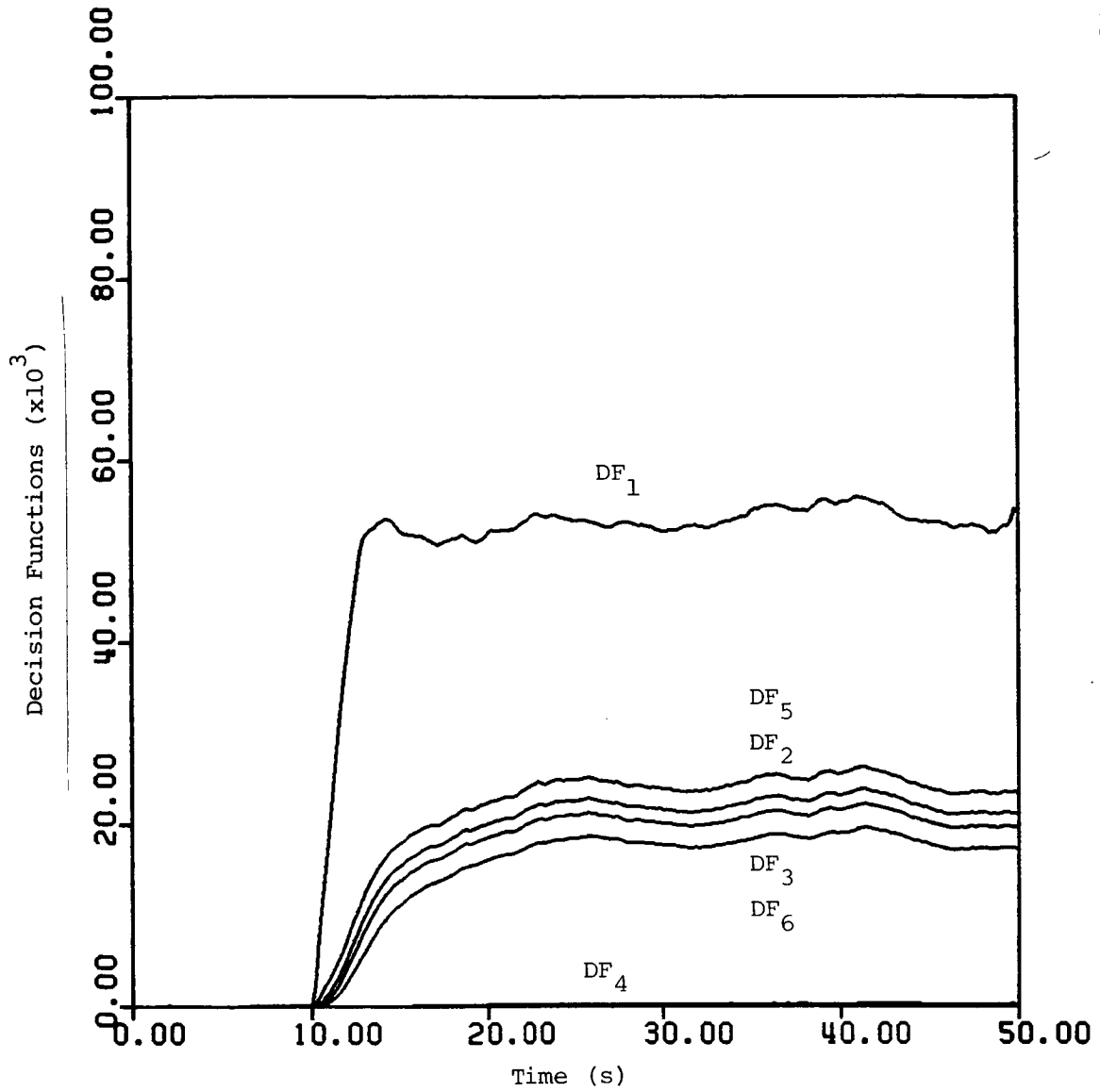


Figure 6.9 Decision functions produced by an age-weighted, scheduled OSGLR algorithm for a -0.0873 rad (-5 deg) elevator bias failure at 90.0 m/s (175 knots) test case

- $46.4, 51.44, 77.2, 102.9$ m/s linear models
- 77.2 m/s age-weighted filter and OSGLR steady-state matrices

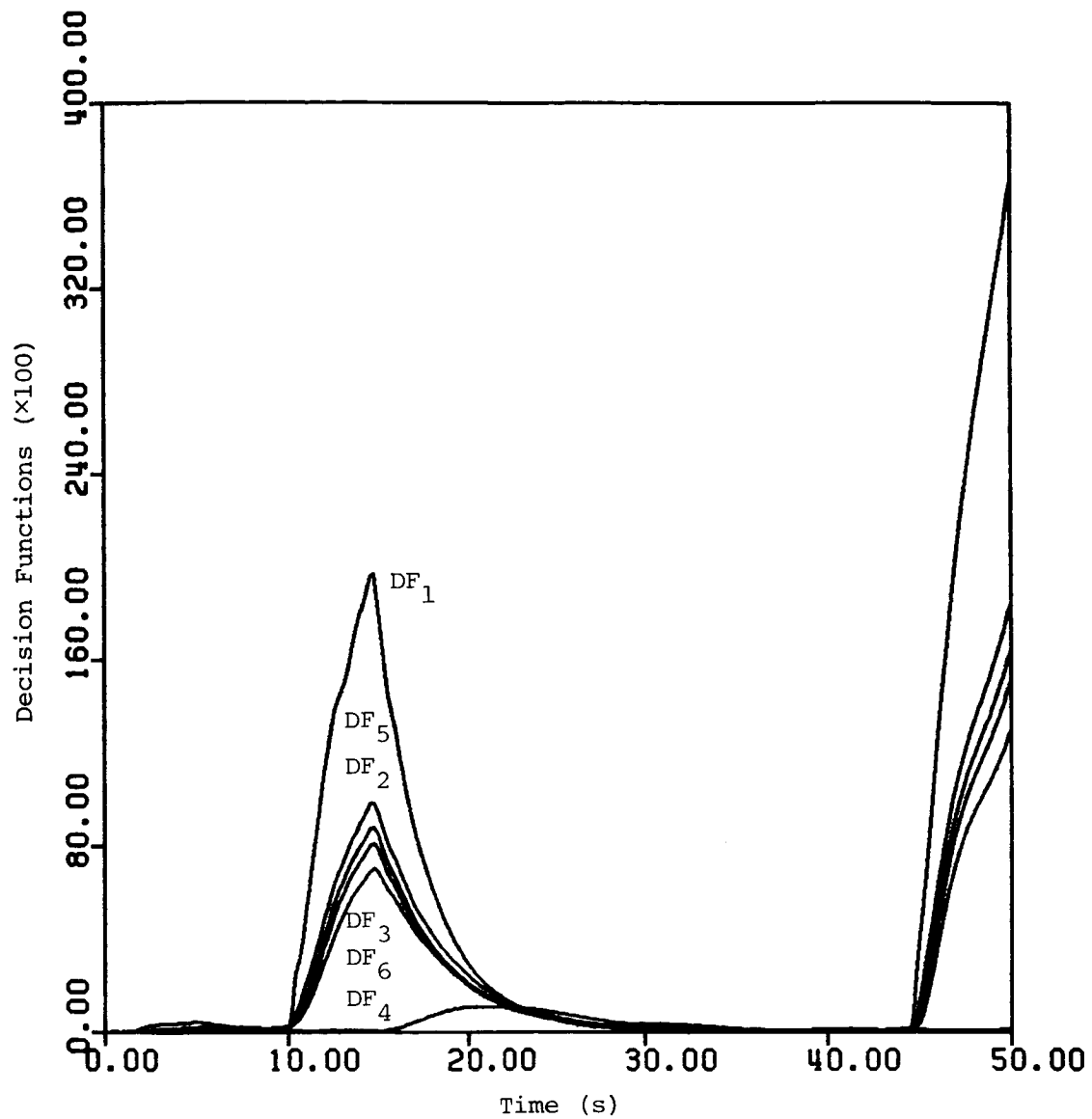


Figure 6.10 Decision functions produced by an age-weighted, scheduled OSGLR algorithm for a -0.0873 rad (-5 deg) elevator bias failure at 64.3 m/s (125 knots) test case

- $46.4, 51.44, 77.2, 102.9$ m/s linear models
- 77.2 m/s age-weighted filter and OSGLR steady-state matrices

weighted filter switches from the 77.2 m/s model to the 51.44 m/s model because the dynamic pressure has decreased, the decision functions decrease significantly. The decision functions increase again when the dynamic pressure increases and the 77.2 m/s model was used again. Two possible reasons for this undesirable behavior are that the 51.44 m/s linear model is inadequate or that the 77.2 m/s age-weighted filter and OSGLR steady-state matrices are not appropriate for the 51.44 m/s linear model. The second possibility is eliminated as a reason for the decrease in the decision functions in the following subsection on scheduling of the age-weighted filter and OSGLR steady-state matrices. The 51.44 m/s linear model was shown in Section 6.2 not to model the 51.44 m/s cruise flight condition well so the first reason is the probable explanation.

6.5 Scheduling of Age-Weighted Filter and OSGLR Steady-State Matrices

Scheduling the linear models used by the age-weighted filter while assuming constant age-weighted filter and OSGLR steady-state matrices is unlikely to be acceptable over an entire flight envelope. Therefore, the scheduling of the steady-state age-weighted filter gain and residual covariance matrices as well as the steady-state OSGLR influence and information matrices was also investigated. (See Appendix B for more details.) The simple scheduling approach used for the linear models was employed (see Section 6.2).

The decision functions for the -0.0873 rad (-5 deg) elevator failure at 64.3 m/s (125 knots) is shown in Figure 6.11. There are several discontinuities in the decision functions due to changes in the steady-state information matrix used to calculate the decision functions. In fact, the elevator decision function jumps to 1.8×10^6 . A smaller vertical scale was chosen to show that even with the correct 51.44 m/s age-weighted filter and OSGLR steady-state matrices, the decision functions decay to very small values with the 51.44 m/s linear model. As discussed in the last subsection, the most probable reason for this undesirable behavior is a poor 51.44 m/s linear model.

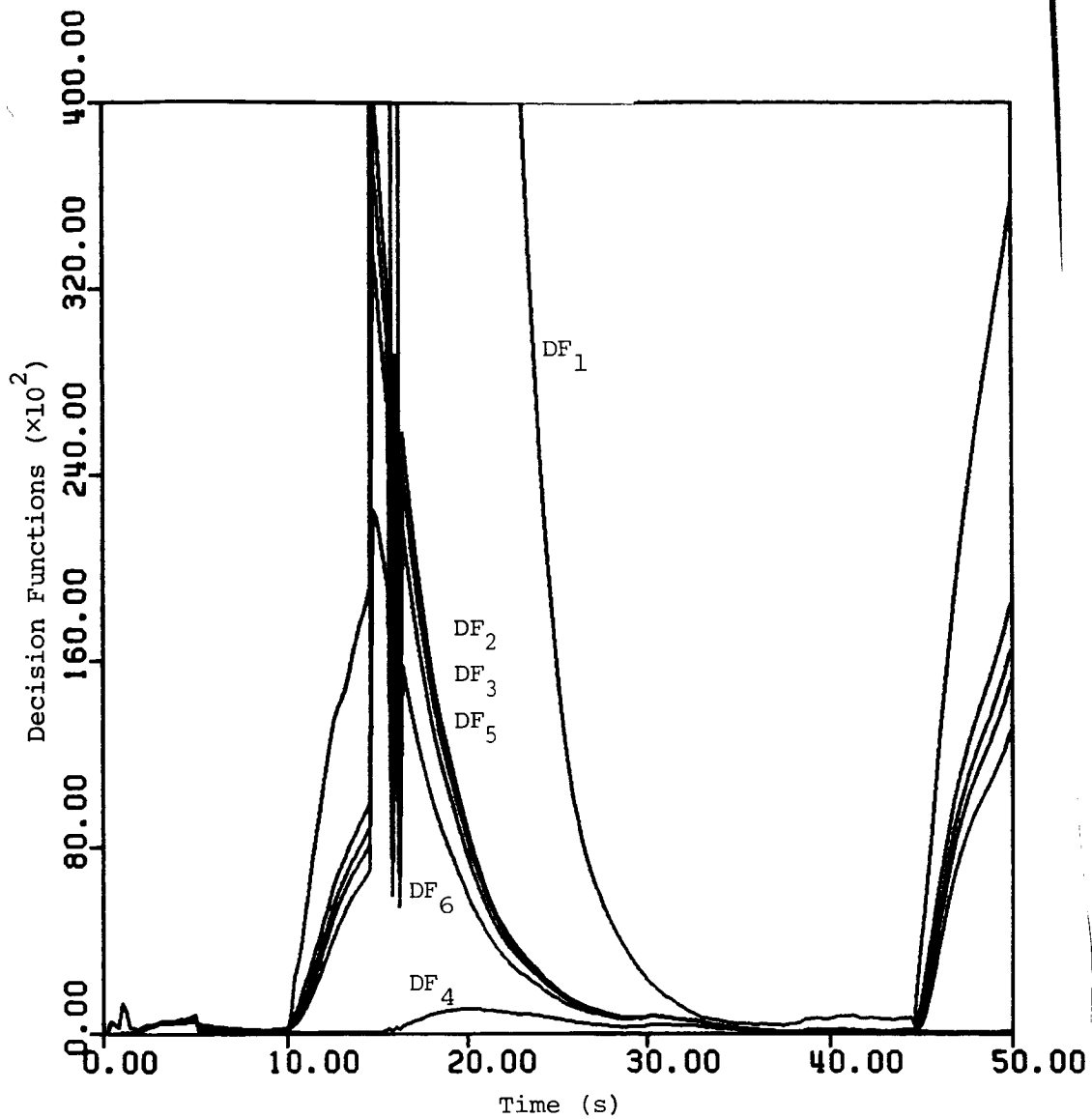


Figure 6.11 Decision functions produced by an age-weighted, scheduled OSGLR algorithm for a -0.0873 rad (-5 deg) elevator bias failure at 64.3 m/s (125 knots) test case

- $46.3, 51.44, 77.2, 102.9$ m/s linear models
- steady-state age-weighted filter and OSGLR matrices also scheduled

The discontinuities resulting from changes in the steady-state information matrix reveal the difficulty with the simple approach of scheduling the steady-state information matrix. Using the simple scheduling, the linear model as well as the age-weighted filter and OSGLR steady-state matrices all change at the same time. The difficulty is that the steady-state information matrix is not valid for the old linear model, age-weighted filter matrices, and the OSGLR influence matrix, all of which were used to produce the information vectors up to the time of the switch of models. In order to avoid this difficulty, one might simply use a constant information matrix. However, in implementing this algorithm over an entire flight envelope, some change in the information matrix will most likely be required.

Another scheduling approach of linearly interpolating between the linear models and their associated age-weighted filter and OSGLR matrices based upon the actual dynamic pressure was tried. The decision functions for the -0.0873 rad (-5 deg) elevator failure at 90.0 m/s (175 knots) test case for this scheduling is shown in Figure 6.12. The effect of turbulence on the dynamic pressure can be seen in the elevator decision function. The dynamic pressure could be smoothed, however. Still, this scheduling approach is not very satisfactory either. The elevator decision function for this test case after the failure occurred using the 77.2 m/s model and associated steady-state age-weighted filter and OSGLR matrices is approximately $55,000$. For the 102.9 m/s model and associated steady-state age-weighted filter and OSGLR matrices, the elevator decision function is approximately $130,000$. For the linear scheduling of the steady-state information matrix to have validity, one would expect the elevator decision functions to be within the range of $55,000$ to $130,000$. Instead, the elevator decision function is much larger. Scheduling the steady-state information matrix probably will not be satisfactory whenever the linear model, age-weighted filter gain and covariance matrices and OSGLR influence matrix are changing. Therefore, the information matrix probably needs to be time-varying.

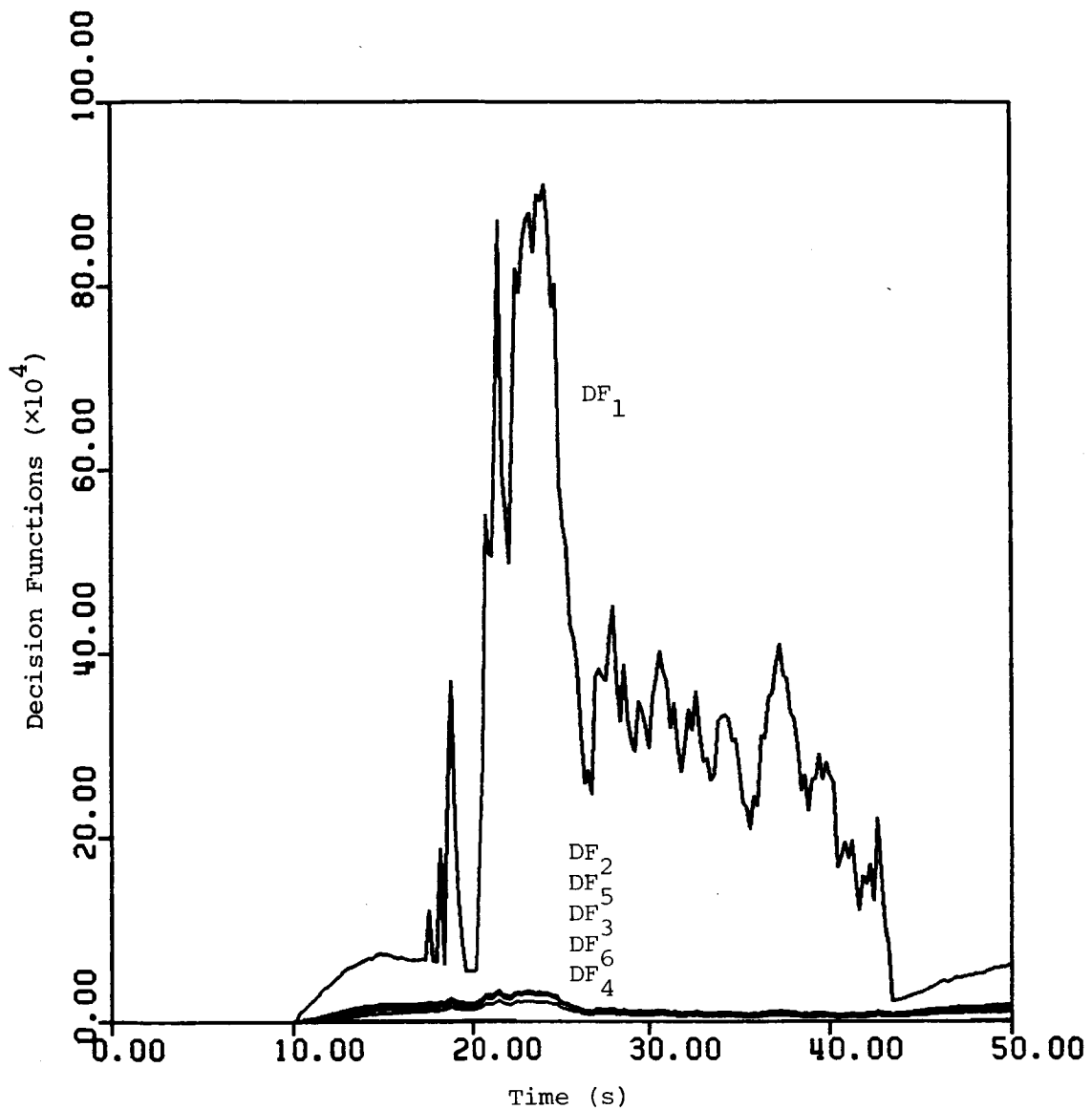


Figure 6.12 Decision functions for a -0.0873 rad (-5 deg) elevator bias failure at 175 knots test case produced by an age-weighted, linearly scheduled OSGLR algorithm

- linear interpolation scheduling approach
- 46.3, 51.44, 77.2, 102.9 m/s linear models
- steady-state age-weighted filter and OSGLR matrices also scheduled

6.6 Summary and Conclusions

Scheduling of the linear models used by the age-weighted filter as a function of dynamic pressure was investigated as a means of reducing the mismodeling effects in the residuals of the filter and, therefore, reducing the no-failure decision functions. The age-weighted filter steady-state gain and covariance matrices and the OSGLR steady-state influence and information matrices were assumed to be constant and corresponded to one of the linear models scheduled. The scheduling approach simply selected the linear model whose dynamic pressure was closest to the actual dynamic pressure. Using this scheduling approach, the decision functions produced by the acceleration from 51.44 m/s test case were reduced from 39,000 to 6,000. This reduced decision function levels are comparable to the decision function levels produced by a maximum rate-of-climb maneuver. Further reductions are possible if a more accurate 51.44 m/s linear model can be developed.

Scheduling linear models as a function of dynamic pressure actually increased the decision function produced by nonzero flap deflections in some cases. As these no-failure decisions are large, scheduling on flap deflection is also necessary. Using linear models with a nominal flap deflection of 50% reduced the decision functions for the 50% and 75% flap deflection test cases to less than 3,000. (The age-weighted filter and OSGLR steady-state matrices corresponded to one of the 50% flap linear models.) However, the decision functions produced by 100% flap deflection test case were very large even with the 50% flap linear models. Using linear models with a nominal flap deflection of 100% did not reduce the decision function levels for the 100% flap test case either. More effort is required to explain why scheduling 100% flap linear models was not sufficient to reduce the decision functions produced by the 100% flap test case.

Two off-nominal elevator failure cases were tested with the linear models scheduled. One case showed no difficulty in detecting the failure with the scheduling. The other case further demonstrated the need for a

better 51.44 m/s linear model. Further testing of failure cases is required to determine the effect of scheduling only the linear models on detecting and isolating failures.

The scheduling of the age-weighted filter steady-state gain and residual covariance matrices and the OSGLR steady-state influence and information matrices was also briefly investigated. Some scheduling of these matrices will be necessary for the OSGLR algorithm to be extended over the entire flight envelope. Two scheduling approaches were tested: the simple approach described earlier and linear interpolation. The same scheduling approach was used for both the linear model and the age-weighted filter and OSGLR steady-state matrices. The results from several failure cases using both scheduling approaches suggested that time-varying information matrix may be required.

The information matrix reflects the uncertainty in the information vector. The two scheduling approaches assume the change in uncertainty in the information vector caused by the change in the filter gain and residual covariance matrices and the OSGLR influence matrix is instantaneous. However, there is a time lag before the effect of the changes in the gain, covariance, and influence matrices is reflected in the information vector. Further work is needed to define the extent of the scheduling required for the age-weighted filter gain and residual covariance matrices and the OSGLR influence matrix.

SUMMARY AND CONCLUSIONS

This report has evaluated the orthogonal series generalized likelihood ratio (OSGLR) test for detecting and isolating commercial aircraft control surface and actuator failures. The OSGLR algorithm was chosen based on a preliminary evaluation of three failure detection and isolation (FDI) algorithms: the detection filter, the generalized likelihood ratio test, and the OSGLR test. The OSGLR test offered the best performance with moderate computational requirements. However, the OSGLR algorithm was also more sensitive to modeling errors than the other two algorithms. This preliminary evaluation is summarized in Section 2. In addition, FDI algorithms are surveyed in Section 3 searching for additional practical techniques that might be applicable for Restructurable Controls. The most promising algorithms appeared to be those already considered and, therefore, the effort concentrated on the OSGLR algorithm.

For the OSGLR algorithm to be feasible, it was necessary to improve its robustness to model uncertainty. Methods of improving the robustness of the algorithm were examined with the incorporation of age-weighting into the algorithm being the most effective approach, significantly reducing the sensitivity of the algorithm. With age-weighting, the covariance of the past measurements and residuals is increased, causing the algorithm to rely more on the new measurements than the past measurements.

In the preliminary evaluation, the algorithms were tested basically at the nominal cruise flight condition of 77.2 m/s (150 knots) at 304.8 m (1000 ft). In this more in-depth evaluation, a number of no-

failure test cases at off-nominal flight conditions including maneuvers, nonzero flap deflections, different turbulence levels and steady winds were used to test the OSGLR algorithm. Maneuvering flight typical of commercial aircraft near the nominal dynamic pressure, light and nominal turbulence levels, and steady winds did not produce significant no-failure decision functions. Large (75% and greater) flap deflections and airspeeds of 51 m/s (100 knots) and less produced large no-failure decision functions. The 77.2 m/s (150 knots) cruise linear model was not valid for these flight conditions.

Since detection thresholds will be chosen such that false alarms are improbable, the no-failure decision functions produced by the off-nominal flight conditions determine the realistic detection thresholds possible in the neighborhood of the nominal flight condition. The detection performance was examined by running a number of failure test cases, mostly at the nominal flight condition. For maneuvering flight near the nominal dynamic pressure, small flap deflections, light and nominal turbulence levels, and steady wind, selecting a threshold to detect 5 deg elevator, 7 deg aileron, 8 deg rudder, and 15% flap bias failures in 1 s at 77.2 m/s (150 knots) appears possible. If there is no compensation for thunderstorm turbulence, a larger detection threshold would be required resulting in slightly worse detection performance.

Finally, extending the validity of the algorithm to off-nominal airspeeds and large flap deflection flight conditions by scheduling was considered. The approach investigated was to schedule the linear models used by the age-weighted filter, choosing the linear model with the nominal dynamic pressure closest to the actual dynamic pressure. The steady-state age-weighted filter and OSGLR matrices corresponded to one of the linear model scheduled. Scheduling on dynamic pressure was used because modeling errors increased with increasing off-nominal dynamic pressure. This approach successfully reduced the no-failure decision functions produced at low airspeeds. Scheduling on flap deflection was also investigated with some success to reduce the no-failure decision

functions produced by large flap deflections. Since simply scheduling the linear models over the entire flight envelope of a commercial aircraft is unlikely to be adequate, scheduling of the age-weighted filter gain and covariance steady-state matrices and the OSGLR influence and information steady-state matrices in the same manner as the linear models was briefly investigated. The scheduling of the steady-state information matrix was unsatisfactory; a time-varying information matrix may be required. Scheduling of the linear model matrices, the age-weighted filter gain and covariance steady-state matrices, and the OSGLR influence steady-state matrix, however, appears feasible.

Depending on the requirements of restructuring the control system, the OSGLR algorithm should be capable of detecting aircraft control surface failures for Restructurable Controls application. Moderate and large failures can be detected quickly. Small failures require longer detection times or cannot be detected. However, failures that are difficult to detect may not be important and could be partially compensated for by a control system robust to small control surface failures. Isolation of some failures may be difficult if there are several surfaces which produce similar effects on the aircraft. Even for these surfaces, isolation may be possible if the failure is moderate or large. If restructuring the control system requires isolation for all failures, position sensors on some of the surfaces will most likely be required. Finally, extending the algorithm over the entire operating envelope of a commercial aircraft, while not demonstrated, appears feasible based on the experience of extending the algorithm to a number of flight conditions.

Further investigation of the scheduling of the linear models and the implementation of the OSGLR algorithm is required, though, before the algorithm can be extended over the entire envelope. Some of the issues requiring consideration are:

- o the number of linear models required to cover the entire flight envelope.

- o the complexity of the implementation approach versus performance.
 - Is the steady-state implementation of the OSGLR algorithm (except for the information matrix) adequate or is the time-varying implementation necessary?
 - Are there significant performance benefits to a time-varying implementation?
 - If scheduling is adequate, how much scheduling of the age-weighted filter gain and covariance matrices and the OSGLR influence matrices is required?
- o the computational and storage requirements of the different approaches.
 - Can the requirements be reduced by, for example, fitting scheduled matrices?

These issues are important since there is not much experience in implementing multivariable systems for practical real-time use.

REFERENCES

1. Montoya, R.J., W.E. Howell, W.T. Bundick, A.J. Ostroff, R.M. Heuschen, and C.M. Belcastro, Restructurable Controls, NASA Conference Publication 2227, NASA Langley Research Center, Hampton, Virginia, September 21-22, 1982.
2. Ostroff, A.J., and R.M. Heuschen, "Investigation of Control Law Reconfigurations to Accommodate a Control Element Failure on a Commercial Aircraft," Proceedings of the 1984 Automatic Control Conference, San Diego, CA, June 6-8, 1984.
3. Looze, D.P., S.M. Krolewski, J.L. Weiss, J.S. Eterno, and S.W. Gully, "An Approach to Restructurable Control System Design," Proceedings of the 23rd Conference on Decision and Control, Las Vegas, NV, December, 1984.
4. "National Transportation Safety Board Accident Report of the American Airlines DC10 Crash at Chicago - O'Hare International Airport, May 25, 1979," NTSB-AAR-79-17, December, 1979.
5. McMahan, J., "Flight 1080," Air Line Pilot, July, 1978.
6. Motyka, P., W. Bonnice, S. Hall, and E. Wagner, The Evaluation of Failure Detection and Isolation Algorithms for Restructurable Control, NASA Contractor Report 177983, November 1985.
7. Beard, R.V., Failure Accommodation in Linear Systems Through Self-Reorganization, Ph.D. Thesis, Dept. of Aeronautics and Astronautics, MIT, Cambridge, MA, February, 1971.
8. Jones, H.L., Failure Detection in Linear Systems, Ph.D. Thesis, Dept. of Aeronautics and Astronautics, MIT, Cambridge, MA, August, 1973.
9. Meserole, Jr. J.S., Detection Filters for Fault-Tolerant Control of Turbofan Engines, Ph.D. Thesis, Dept. of Aeronautics and Astronautics, MIT, Cambridge, MA, June, 1981.

10. Willsky, A.S. and H.L. Jones, "A Generalized Likelihood Ratio Approach to the Detection and Estimation of Jumps in Linear Systems," IEEE Transactions on Automatic Control, Vol. AC-21, No. 1, pp. 108-112, February, 1976.
11. Hall, S.R., A Failure Detection Algorithm for Linear Dynamic Systems, Sc.D. Thesis, Department of Aeronautics and Astronautics, Massachusetts Institute of Technology, Cambridge, MA, June, 1985 (also CSDL-T-874, June, 1985).
12. Chalk, C.R., et al, (1969) Background Information and User Guide for MIL-F-8785B (ASG), "Military Specification - Flying Qualities of Piloted Airplanes", Technical Report AFFDL-TR-69-72, Air Force Flight Dynamics Laboratory, Wright-Patterson Air Force Base, Ohio, August, 1969.
13. Bonnice, W.F., E. Wagner, P. Motyka, and S.R. Hall, "The Application of the Detection Filter to Aircraft Control Surface and Actuator Failure Detection and Isolation," AIAA Paper 85-1973-CP, AIAA Guidance, Navigation and Control Conference, Snowmass, CO., August 1985.
14. Hall, S.R. and B.K. Walker, "The Orthogonal Series Generalized Likelihood Ratio Test," presented at the American Control Conference, June 1985.
15. Van Trees, H.L., Detection, Estimation, and Modulation Theory, Part I, John Wiley & Sons, New York, 1968.
16. Pallett, E.H.J., Automatic Flight Control, Granada, 1983, pp. 264-270+.
17. Weirather, L.H., "Transducers," Chapter 4 in Basic Principles of Flight Test Instrumentation Engineering, Vol. 1, AGARDograph No. 160, April 1974.
18. Willsky, A.S., "A Survey of Design Methods for Failure Detection in Dynamic Systems," Automatica, 12 (1976), pp. 601-611.
19. Caglayan, A.K., and R.E. Lancraft, A Fault Tolerant System for an Integrated Avionics Sensor Configuration, NASA Contractor Report 3834, September 1984.
20. Chow, E.Y. and A.S. Willsky, "Bayesian Design of Decision Rules for Failure Detection," IEEE Transactions and Aerospace and Electronic Systems, November 1984, pp. 761-774.

21. Deckert, J.C., M.N. Desai, J.J. Deyst, and A.S. Willsky, "F8-DFBW Sensor Failure Identification Using Analytic Redundancy," IEEE Transactions on Automatic Control, October 1977, pp. 795-803.
22. Desai, M.N., J.C. Deckert, and J.J. Deyst, "Dual-Sensor Failure Identification Using Analytic Redundancy," Journal of Guidance and Control, May-June 1979, pp 213-220.
23. Gelb, A., Ed., Applied Optimal Estimation, The M.I.T. Press, Cambridge, MA, 1974.

APPENDIX A

SUMMARY OF TEST CASES

This appendix contains a table (Table A-1) summarizing the test cases presented in this report for easy reference and comparison. Only the steady-state implementation of the OSGLR algorithm was tested. In addition, all the test cases included the effects of sensor noise, errors, and dynamics.

Table A-1 Summary of Test Cases

Figure	Page No.	Flight Condition(s)	Failure	Process Noise Added*	Age-Weighting	Linear Models Used by the Filter	Thrust as an Input	Steady-State Filter Gain and Covariance Matrices and OSGLR Matrices**	Scheduling Approach
4.3	55	Cruise at 77.2 m/s (150k) and 304.8 m (1000 ft)	None	None	None	Cruise at 77.2 m/s (150 k) and 304.8 m (1000 ft)	No	Cruise at 77.2 m/s (150 k) and 304.8 m (1000 ft)	None
4.4	57	Cruise at 77.2 m/s (150k) and 304.8 m (1000 ft) at the time of failure	-0.01745 rad (-1 deg) elevator at 10s	None	None	Cruise at 77.2 m/s (150 k) and 304.8 m (1000 ft)	No	Cruise at 77.2 m/s (150k) and 304.8 m (1000 ft)	None
4.5	58	Cruise at 102.9 m/s (200 k) and 1524 m (5000 ft)	None	None	None	Cruise at 77.2 m/s (150 k) and 304.8 m (1000 ft)	No	Cruise at 77.2 m/s (150 k) and 304.8 m (1000 ft)	None
4.6	59	Cruise at 77.2 m/s (150k) and 304.8 m (1000 ft)	-0.01745 rad (-1 deg) elevator a 10s	Yes	None	Cruise at 77.2 m/s (150 k) and 304.8 m (1000 ft)	No	Cruise at 77.2 m/s (150 k) and 304.8 m (1000 ft)	None
4.7	60	Cruise at 102.9 m/s (200k) and 1524 m (5000 ft)	None	Yes	None	Cruise at 77.2 m/s (150 k) and 304.8 m (1000 ft)	No	Cruise at 77.2 m/s (150 k) and 304.8 m (1000 ft)	None
4.8	64	Cruise at 102.9 m/s (200k) and 1524 m (5000 ft)	None	None	15 s time constant	Cruise at 77.2 m/s (150 k) and 304.8 m (1000 ft)	No	Cruise at 77.2 m/s (150 k) and 304.8 m (1000 ft)	None
4.9	65	Cruise at 77.2 m/s (150k) and 304.8 m (1000 ft)	-0.01745 rad (-1 deg) elevator at 10s	None	15 s time constant	Cruise at 77.2 m/s (150 k) and 304.8 m (1000 ft)	No	Cruise at 77.2 m/s (150 k) and 304.8 m (1000 ft)	None
4.11	68	Cruise at 102.9 m/s (200k) and 1524 m (5000 ft)	None	None	3 s time constant	Cruise at 77.2 m/s (150 k) and 304.8 m (1000 ft)	No	Cruise at 77.2 m/s (150 k) and 304.8 m (1000 ft)	None

* in addition to turbulence process noise
 **correspond to linear models shown

Table A-1 Summary of Test Cases (Cont.-2)

Figure	Page No.	Flight Condition(s)	Failure	Process Noise Added*	Age-Weighting	Linear Models Used by the Filter	Thrust as an Input	Steady-State Filter Gain and Covariance Matrices and OSGLR Matrices**	Scheduling Approach
4.12	69	Cruise at 77.2 m/s (150k) and 304.8 m (1000 ft)	-0.01745 rad (-1 deg) elevator at 10s	None	3 s time constant	Cruise at 77.2 m/s (150 k) and 304.8 m (1000 ft)	No	Cruise at 77.2 m/s (150 k) and 304.8 m (1000 ft)	None
5.1	76	Maneuvering (turn, acceleration, climb)	None	None	3 s time constant	Cruise at 77.2 m/s (150 k) and 304.8 m (1000 ft)	No	Cruise at 77.2 m/s (150 k) and 304.8 m (1000 ft)	None
5.2	78	Maneuvering (turn, acceleration, climb)	None	None	3 s time constant	Cruise at 77.2 m/s (150 k) and 304.8 m (1000 ft)	Yes	Cruise at 77.2 m/s (150 k) and 304.8 m (1000 ft)	None
5.3	79	S turn	None	None	3 s time constant	Cruise at 77.2 m/s (150 k) and 304.8 m (1000 ft)	Yes	Cruise at 77.2 m/s (150 k) and 304.8 m (1000 ft)	None
5.4	81	Maximum rate of climb	None	None	3 s time constant	Cruise at 77.2 m/s (150 k) and 304.8 m (1000 ft)	Yes	Cruise at 77.2 m/s (150 k) and 304.8 m (1000 ft)	None
5.5	82	Acceleration from 51.44 m/s (100 k) to 102.9 m/s (200 k)	None	None	3 s time constant	Cruise at 77.2 m/s (150 k) and 304.8 m (1000 ft)	Yes	Cruise at 77.2 m/s (150 k) and 304.8 m (1000 ft)	None
5.6	84	Deceleration at constant altitude from 102.9 m/s (200 k) to 51.44 m/s (100 k)	None	None	3 s time constant	Cruise at 77.2 m/s (150 k) and 304.8 m (1000 ft)	Yes	Cruise at 77.2 m/s (150 k) and 304.8 m (1000 ft)	None
5.7	85	Descending from 1524 m (5000 ft)	None	None	3 s time constant	Cruise at 77.2 m/s (150 k) and 304.8 m (1000 ft)	Yes	Cruise at 77.2 m/s (150 k) and 304.8 m (1000 ft)	None

* in addition to turbulence process noise
 **correspond to linear models shown

Table A-1 Summary of Test Cases (Cont.-3)

Figure	Page No.	Flight Condition(s)	Failure	Process Noise Added*	Age-Weighting	Linear Models Used by the Filter	Thrust as an Input	Steady-State Filter Gain and Covariance Matrices and OSGLR Matrices**	Scheduling Approach
5.8	86	50% flap deflection (starting at 5 s, reaching 50% in about 10 s; aircraft at 77.2 m/s (150 k) and 304.8 m (1000 ft) before flaps deflected)	None	None	3 s time constant	Cruise at 77.2 m/s (150 k) and 304.8 m (1000 ft)	Yes	Cruise at 77.2 m/s (150 k) and 304.8 m (1000 ft)	None
5.9	87	75% flap deflection (starting at 5 s, reaching 50% in about 10 s; aircraft at 51.44 m/s (150 k) and 304.8 m (1000 ft) before flaps deflected)	None	None	3 s time constant	Cruise at 77.2 m/s (150 k) and 304.8 m (1000 ft)	Yes	Cruise at 77.2 m/s (150 k) and 304.8 m (1000 ft)	None
5.10	89	Maneuvering (turn, acceleration, climb) with light turbulence	None	None	3 s time constant	Cruise at 77.2 m/s (150 k) and 304.8 m (1000 ft)	Yes	Cruise at 77.2 m/s (150 k) and 304.8 m (1000 ft)	None
5.11	90	Cruise at 77.2 m/s (150 k) at 304.8 m (1000 ft) in thunderstorm turbulence	None	None	3 s time constant	Cruise at 77.2 m/s (150 k) and 304.8 m (1000 ft)	Yes	Cruise at 77.2 m/s (150 k) and 304.8 m (1000 ft)	None
5.12	92	Cruise at 77.2 m/s (150 k) at 304.8 m (1000 ft) in a 10.3 m/s (20 k) crosswind	None	None	3 s time constant	Cruise at 77.2 m/s (150 k) and 304.8 m (1000 ft)	Yes	Cruise at 77.2 m/s (150 k) and 304.8 m (1000 ft)	None
5.13	93	Cruise at 77.2 m/s (150 k) and 304.8 m (1000 ft) at the time of failure	-0.0873 rad (-5 deg) elevator at 10 s	None	3 s time constant	Cruise at 77.2 m/s (150 k) and 304.8 m (1000 ft)	Yes	Cruise at 77.2 m/s (150 k) and 304.8 m (1000 ft)	None

* in addition to turbulence process noise
 **correspond to linear models shown

Table A-1 Summary of Test Cases (Cont.-4)

Figure	Page No.	Flight Condition(s)	Failure	Process Noise Added*	Age-Weighting	Linear Models Used by the Filter	Thrust as an Input	Steady-State Filter Gain and Covariance Matrices and OSGLR Matrices**	Scheduling Approach
5.15	96	Cruise at 64.3 m/s (125 k) and 304.8 m/s (1000 ft) at the time of failure	-0.0873 rad (-5 deg) elevator at 10 s	None	3 s time constant	Cruise at 77.2 m/s (150 k) and 304.8 m (1000 ft)	Yes	Cruise at 77.2 m/s (150 k) and 304.8 m (1000 ft)	None
5.16	97	Cruise at 90 m/s (175 k) and 304.8 m/s (1000 ft) at the time of failure	-0.0873 rad (-5 deg) elevator at 10 s	None	3 s time constant	Cruise at 77.2 m/s (150 k) and 304.8 m (1000 ft)	Yes	Cruise at 77.2 m/s (150 k) and 304.8 m (1000 ft)	None
5.17	99	Cruise at 77.2 m/s (150 k) and 304.8 m/s (1000 ft) at the time of failure	0.0873 rad (5 deg) right aileron at 10 s	None	3 s time constant	Cruise at 77.2 m/s (150 k) and 304.8 m (1000 ft)	Yes	Cruise at 77.2 m/s (150 k) and 304.8 m (1000 ft)	None
5.19	101	Cruise at 77.2 m/s (150 k) and 304.8 m/s (1000 ft) at the time of failure	-0.0873 rad (-5 deg) rudder at 10 s	None	3 s time constant	Cruise at 77.2 m/s (150 k) and 304.8 m (1000 ft)	Yes	Cruise at 77.2 m/s (150 k) and 304.8 m (1000 ft)	None
5.20	103	Cruise at 77.2 m/s (150 k) and 304.8 m (1000 ft) at the time of failure	5% right flap at 10 s	None	3 s time constant	Cruise at 77.2 m/s (150 k) and 304.8 m (1000 ft)	Yes	Cruise at 77.2 m/s (150 k) and 304.8 m (1000 ft)	None
6.1	121	Acceleration from 51.44 m/s (100k) to 107.9 m/s (200 k)	None	None	3 s time constant	Cruise at airspeeds of 51.44, 77.2, and 102.9 m/s (100, 150, and 200 k) and 304.8 m (1000 ft)	Yes	Cruise at 77.2 m/s (150 k) and 304.8 m (1000 ft)	Simple scheduling on dynamic pressure of the linear models used by the filter

* in addition to turbulence process noise
 **correspond to linear models shown

Table A-1 Summary of test cases (Cont.-5)

Figure	Page No.	Flight Condition(s)	Failure	Process Noise Added*	Age-Weighting	Linear Models Used by the Filter	Thrust as an Input	Steady-State Filter Gain and Covariance Matrices and OSGLR Matrices**	Scheduling Approach
6.2	123	Acceleration from 51.44 m/s (100 k) to 107.9 m/s (200 k)	None	None	3 s time constant	Cruise at airspeeds of 46.3, 51.44, 77.3 and 102.9 m/s (90, 100, 150, and 200 k) and 304.8 m (1000 ft)	Yes	Cruise at 77.2 m/s (150 k) and 304.8 m (1000 ft)	Simple scheduling on dynamic pressure of the linear models used by the filter
6.3	124	Cruise of 51.44 m/s (100 k) and 304.8 m (1000 ft)	None	None	None	Cruise of 51.44 m/s (100 k) and 304.8 m (1000 ft)	Yes	Cruise at 51.44 m/s (100 k) and 304.8 m (1000 ft)	None
6.4	125	Cruise at 77.2 m/s (150 k) and 304.8 m (1000 ft)	None	None	None	Cruise of 77.2 m/s (150 k) and 304.8 m (1000 ft)	Yes	Cruise at 77.2 m/s (150 k) and 304.8 m (1000 ft)	None
6.5	127	50% flap deflection (starting at 5 s, reading 50% in about 10 s; aircraft at 77.2 m/s (150 k) and 304.8 m (1000 ft) before flaps are deflected)	None	None	3 s time constant	Cruise at airspeeds of 46.3, 51.44, 77.3 and 102.9 m/s (90, 100, 150, and 200 k) and 304.8 m (1000 ft)	Yes	Cruise at 77.2 m/s (150 k) and 304.8 m (1000 ft)	Simple scheduling on dynamic pressure of the linear models used by the filter
6.6	129	50% flap deflection (starting at 5 s, reading 50% in about 10 s; aircraft at 77.2 m/s (150 k) and 304.8 m (1000 ft) before flaps are deflected)	None	None	3 s time constant	Cruise at airspeeds of 38.6, 51.44, and 77.2 m/s (75, 100, and 150 k) at 304.8 m (1000 ft) with 50% nominal flap deflection	Yes	Cruise at 77.2 m/s (150 k) and 304.8 m (1000 ft) with 50% nominal flap deflection	Simple scheduling on dynamic pressure of the linear models used by the filter

* in addition to turbulence process noise
 **correspond to linear models shown

Table A-1 Summary of Test Cases (Cont.-6)

Figure	Page No.	Flight Condition(s)	Failure	Process Noise Added*	Age-Weighting	Linear Models Used by the Filter	Thrust as an Input	Steady-State Filter Gain and Covariance Matrices and OSGLR Matrices**	Scheduling Approach
6.7	130	75% flap deflection (starting at 5 s, reaching 50% in about 10 s; aircraft at 51.44 m/s (150 k) and 304.8 m (1000 ft) before flap are deflected	None	None	3 s time constant	Cruise at airspeeds of 38.6, 51.44, and 77.2 m/s (75, 100, and 150 k) at 304.8 m (1000 ft) with 50% nominal flap deflection	Yes	Cruise at 77.2 m/s (150 k) and 304.8 m (1000 ft) with 50% nominal flap deflection	Simple scheduling on dynamic pressure of the linear models used by the filter
6.8	131	100% flap deflection from the start of the test case (aircraft started at 77.2 m/s (150 k) and 304.8 m (1000 ft))	None	None	3 s time constant	Cruise at airspeeds of 38.6, 51.44, and 77.2 m/s (75, 100, and 150 k) at 304.8 m (1000 ft) with 100% nominal flap deflection	Yes	Cruise at 77.2 m/s (150 k) and 304.8 m (1000 ft) with 100% nominal flap deflection	Simple scheduling on dynamic pressure of the linear models used by the filter
6.9	132	Cruise at 90 m/s (175 k) and 304.8 m (1000 ft) at the time of failure	-0.0873 rad (-5 deg) elevation at 10 s	None	3 s time constant	Cruise at airspeeds of 46.3, 51.44, 77.2 and 102.9 m/s (90, 100, 150, and 200 k) and 304.8 m (1000 ft)	Yes	Cruise at 77.2 m/s (150 k) and 304.8 m (1000 ft)	Simple scheduling on dynamic pressure of the linear models used by the filter
6.10	133	Cruise at 64.3 m/s (125 k) and 304.8 m (1000 ft) at the time of failure	-0.0873 rad (-5 deg) elevation at 10 s	None	3 s time constant	Cruise at airspeeds of 46.3, 51.44, 77.2 and 102.9 m/s (90, 100, 150, and 200 k) and 304.8 m (1000 ft)	Yes	Cruise at 77.2 m/s (150 k) and 304.8 m (1000 ft)	Simple scheduling on dynamic pressure of the linear models used by the filter
6.11	135	Cruise at 64.3 m/s (125 k) and 304.8 m (1000 ft) at the time of failure	-0.0873 rad (-5 deg) elevation at 10 s	None	3 s time constant	Cruise at airspeeds of 46.3, 51.44, 77.2 and 102.9 m/s (90, 100, 150, and 200 k) and 304.8 m (1000 ft)	Yes	Cruise models used by the filter	Simple scheduling on dynamic pressure of the linear models and steady-state matrices

* in addition to turbulence process noise
 **correspond to linear models shown

Table A-1 Summary of Test Cases (Cont.-7)

Figure	Page No.	Flight Condition(s)	Failure	Process Noise Added*	Age-Weighting	Linear Models Used by the Filter	Thrust as an Input	Steady-State Filter Gain and Covariance Matrices and OSGLR Matrices**	Scheduling Approach
6.12	137	Cruise at 90 m/s (175 k) and 304.8 m (1000 ft) at the time of failure	-0.0873 rad (-5 deg) elevation at 10 s	None	3 s time constant	Cruise at airspeeds of 46.3, 51.44, 77.2 and 102.9 m/s (90, 100, 150, and 200 k) and 304.8 m (1000 ft)	Yes	Cruise models used by the filter	Linear interpolation on dynamic pressure of linear models and steady-state matrices

* in addition to turbulence process noise

**correspond to linear models shown

APPENDIX B

SCHEDULING IMPLEMENTATION DETAILS

B.1 Introduction

This appendix describes in more detail the scheduling considered in this report. First, the linear model formulation and the OSGLR steady-state equations will be presented and then the scheduling of the linear models and OSGLR steady-state algorithm described.

B.2 Linear Model Formulation

The continuous-time linear model can be written

$$\dot{\underline{\Delta x}} = \underline{f}(\underline{x}_0, \underline{u}_0) + \underline{A} \underline{\Delta x} + \underline{B} \underline{\Delta u} \quad (\text{B.1})$$

$$\underline{y} = \underline{g}(\underline{x}_0, \underline{u}_0) + \underline{C} \underline{\Delta x} + \underline{D} \underline{\Delta u} \quad (\text{B.2})$$

where

$$\dot{\underline{x}} = \underline{f}(\underline{x}, \underline{u}) \quad (\text{B.3})$$

$$\underline{y} = \underline{g}(\underline{x}, \underline{u}) \quad (\text{B.4})$$

are the nonlinear state differential and output equations. \underline{x}_0 and \underline{u}_0 are the nominal state and input vectors. $\underline{\Delta x}$ and $\underline{\Delta u}$ are defined to be

$$\underline{\Delta x} \equiv \underline{x} - \underline{x}_0 \quad (\text{B.5})$$

$$\underline{\Delta u} \equiv \underline{u} - \underline{u}_0 \quad (\text{B.6})$$

An equivalent discrete-time linear model can be written

$$\Delta \underline{x}(k+1) = \underline{f}_d(\underline{x}_o, \underline{u}_o) + \Phi \Delta \underline{x}(k) + B \Delta \underline{u}(k) \quad (\text{B.7})$$

$$\underline{y}(k) = \underline{g}_d(\underline{x}_o, \underline{u}_o) + C \Delta \underline{x}(k) + D \Delta \underline{u}(k) \quad (\text{B.8})$$

where the matrix B now is the discrete state input matrix (consistent with Eq. (2.17)). The discrete linear model may be rewritten as

$$\underline{x}(k+1) = \Phi \underline{x}(k) + B \underline{u}(k) + \underline{g}(k) \quad (\text{B.9})$$

$$\underline{y}(k) = C \underline{x}(k) + D \underline{u}(k) + \underline{h}(k) \quad (\text{B.10})$$

by using Eqs. (B.5) and (B.6). The constant bias vectors, $\underline{g}(k)$ and $\underline{h}(k)$, are given by

$$\underline{g}(k) = \underline{f}_d(\underline{x}_o, \underline{u}_o) + \underline{x}_o - \Phi \underline{x}_o - B \underline{u}_o \quad (\text{B.11})$$

$$\underline{h}(k) = \underline{g}_d(\underline{x}_o, \underline{u}_o) - C \underline{x}_o - D \underline{u}_o \quad (\text{B.12})$$

B.3 Steady-State OSGLR Equations

The steady-state OSGLR equations consist of the steady-state age-weighted filter equations and the OSGLR information vectors and decision function equations.

The steady-state age-weighted filter equations are

$$\hat{\underline{x}}^-(k+1) = \Phi \hat{\underline{x}}^+(k) + B \underline{u}(k) + \underline{g}(k) \quad (\text{B.13})$$

$$\hat{\underline{x}}^+(k) = \hat{\underline{x}}^-(k) + K \underline{\gamma}(k) \quad (\text{B.14})$$

$$\underline{\gamma}(k) = \underline{y}(k) - \hat{\underline{y}}(k) \quad (\text{B.15})$$

$$\hat{\underline{y}}(k) = C \hat{\underline{x}}(k) + D \underline{u}(k) + \underline{h}(k) \quad (\text{B.16})$$

The steady-state information vector equation is

$$\underline{\chi}(k+1) = \frac{1}{s} A_{\phi} \underline{\chi}(k) + G^T M^{-1} \underline{y}(k+1) \quad (\text{B.17})$$

where s is the age-weighting constant, A_{ϕ} is the basis function transition matrix, G is the steady-state influence matrix, and M is the residual covariance matrix (with the effects of age-weighting included).

The decision function is given by

$$\text{DF}(k) = \underline{\chi}^T(k) S^{-1} \underline{\chi}(k) \quad (\text{B.18})$$

where S is the steady-state information matrix.

B.4 Scheduling

The scheduling approach given the most consideration was the approach of scheduling the linear model used by the age-weighted filter (Eqs. B.13 and B.16) as a function of dynamic pressure. At each time step, the linear model whose nominal dynamic pressure was closest to the actual dynamic pressure was chosen. While scheduling of all the ϕ , B , C , and D matrices and the \underline{g} and \underline{h} vectors which represent the linear model may not be necessary in practice, this was the approach taken in this report.

The scheduling of the steady-state age-weighted filter gain and residual covariance matrices (K and M respectively) and the steady-state OSGLR influence and information matrices (G and S respectively) was also briefly examined. Scheduling of the A_{ϕ} matrix and the age-weighting factor s is not necessary as they remain constant. Actually, the product $G^T M^{-1}$ found in Eq. B.17 was scheduled instead of scheduling the steady-state influence and residual covariance matrices (G and M) separately.

TECHNICAL REPORT STANDARD TITLE PAGE

1. Report No.	2. Government Accession No.	3. Recipient's Catalog No.	
4. Title and Subtitle The Evaluation of the OSGLR Algorithm for Restructurable Controls		5. Report Date March 1986	
		6. Performing Organization Code	
7. Author(s) W.F. Bonnice, E. Wagner, S.R. Hall, P. Motyka		8. Performing Organization Report No. CSDL-R-1849	
9. Performing Organization Name and Address The Charles Stark Draper Laboratory, Inc. 555 Technology Square Cambridge, Massachusetts 02139		10. Work Unit No.	
		11. Contract or Grant No. NAS1-17556	
12. Sponsoring Agency Name and Address National Aeronautics and Space Administration Washington, D.C. 20546		13. Type of Report and Period Covered Final Report Dec. 1983 - April 1986	
		14. Sponsoring Agency Code	
15. Supplementary Notes Langley Technical Monitor: W. Thomas Bundick			
16. Abstract The detection and isolation of commercial aircraft control surface and actuator failures using the orthogonal series generalized likelihood ratio (OSGLR) test was evaluated. The OSGLR algorithm was chosen as the most promising algorithm based on a preliminary evaluation of three failure detection and isolation (FDI) algorithms (the detection filter, the generalized likelihood ratio test, and the OSGLR test) and a survey of the literature. One difficulty of analytic FDI techniques and the OSGLR algorithm in particular is their sensitivity to modeling errors. Therefore, methods of improving the robustness of the algorithm were examined with the incorporation of age-weighting into the algorithm being the most effective approach, significantly reducing the sensitivity of the algorithm to modeling errors. The steady-state implementation of the algorithm based on a single cruise linear model was evaluated using a nonlinear simulation of a C-130 aircraft. A number of off-nominal no-failure flight conditions including maneuvers, nonzero flap deflections, different turbulence levels and steady winds were tested. Based on the no-failure decision functions produced by off-nominal flight conditions, the failure detection performance at the nominal flight condition was determined. The extension of the algorithm to a wider flight envelope by scheduling the linear models used by the algorithm on dynamic pressure and flap deflection was also considered. Since simply scheduling the linear models over the entire flight envelope is unlikely to be adequate, scheduling of the steady-state implementation of the algorithm was briefly investigated.			
17. Key Words Suggested by Author Failure Detection and Isolation Restructurable Controls Generalized Likelihood Ratio		18. Distribution Statement Unclassified - Unlimited Subject Category - 04	
19. Security Classif. (of this report) Unclassified	20. Security Classif. (of this page) Unclassified	21. No. of Pages 158	22. Price